Fragile Phases as Affine Monoids: Classification and Material Examples

Zhi-Da Song,[1,†] Luis Elcoro,[2,†] Yuan-Feng Xu,[3] Nicolas Regnault,[4,1] and B. Andrei Bernevig[1,3,5,*]

[1]*Department of Physics, Princeton University, Princeton, New Jersey 08544, USA*
[2]*Department of Condensed Matter Physics, University of the Basque Country UPV/EHU, Apartado 644, 48080 Bilbao, Spain*
[3]*Max Planck Institute of Microstructure Physics, 06120 Halle, Germany*
[4]*Laboratoire de Physique de l'Ecole normale supérieure PSL University, CNRS, Sorbonne Université, Université Paris Diderot, Sorbonne Paris Cité, 24 rue Lhomond, 75005 Paris France*
[5]*Physics Department, Freie Universitat Berlin, Arnimallee 14, 14195 Berlin, Germany*

(Received 24 August 2019; revised 4 February 2020; accepted 22 April 2020; published 1 July 2020)

Topological phases in electronic structures contain a new type of topology, called fragile, which can arise, for example, when an elementary band representation (atomic limit band) splits into a particular set of bands. For the first time, we obtain a complete classification of the fragile topological phases, which can be diagnosed by symmetry eigenvalues, to find an incredibly rich structure that far surpasses that of stable or strong topological states. We find and enumerate hundreds of thousands of different fragile topological phases diagnosed by symmetry eigenvalues, and we link the mathematical structure of these phases to that of affine monoids in mathematics. Furthermore, for the first time, we predict and calculate (hundreds of realistic) materials where fragile topological bands appear, and we showcase the very best ones.

DOI: 10.1103/PhysRevX.10.031001 Subject Areas: Condensed Matter Physics

I. INTRODUCTION

Since the birth of topological insulators (TIs) [1–9], researchers have found topological states of matter to be a theoretically and experimentally versatile field where new phenomena are uncovered every year [10–12]. From topological semimetals [13–22] to topological crystalline insulators with symmorphic and nonsymmorphic symmetries [23–29] to higher-order topological insulators (HOTIs) [30–36], the field of topological electronic phases of matter keeps evolving. As researchers steadily theoretically solve and experimentally find materials for several topological phases, new further-unknown types of topological phases arise.

Recent substantial progress in the field has led to the development of techniques [37–45] that can be used for a high-throughput discovery of topological materials, the beginning of which has been undertaken in Refs. [46–49]. Topological quantum chemistry (TQC) [37,40,41,50] and the associated Bilbao Crystallographic Server (BCS) [37,40,51] have provided a classification of *all* the atomic limits—whose bases are the so-called elementary band representations (EBRs)—that exist in the 230 nonmagnetic space groups (SGs). TQC defines topological phases as the phases not adiabatically continuable to a sum of EBRs. This definition leads to different large series of topological states. The first series includes the so-called eigenvalue-stable (strong, weak, and crystalline) topological states, whose characters at high symmetry points cannot be expressed as a linear combination (sum or difference) of characters of EBRs. These states have been fully classified, and progress towards material high-throughput has been made [37,38,43,44,46–48], with several partial catalogues of topological materials that already existed. The second series are the so-called fragile states of matter, which we call eigenvalue fragile phases (EFPs); they cannot be written purely as a sum of characters (traces of representations) of EBRs, but they can be written as sums and differences of characters of EBRs. Last, there exist stable or fragile states that are not characterized by characters or irreducible representations (irreps); they are characterized by the flow of Berry phases. These fragile phases currently lack classifications, and they lack any material examples. A schematic of the classifications is shown in Fig. 1.

Fragile states show up in the examples of TQC [37,56], although their full potential has only been identified after Refs. [38,42,54,55,57–62]. References [55–59] discovered a small number of models of EFP by applying the methods of TQC, but neither a general, complete (or even partial) classification, nor *any* material examples for these phases, is known. This fact leaves us in the unenviable situation of being far from a theoretical understanding of a so-far purely

*bernevig@princeton.edu
†Z. S. and L. E. contributed equally to this work.

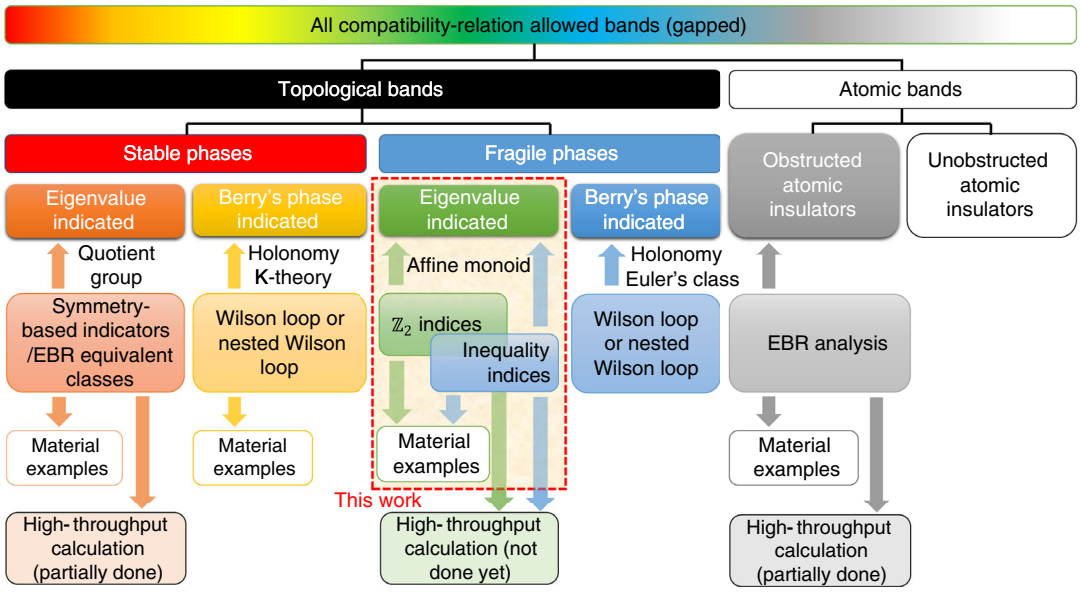

FIG. 1. The classification of topological bands, where the shaded area represents the contents of the present work. All the band structures are classified into three categories: stable topological bands, fragile topological bands, and atomic (trivial) bands. The stable or fragile topological bands are further classified into two subcategories: those indicated by symmetry eigenvalues and those not indicated by symmetry eigenvalues. The atomic bands are also classified into two subcategories depending on whether the Wannier functions are located at the positions of atoms. The topological states that are not eigenvalue indicated are usually identified by the Wilson loop method [30,52–55], but the general framework to calculate their topological invariants is still unknown. The eigenvalue-indicated stable topological states are classified by the TQC [37] and other theories [38,50]. The present work finishes the classification of EFPs.

theoretical phase of matter. In this work, we perform, for the first time, three separate tasks. (1) We provide an elegant, mathematical framework to *fully* classify and diagnose *all* the EFPs. (2) We apply this formalism to the spin-orbit-coupling (SOC) doubled groups with time-reversal symmetry (TRS) and classify all the 340590 EFPs that can exist—a much richer structure than in stable or strong topological phases. (3) We provide examples of 100 fragile bands in different real materials, some of which are extremely well isolated in energy from other bands. Our framework is closely related to the mathematical theories of polyhedra and affine monoids, bringing highly esoteric mathematical concepts into real material structures. (See the Appendix F for a mathematical definition.) Thus, we call our method the polyhedron method. To underscore the importance of fragile topology, the low-lying states of twisted bilayer graphene (TBG), a wonder material engineered of two twisted layers of graphene [63–68], are predicted to exhibit a fragile topology [55,58,59,69,70].

II. EFPS IN VIEWPOINT OF TQC

To obtain the mathematical structure of EFPs, we first review their definition from the viewpoint of TQC. A band structure is *partially* indexed by its decomposition into irreps at the high symmetry momenta [37–39]. Such a decomposition is described by a "symmetry data vector," where entries give the multiplicities of the irreps in the decomposition. To be specific, we write the symmetry data vector as

$$B = (m_{1_{K_1}}, m_{2_{K_1}}, \ldots, m_{1_{K_2}}, m_{2_{K_2}}, \cdots)^T. \tag{1}$$

Here, K_1, K_2, $\cdots$ are a known set of sufficient high symmetry momenta (maximal k-vectors in Ref. [40]), and m_{i_K} is the multiplicity of the ith irrep of the little group at K. (Different maximal k-vectors can have different irreps.) For example, for a one-dimensional system with only inversion symmetry, the symmetry data vector is written as $B = (m_{+_0}, m_{-_0}, m_{+_\pi}, m_{-_\pi})$, where the four entries represent the multiplicities of the inversion even (+) or odd (-) irrep at $k = 0, \pi$, respectively. The symmetry data vector of a gapped band structure necessarily satisfies a set of rules called "compatibility relations" (available for all SGs on the BCS [37–41,51]), which dictate if a given band structure can exist in the Brillouin zone (BZ). In the 1D example, the compatibility relation is trivial, and it enforces an equal band number at $k = 0, \pi$: $m_{+_0} + m_{-_0} = m_{+_\pi} + m_{-_\pi}$. We always assume that the symmetry data vector satisfies the compatibility relations. For the symmetry data to be consistent with a *trivial* insulator, it should be induced by local orbitals forming representations of the SG in real space. Such trivial insulators are labeled as band representations (BRs); their symmetry data vectors are defined as "trivial." The generators of BRs are the EBRs [71,72].

In the 1D example, there are four EBRs, induced by the even (+)/odd (−) orbital at $x = 0/\frac{1}{2}$, respectively. They are $\mathrm{ebr}_1 = (1,0,1,0)^T$, $\mathrm{ebr}_2 = (0,1,0,1)^T$, $\mathrm{ebr}_3 = (1,0,0,1)^T$, and $\mathrm{ebr}_4 = (0,1,1,0)^T$, respectively. In general, we can

define the EBR matrix as $\mathrm{EBR} = (\mathrm{ebr}_1, \mathrm{ebr}_2, \cdots)$, where the ith column of the EBR matrix ebr_i is the ith EBR of the corresponding SG. A symmetry data vector B is trivial if and only if there exist $p_1, p_2, \cdots \in \mathbb{N}$ ($\mathbb{N}$ stands for the nonnegative integers) such that $B = p_1\mathrm{ebr}_1 + p_2\mathrm{ebr}_2 + \cdots$, or, equivalently,

$$\exists\, p = (p_1, p_2, \ldots)^T \in \mathbb{N}^{N_{\mathrm{EBR}}} \quad \text{s.t.} \quad B = \mathrm{EBR} \cdot p. \tag{2}$$

Here, N_{EBR} is the number of EBRs in the SG. Crucially, the EBRs may not be linearly independent: Given B, the corresponding p may not be unique.

Because bands are only partially defined by symmetry data vectors, not all trivial symmetry data vectors imply trivial insulators (topological insulators in space group $P1$ have trivial symmetry data vectors). Hence, nontrivial symmetry data are a sufficient but not necessary condition for a band to be topologically nontrivial.

For any symmetry data vector B satisfying compatibility relations, there always exists $p \in \mathbb{Q}^{N_{\mathrm{EBR}}}$ (rational number) such that $B = \mathrm{EBR} \cdot p$ (for a proof, see Ref. [38] and also, in more detail, Ref. [73]). Because of this property, *nontrivial* symmetry data vectors can be further classified into two cases, both included in the TQC formalism [37,42]: (i) B cannot be written as an integer combination of EBRs but can only be written as a fractional rational combination of EBRs; (ii) B can be written as an integer combination of EBRs, and at least one of the coefficients is *necessarily* negative. Case (i) is characterized by topological indices—symmetry-based indicators [38,44] or EBR equivalence classes [37]—and implies robust topology [38,43,44]. Case (ii), on the other hand, implies fragile topology [42,54–57], and no classification, indices, or material examples are known for it. We provide a full classification and 100 material examples below. A symmetry data vector in case (ii) can be generally written as $B = \sum_i p_i\mathrm{ebr}_i - \sum_j q_j\mathrm{ebr}_j$, with $p_i, q_j \in \mathbb{N}$ and $p_i q_i = 0$ for all i. (However, not all vectors written in such a form represent fragile phases. For example, if $\mathrm{ebr}_1 + \mathrm{ebr}_2 = \mathrm{ebr}_3$, then $\mathrm{ebr}_3 - \mathrm{ebr}_2 = \mathrm{ebr}_1$ is not fragile.) The topologically nontrivial restriction is that B does not decompose to a sum of EBRs. Once coupled to an atomic insulator BR $\sum_j q_j\mathrm{ebr}_j$, the total band structure, i.e., $\sum_i p_i\mathrm{ebr}_i$, represents a trivial symmetry data vector, removing the topology imposed by symmetry eigenvalues; thus, it is "fragile."

We now introduce a convenient parametrization of the symmetry data. We can always write the Smith decomposition of the EBR matrix as $\mathrm{EBR} = L\Lambda R$, with L (correspondingly R) an $N_B \times N_B$ (correspondingly $N_{\mathrm{EBR}} \times N_{\mathrm{EBR}}$) unimodular integer matrices, N_B the length of the symmetry data vector, and Λ an $N_B \times N_{\mathrm{EBR}}$ matrix with diagonal integer entries $\Lambda_{ij} = \delta_{ij}\lambda_i$ for $i = 1, 2 \cdots N_B$, $j = 1, 2 \cdots N_{\mathrm{EBR}}$, where $\lambda_i > 0$ for $r = 1 \cdots r$ and $\lambda_i = 0$ for $i > r$, with r the EBR matrix rank (Appendix A).

For $B = \mathrm{EBR} \cdot p$, for some $p \in \mathbb{Q}^{N_{\mathrm{EBR}}}$, we can equivalently write the symmetry data vector as

$$B_i = \sum_{j=1}^{r} L_{ij}\lambda_j y_j, \tag{3}$$

where y is defined as $y_j = (Rp)_j$ ($j = 1 \cdots r$). While, in general, the map from p to y is many-to-one mapping due to linear dependence of EBRs, the map from y to B is one-to-one mapping: If y and y' map to the same B, ($\sum_j L_{ij}\lambda_j y_j = \sum_j L_{ij}\lambda_j y'_j$), multiplying L^{-1} on both sides gives $y = y'$. Table S1 in Ref. [74] tabulates the parametrizations in all SGs.

As the symmetry data vector B entries represent the multiplicities of the irreps, they should be integer nonnegative valued for any physical band structure, a condition which is not automatically guaranteed by the parametrization in Eq. (3). What conditions should the y vector satisfy so that B is (1) non-negative (zero and strictly positive) and (2) an integer? For condition (2), since the L matrix is unimodular, B is an integer vector iff $\lambda_i y_i$ ($i = 1 \cdots r$) are all integers, or $y_i = c_i/\lambda_i$, where $c_i = (L^{-1}B)_i \in \mathbb{Z}$. For the trivial and the nontrivial fragile [case (ii)] symmetry data vectors, both of which can be written as integer combinations of EBRs, $p \in \mathbb{Z}^{N_{\mathrm{EBR}}}$, the corresponding $y_i = (Rp)_i$ vector must be an integer. A fractional y, where $c_i \neq 0 \bmod \lambda_i$ for some i, corresponds to a symmetry data vector B in the nontrivial case (i). In fact, $c_i = (L^{-1}B)_i \bmod \lambda_i$ are the symmetry-based indicators [38,43,44] or, equivalently, the distinct EBR equivalence classes of Ref. [37]. In this article, we take the y vector to always be an integer and consider trivial and nontrivial fragile [case (ii)] symmetry data vectors B.

All the EFPs [nontrivial case (ii)] have trivial symmetry-based indicators. Instead, the EFPs are diagnosed by the fragile indices. We prove that all band structures with time-reversal symmetry and SOC have only two kinds of fragile indices: a $\mathbb{Z}_2$ type (modulo 2) and an inequality type (Appendix C). We give examples of both of these cases.

III. EXAMPLES OF FRAGILE INDICES

A. Example of $\mathbb{Z}_2$-type fragile indices

We consider SG 199 ($I2_13$). SG 199 has three EBRs, as shown in Fig. 2. Note that ebr_1 and ebr_3 split into disconnected branches. According to Ref. [37], in each of the split EBRs, at least one branch is topological. For example, the upper branch in ebr_1 is not an EBR and hence must be topological. Since it can be written as $\mathrm{ebr}_3 - \mathrm{ebr}_2$, it at least has a fragile topology.

Now, we apply a complete analysis on the EFPs in SG 199. Since there are only three EBRs, the EBR matrix has three columns. Arranging the irreps in the order $\bar{\Gamma}_5$, $\bar{\Gamma}_6\bar{\Gamma}_7$, $\bar{\mathrm{H}}_5$, $\bar{\mathrm{H}}_6\bar{\mathrm{H}}_7$, $\bar{\mathrm{P}}_4$, $\bar{\mathrm{P}}_5$, $\bar{\mathrm{P}}_6$, $\bar{\mathrm{P}}_7$, we can write the EBR matrix as

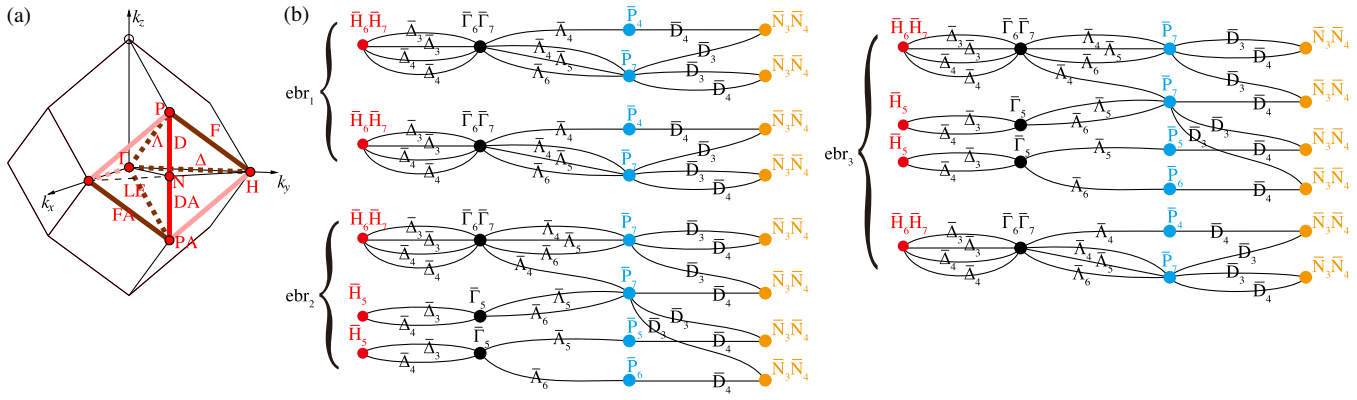

FIG. 2. (a) BZ of SG 199 ($I2_13$). (b) The EBRs of SG 199. The dots and lines represent high symmetry points and the high symmetry lines connecting the high symmetry points, respectively. The symbols of the irreps, e.g., $\Gamma_6\Gamma_7$, are defined on the REPRESENTATIONS DSG tool of the BCS [37,40,51].

$$\mathrm{EBR} = \begin{pmatrix} 0 & 2 & 2 \\ 2 & 1 & 2 \\ 0 & 2 & 2 \\ 2 & 1 & 2 \\ 2 & 0 & 1 \\ 0 & 1 & 1 \\ 0 & 1 & 1 \\ 2 & 2 & 3 \end{pmatrix}. \tag{4}$$

Here, we have omitted the N point because N has only one type of irrep. The Smith decomposition of the EBR $= L\Lambda R$ matrix is

$$\begin{pmatrix} 2 & 0 & 1 & 0 & 0 & 0 & 0 & 0 \\ -1 & 1 & 0 & 0 & 0 & 0 & 0 & 0 \\ 2 & 0 & 0 & 1 & 0 & 0 & 0 & 0 \\ -1 & 1 & 0 & 0 & 1 & 0 & 0 & 0 \\ -2 & 1 & 0 & 0 & 0 & 1 & 0 & 0 \\ 1 & 0 & 0 & 0 & 0 & 0 & 1 & 0 \\ 1 & 0 & 0 & 0 & 0 & 0 & 0 & 1 \\ 0 & 1 & 0 & 0 & 0 & 0 & 0 & 0 \end{pmatrix} \begin{pmatrix} 1 & 0 & 0 \\ 0 & 1 & 0 \\ 0 & 0 & 0 \\ 0 & 0 & 0 \\ 0 & 0 & 0 \\ 0 & 0 & 0 \\ 0 & 0 & 0 \\ 0 & 0 & 0 \end{pmatrix} \times \begin{pmatrix} 0 & 1 & 1 \\ 2 & 2 & 3 \\ -1 & -1 & -1 \end{pmatrix}. \tag{5}$$

The Λ matrix has only two nonzero elements, meaning $r = 2$, so the symmetry data are parametrized by a two-component integer vector $y = (y_1, y_2)^T$. From Eq. (3), the symmetry data vector is then given by

$$B = (2y_1, -y_1 + y_2, 2y_1, -y_1 + y_2, -2y_1 + y_2, y_1, y_1, y_2)^T. \tag{6}$$

To ensure $B \geq 0$, the y vector should satisfy $y_2 \geq 2y_1 \geq 0$. Therefore, the physical symmetry data vectors, i.e., B's, belong to the set of integer points $\bar{Y}$ in the 2D cone (open triangle), $Y = \{y \in \mathbb{R}^2 | y_2 \geq 2y_1 \geq 0\}$, defined as

$$\bar{Y} = \mathbb{Z}^2 \cap Y = \{y \in \mathbb{Z}^2 | y_2 \geq 2y_1 \geq 0\} \tag{7}$$

and shown in Fig. 3(a). The trivial symmetry data vectors can be written as sums of EBRs, i.e., $B = \mathrm{EBR} \cdot p$ for $p \in \mathbb{N}^{N_{\mathrm{EBR}}}$. They are represented by the y vectors belonging to

$$\bar{X} = \{y \in \mathbb{Z}^r | y_i = (Rp)_i p \in \mathbb{N}^{N_{\mathrm{EBR}}}\}. \tag{8}$$

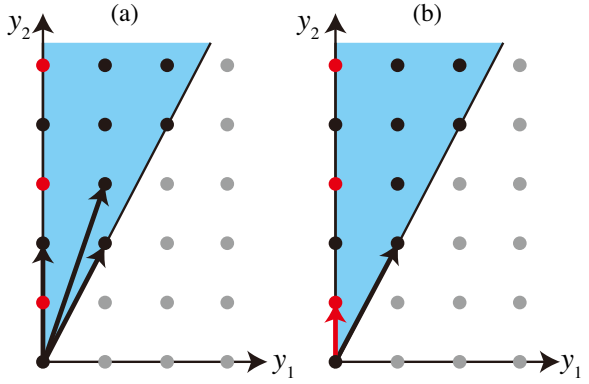

FIG. 3. (a) EFPs in SG 199 ($I2_13$). The shaded area represents the cone Y, the black points represent the trivial points in $\bar{Y}$, the red points represent the EFPs, and the grey points correspond to unphysical symmetry data. The three bold vectors $(0,2)^T$, $(1,2)^T$, $(1,3)^T$ are the generators of trivial points. (b) The Hilbert bases of $\bar{Y}$. The two bold vectors, i.e., $(0,1)^T$, $(1,2)^T$, generate all the points in $\bar{Y}$. Here, $(0,1)^T$ is nontrivial and corresponds to a fragile root, and $(1,2)^T$ is trivial and corresponds to an EBR.

In the case of Eq. (5), we can write the trivial points as

$$\bar{X} = \{p_1(0,2)^T + p_2(1,2)^T + p_3(1,3)^T | p_{1,2,3} \in \mathbb{N}\}, \quad (9)$$

i.e., the black points in Fig. 3(a), generated by non-negative p combinations of the three vectors $(0,2)^T$, $(1,2)^T$, $(1,3)^T$. One can find that $(0,2)^T$, $(1,2)^T$, $(1,3)^T$ correspond to the ebr_1, ebr_2, and ebr_3 shown in Fig. 2, respectively. We deduce that the nontrivial fragile symmetry data vectors, or the EFPs, are represented by the points in $\bar{Y} - \bar{X}$; these are the red points in Fig. 3(a).

We provide the explicit index for EFPs in SG 199. Consider the subset $y_1 = 0$ of $\bar{Y}$. Only one generator, i.e., $(0,2)^T$, satisfies this constraint. All the *trivial* points in the $y_1 = 0$ subset of $\bar{Y}$ are generated by it. The points $(0, 2p+1)^T$ ($p \in \mathbb{N}$) cannot be reached by non-negative combinations p of EBRs and are nontrivial (fragile). Thus, one fragile criterion of SG 199 is given by

$$y_1 = 0, \quad \text{and} \quad y_2 = 1 \mod 2, \quad (10)$$

where $y_2 \mod 2$ is the $\mathbb{Z}_2$ index and $y_1 = 0$ is the condition for the EFP to be diagnosable. Are there any other fragile indices (for other points in $\bar{Y}$)? For y_2 even (remembering $y_2 \geq 2y_1$), we can rewrite y as $y = y_1(1,2)^T + (\frac{1}{2}y_2 - y_1)(0,2)^T$ and reach all points in this subspace of $\bar{Y}$; for y_2 odd and $y_1 \geq 1$, Eq. (7) implies $y_2 \geq 2y_1 + 1$, and we can rewrite y as $y = (1,3)^T + (y_1 - 1)(1,2)^T + (\frac{1}{2}y_2 - \frac{1}{2} - y_1)(0,2)^T$ and reach all points in this subspace of $\bar{Y}$. In both cases, we find that the points are trivial. Hence, only y_2 odd and $y_1 = 0$ are fragile, and Eq. (10) is the only fragile index in SG 199. In Fig. 3, we present a diagrammatic illustration of the points in $\bar{Y}$ and points in $\bar{X}$, from which one immediately obtains Eq. (10). A (Hilbert) basis for all points in $\bar{Y}$ will be provided later.

B. Example of inequality-type fragile indices

We consider SG 70 ($Fddd$). The Smith decomposition of the EBR $= L\Lambda R$ matrix is

$$\begin{pmatrix} -2 & -1 & -1 & 0 & 1 \\ 2 & 3 & 1 & 0 & 0 \\ 0 & 1 & 0 & 0 & 1 \\ -1 & 2 & 0 & 0 & 0 \\ 1 & 0 & 0 & 1 & 0 \end{pmatrix} \begin{pmatrix} 1 & 0 & 0 & 0 & 0 \\ 0 & 1 & 0 & 0 & 0 \\ 0 & 0 & 4 & 0 & 0 \\ 0 & 0 & 0 & 0 & 0 \\ 0 & 0 & 0 & 0 & 0 \end{pmatrix} \times \begin{pmatrix} 1 & 1 & 3 & 3 & 1 \\ 1 & 2 & 2 & 2 & 2 \\ -1 & -2 & -2 & -3 & -1 \\ 0 & 0 & 0 & 0 & 1 \\ 0 & 0 & 1 & 0 & 0 \end{pmatrix}, \quad (11)$$

where the corresponding TRS and double-group irreps are $\bar{\Gamma}_5$, $\bar{\Gamma}_6$, $\bar{\Gamma}_3\bar{\Gamma}_4$, $\bar{L}_2\bar{L}_2$, $\bar{L}_3\bar{L}_3$, respectively. Irreps at the maximal k-vectors Y and Z (not shown) are determined by the irreps at Γ using TRS and compatibility relations (see Refs. [37–41,51]).

The Λ matrix has only three nonzero elements ($r = 3$), so the symmetry data are parametrized by a three-component integer vector $y = (y_1, y_2, y_3)^T$. By requiring the symmetry data vector $B \geq 0$, we obtain a set of inequalities for y defining a 3D cone

$$Y = \{y \in \mathbb{R}^3 | 2y_2 \geq y_1 \geq 0, -2y_1 - y_2 \geq 4y_3 \geq -2y_1 - 3y_2\}. \quad (12)$$

The physical symmetry data vectors B's are represented by integer points in Y, i.e., $\bar{Y} = \mathbb{Z}^3 \cap Y$. Each inequality in Eq. (12) specifies a plane in $\mathbb{R}^3$: The plane separates the points that do or do not satisfy the inequality. The cone Y is cut out by four such planes specified by the four inequalities in Eq. (12). As shown in Eq. (3a), these planes cross each other at four rays contained in this cone. We obtain the directions of the four rays as $\mathbf{r}_1 = (0,4,-1)^T$, $\mathbf{r}_2 = (0,4,-3)^T$, $\mathbf{r}_3 = (8,4,-7)^T$, $\mathbf{r}_4 = (8,4,-5)^T$. For example, the planes $y_1 = 0$ and $-2y_1 - y_2 = 4y_3$ intersect each other on the line $t \cdot \mathbf{r}_1$, $t \in \mathbb{R}$; the planes $y_1 = 0$ and $2y_2 = y_1$ intersect on the line $t \cdot (0,0,1)$, $t \in \mathbb{R}$, which (except for $t = 0$, a point that is already included in the other ray $t \cdot \mathbf{r}_1$) does not satisfy the second inequality in Eq. (12), and hence does not provide a separate ray.

The trivial points in Y (and $\bar{Y}$) are given by Eq. (8). For simplicity, we first consider points in the cone,

$$X = \{y \in \mathbb{R}^r | y_i = (Rp)_i p \in \mathbb{R}_+^{N_{\text{EBR}}}\}. \quad (13)$$

In the general case, $\mathbb{Z}^r \cap X$ is a superset of $\bar{X}$ (their difference being the noninteger $p > 0$, such that $y \in \mathbb{Z}^r$). Because of the definition of X, and since $r = 3$ in Eq. (13) for SG 70, it seems that (the first three rows of) each column of R corresponds to a generator of X. However, in Eq. (11), (the first three rows of) the first column of R, i.e., $(1,1,-1)^T$, can be spanned by the second and third columns as $\frac{1}{4}(1,2,-2)^T + \frac{1}{4}(3,2,-2)^T$; thus, X is generated by the last four columns of R. (There exists a linear dependence between the four vectors defined by the first three rows of each of the last four columns of R, but it involves negative coefficients; hence, the vectors are linearly independent in X.) As shown in Fig. 4(a), each of the four generators corresponds to a ray of X: $\mathbf{r}'_1 = (2,4,-2)^T$, $\mathbf{r}'_2 = (2,4,-4)^T$, $\mathbf{r}'_3 = (6,4,-6)^T$, $\mathbf{r}'_4 = (6,4,-4)^T$ [the rays are chosen as twice the generators for aesthetical purposes in Fig. 4(a)]. Using elementary vector algebra, as explained in Appendix B, one finds the inequalities defining X,

$$X = \{y \in \mathbb{R}^3 | 3y_2 \geq 2y_1 \geq y_2, -2y_1 - y_2 \geq 4y_3 \geq -2y_1 - 3y_2\}. \quad (14)$$

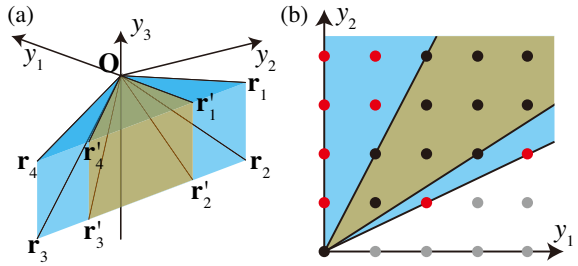

FIG. 4. (a) The cones Y and X for SG 70 ($Fddd$). The blue and yellow regions represent Y and X, respectively. The ray vectors for Y/X are $\mathbf{r}_{1,2,3,4}/\mathbf{r}'_{1,2,3,4}$, respectively, given in the main text. (b) The projections of Y and X in the y_1y_2 plane. The black points correspond to trivial symmetry data vectors B, the red points correspond to EFPs, and the grey points are unphysical.

Illustrated in Fig. 4(a), X is, as it should be, a subset of Y. The first (last) two defining inequalities of X are tighter than (identical to) the first (last) two of Y, respectively. For a point in Y to be outside the trivial X, at least one of the first two inequalities of X should be violated, i.e.,

$$2y_1 - 3y_2 > 0 \quad \text{or} \quad y_2 - 2y_1 > 0. \tag{15}$$

Equation (15) gives two inequality-type fragile indices for SG 70, which can also be obtained in a diagrammatic method. From Fig. 4(a), we see that the boundaries separating X and Y, i.e., $\mathbf{O}\mathbf{r}'_1\mathbf{r}'_2$ and $\mathbf{O}\mathbf{r}'_3\mathbf{r}'_4$, are parallel to the y_3 axis, where $\mathbf{O}$ stands for the origin. (Notice that all $\mathbf{r}_1 - \mathbf{r}_2, \mathbf{r}_3 - \mathbf{r}_4$, $\mathbf{r}'_1 - \mathbf{r}'_2, \mathbf{r}'_3 - \mathbf{r}'_4$ are parallel to y_3.) We project the cones to the y_1y_2 plane to obtain Fig. 4(b), from which we immediately obtain Eq. (15).

Since, in general, $\mathbb{Z}^r \cap X$ is a superset of $\bar{X}$, in principle, there can be nontrivial points in $\mathbb{Z}^r \cap X - \bar{X}$. For example, for SG 199, X [defined by Eq. (13)] is spanned by the rays $(0,1)^T$ and $(1,2)^T$ and is hence identical to Y [Fig. 4(a)]. Thus, Eq. (10) identifies points in $\mathbb{Z}^2 \cap X - \bar{X}$. However, for SG 70, there is no such point in $\mathbb{Z}^3 \cap X - \bar{X}$. We verify this case by explicitly listing the integer points in X and by applying a general technique that we introduce in Appendix C to calculate $\mathbb{Z}^r \cap X - \bar{X}$.

IV. POLYHEDRON METHOD

We have outlined the polyhedron method through the two previous examples. Now, we summarize its general principle.

A. Polyhedron description of symmetry data vectors

In Eq. (3), we parametrized the symmetry data as $B = \sum_j (L\Lambda)_j y_j$, where $(L\Lambda)_j$ represents the jth column of $(L\Lambda)$. Now, we define a polyhedral cone as

$$Y = \left\{ y \in \mathbb{R}^r | \sum_j (L\Lambda)_j y_j \geq 0 \right\}. \tag{16}$$

The physical symmetry data vectors $B \in \mathbb{N}$ are faithfully represented by integer points $\bar{Y} = \mathbb{Z}^r \cap Y$. Using Theorem 4 in Appendix F, Y can be represented by its rays and lines as

$$Y = \{\text{Ray} \cdot p + \text{Line} \cdot q | p \in \mathbb{R}^m_+, q \in \mathbb{R}^n\}, \tag{17}$$

where $\text{Ray} = (\text{Ray}_1, \text{Ray}_2, \cdots)$ is an $r \times m$ matrix and $\text{Line} = (\text{Line}_1, \text{Line}_2, \cdots)$ is an $r \times n$ matrix. The difference between rays and lines is that rays have directions but lines do not. Correspondingly, the coefficients on rays (p_i's) are non-negative, but the coefficients on lines (q_j's) can be either non-negative or negative. For example, in Fig. 3, Y has two rays, $(0,1)^T$ and $(1,2)^T$, but no lines. A polyhedral cone is called *pointed* if it does not contain lines. Now, we show that, for any space group, Y is a pointed polyhedral cone. Choosing $p = 0$ and arbitrary q, due to Eq. (16), we have $L\Lambda_{:,1:r}\text{Line} \cdot q \geq 0$, as well as $L\Lambda_{:,1:r}\text{Line} \cdot q \leq 0$ since we can replace q with $-q$, and thus $\forall\, q \in \mathbb{R}^n$, $L\Lambda_{:,1:r}\text{Line} \cdot q = 0$. As $L\Lambda_{:,1:r}$ is a rank-r matrix, there must be $\text{Line} = 0$. In this paper, Eq. (16) is called the H-representation of polyhedron, and Eq. (17) is called the V-representation. The algorithm to determine the V-representation from the H-representation and vice versa is available in many mathematics packages such as the sageMath package [75].

The trivial B vectors, which decompose into positive sums of EBRs, are given as $\bar{X}$ [Eq. (8)]. Note that $\bar{X}$ is a subset of $\bar{Y}$; thus, fragile symmetry data vectors are generated from points in $\bar{Y} - \bar{X}$. To classify them, we introduce an auxiliary polyhedral cone X [Eq. (13)], which can be thought of as an extension of $\bar{X}$ to allow non-negative real (not only integer) combination coefficients p_i. The nontrivial points can then be divided into two parts: $\bar{Y} - \mathbb{Z}^r \cap X$ and $\mathbb{Z}^r \cap X - \bar{X}$. Points in $\bar{Y} - \mathbb{Z}^r \cap X = \mathbb{Z}^r \cap (Y - X)$ correspond to symmetry data vectors B that cannot be written as non-negative combinations of the EBRs, even if the combination coefficients p_i are allowed to be rational numbers. Points in $\mathbb{Z}^r \cap X - \bar{X}$, on the other hand, correspond to symmetry data that can be written as non-negative rational combinations of EBRs but cannot be written as non-negative integer combinations of EBRs. (Refer to Appendix B 1 for more examples of X and Y.)

Points in $\mathbb{Z}^r \cap (Y - X)$ are outside X and therefore violate the inequalities of X. Thus, in general, points in $\mathbb{Z}^r \cap (Y - X)$ are diagnosed by the inequality-type indices, as in SG 70. On the other hand, points in $\mathbb{Z}^r \cap X - \bar{X}$ are always near the boundary of X and are diagnosed by the $\mathbb{Z}_2$-type indices. In the following, we discuss these two types of indices in detail.

B. Inequality-type fragile indices

Now, let us work out the inequality-type fragile criteria for $\mathbb{Z}^r \cap (Y - X)$. First, we assume the H-representation

of X as $X = \{y \in \mathbb{R}^r | Ay \geq 0, Bx = 0\}$, where $A \in \mathbb{Q}^{n\times r}$ $B \in \mathbb{Q}^{m\times r}$, r is the rank of EBR, and n, m are some positive integers. (See Theorem 4 for the general form of the H-representation.) Now, we show that B must be zero. Since the first r row of R has the rank r, X is an r-dimensional object. The presence of nonzero B implies constraints on the points in X and hence a lower dimension of X. Thus, B has to be zero, and the H-representation of X can always be written as

$$X = \{x \in \mathbb{R}^r | Ax \geq 0\}. \tag{18}$$

For a point y in $\mathbb{Z}^r \cap (Y - X)$, there should be some row in A, denoted as a, such that $ay < 0$, so $y \notin X$. Therefore, in principle, each row of A gives an inequality-type fragile index $-ay$, and $-ay > 0$ implies the fragile phase. One needs to check whether $ay < 0$ is allowed in Y: If it is not allowed, there is no need to introduce the corresponding fragile index. The method (with an example) to remove such unallowed criteria is given in Appendix C 1.

C. $\mathbb{Z}_2$-type fragile indices

As proved in Appendix C, points in $\mathbb{Z}^r \cap X - \bar{X}$ are always near the boundary of X—the distances from these points to the boundary are always 0 or 1—and thus belong to some lower-dimensional subpolyhedron of X. Integer sums [per Eq. (8)] of the generators of $\bar{X}$ belonging to this lower-dimensional subspace may not reach every integer point in this subspace. For example, in SG 199, all the points in $\mathbb{Z}^r \cap X - \bar{X}$ also belong to the subcone $\{y \in \mathbb{Z}^2 | y_1 = 0, y_2 \geq 0\}$. The only $\bar{X}$ generator in this subcone is $(0, 2)^T$. Thus, $(0, y_2)$ cannot be generated if y_2 is odd, and $\mathbb{Z}^r \cap X - \bar{X} = \{y \in \mathbb{Z}^2 | y_1 = 0, y_2 \geq 0, y_2 \bmod 2 = 1\}$. As detailed in Appendix C, points in $\mathbb{Z}^r \cap X - \bar{X}$ can always be characterized by the decomposition coefficients of the $\bar{X}$ generators that are restricted in some lower-dimensional subspace. If these coefficients are fractional, the corresponding symmetry data vectors B are nontrivial. Because of these fractional coefficients, in principle, such a diagnosis involves the modulo operation [see Eq. (10)]. We find that only the modulo 2 operation is involved [see Eq. (10)], and we call these indices $\mathbb{Z}_2$-type indices.

D. Fragile indices in all SGs

In Table I, we summarize the numbers of inequality-type and $\mathbb{Z}_2$-type indices in all SGs; in Table S2 of Ref. [74], we explicitly tabulate all the fragile indices.

The mathematics of EFPs is much richer than that of robust topology. The latter usually forms a group. For example, in the absence of TRS, according to the Chern number, the band insulators form an additive group $\mathbb{Z}$ [76–78]; in the presence of TRS (and without any other symmetries), according to the $\mathbb{Z}_2$ invariant, the band insulators form a $\mathbb{Z}_2$ group [1–3]. However, neither $\bar{Y}$ nor $\bar{X}$ form a group. Instead, $\bar{Y}$ and $\bar{X}$ are semigroups: A general element, except the identity, does not have an inverse. To be specific, both $\bar{Y}$ and $\bar{X}$ can be written as $M = \{r_1 p_1 + r_2 p_2 + \cdots r_n p_n | p_1 \cdots p_n \in \mathbb{N}\}$, for some n, and $r_1 p_1 + r_2 p_2 + \cdots r_n p_n = 0 \Rightarrow p = 0$, where r_i's are the generators that are no longer constrained to be the columns of R. (See Appendix B for the proof that $\bar{Y}$ can be written in this form.) For example, in SG 199, $\bar{Y}$ can be written as $\{p_1(0, 1)^T + p_2(1, 2)^T | p_{1,2} \in \mathbb{N}\}$ (see Fig. 3). Here, M is a positive affine monoid in mathematics, and we make use of monoid properties to obtain the EFP roots.

V. EFP ROOTS

We find that the EFPs and the trivial states are always generated by a finite set of generators. [$\bar{Y}$ in SG 199 is generated by $(0, 1)^T$ and $(1, 2)^T$; see Fig. 3(b)]. We call the nontrivial states in the generators of $\bar{Y}$ the EFP roots. (Trivial states in the generators of $\bar{Y}$ are EBRs.) By definition, an EFP can always be written as a sum of EFP roots plus some EBRs. Thus, the EFP roots can be thought of as the nonredundant representatives of the EFPs. We worked out all the EFP roots in all SGs in the presence of the TRS and the SOC, as tabulated in Table S3 of Ref. [74]. The numbers of EFP roots in all SGs are summarized in Table I. As discussed in Appendix B, as a positive affine monoid, $\bar{Y}$ is generated by the Hilbert bases: All of the elements $\bar{Y}$ can be written as a sum of Hilbert bases with positive coefficients, and none of the Hilbert bases can be written as a sum of other elements with positive coefficients. The Hilbert bases form a *unique* minimal set of generators of $\bar{Y}$. For a given SG, we first calculate the Hilbert bases and then identify the topological nontrivial ones as the EFP roots. There are two commonly used algorithms to get the Hilbert bases—the Normaliz algorithm [79] and the Hemmecke algorithm [80]. In this work, we mainly use the Hemmecke algorithm. In Table I, we tabulate the numbers of EBRs and EFP roots in the Hilbert bases in all SGs.

We now present some examples of the roots for two known fragile phases. First, we look at the SG 2 ($P\bar{1}$). Here, Γ, R, T, U, V, X, Y, and Z stand for the TRS momenta (0,0,0), (π, π, π), $(0, \pi, \pi)$, $(\pi, 0, \pi)$, $(\pi, \pi, 0)$, $(\pi, 0, 0)$, $(0, \pi, 0)$, and $(0, 0, \pi)$, respectively. We find 1136 EFP roots in SG 2 (Table I). (We finally find that, upon coordinate rotation and gauge transformation, only three fragile roots are independent. See Table S8 of the supplemental material of Ref. [73].) Two of the roots are given by

$$2\bar{\Gamma}_2\bar{\Gamma}_2 + 2\bar{\mathrm{R}}_3\bar{\mathrm{R}}_3 + 2\bar{\mathrm{T}}_3\bar{\mathrm{T}}_3 + 2\bar{\mathrm{U}}_3\bar{\mathrm{U}}_3 + 2\bar{\mathrm{V}}_3\bar{\mathrm{V}}_3 + 2\bar{\mathrm{X}}_3\bar{\mathrm{X}}_3 + 2\bar{\mathrm{Y}}_3\bar{\mathrm{Y}}_3 + 2\bar{\mathrm{Z}}_2\bar{\mathrm{Z}}_2 \tag{19}$$

and

TABLE I. Sizes of Hilbert bases and numbers of fragile indices in SGs with time-reversal symmetry and significant SOC. SGs that do not have fragile indices are not tabulated. Here, "r" represents the rank of the EBR matrix. The terms "ebr" and "root" represent the numbers of EBRs and fragile roots in the Hilbert bases of $\bar{Y}$, respectively, and, "ieq" and "$\mathbb{Z}_2$" represent the numbers of inequality-type indices and $\mathbb{Z}_2$-type indices, respectively.

		Basis		Index				Basis		Index				Basis		Index				Basis		Index	
r	SG	ebr	Root	ieq	$\mathbb{Z}_2$	r	SG	ebr	Root	ieq	$\mathbb{Z}_2$	r	SG	ebr	Root	ieq	$\mathbb{Z}_2$	r	SG	ebr	Root	ieq	$\mathbb{Z}_2$
2	199	1	1	0	1	4	218	2	6	6	0	6	69	10	52	24	0	8	148	8	140	24	0
	208	1	1	0	1		219	2	6	6	0		71	10	132	28	0		166	8	140	24	0
	210	1	1	0	1		220	5	5	4	4		85	10	16	24	0		193	9	975	30	24
	214	1	1	0	1	5	11	9	8	8	0		125	10	16	24	0		200	8	64	24	0
3	70	5	10	2	0		13	9	8	8	0		129	10	16	24	0		224	11	90	40	0
	150	2	2	1	3		14	8	8	8	0		132	10	92	24	0		226	11	334	28	0
	157	2	2	1	3		15	9	60	12	0		163	8	68	12	4		227	13	464	26	0
	159	4	2	1	1		49	9	8	8	0		165	6	40	12	12	9	2	16	1136	240	0
	173	4	2	1	1		51	9	8	8	0		190	9	51	10	0		10	16	1136	240	0
	182	4	2	1	1		53	8	8	8	0		201	10	8	12	0		47	16	1136	240	0
	185	2	2	1	3		55	8	8	8	0		203	10	84	16	0		87	14	1188	56	0
	186	4	2	1	1		58	8	8	8	0		205	8	6	2	0		139	14	1188	56	0
4	63	7	4	4	0		66	9	60	12	0		206	8	13	4	4		147	8	668	56	16
	64	6	4	4	0		67	9	8	8	0		215	5	16	16	0		162	8	668	56	16
	72	7	4	4	0		74	9	60	12	0		216	9	36	14	0		164	8	668	56	16
	121	6	4	4	0		81	8	8	8	0		222	7	22	12	0		176	12	3070	54	0
	126	6	8	4	0		82	8	8	8	0	7	12	12	224	56	0		192	11	723	30	24
	130	7	8	4	0		86	8	16	8	0		65	12	224	56	0		194	12	3070	54	0
	135	7	8	4	0		88	8	78	12	0		84	12	700	56	0	10	174	15	615	108	0
	137	6	8	4	0		111	8	8	8	0		128	11	128	12	0		187	15	615	108	0
	138	7	8	4	0		115	8	8	8	0		131	12	700	56	0	11	225	14	3208	34	0
	143	6	6	3	5		119	8	8	8	0		140	12	220	24	0		229	14	868	88	0
	149	6	6	3	5		134	8	16	8	0		188	12	102	18	28	13	83	20	58840	240	0
	156	6	6	3	5		136	8	44	12	0		189	10	49	20	0		123	20	58840	240	0
	158	6	6	3	5		141	8	78	12	0		202	8	48	12	0	14	175	17	72598	228	0
	168	3	3	2	3		167	6	10	4	0		204	8	24	16	0		191	17	72598	228	0
	177	3	3	2	3		217	3	8	8	0		223	4	57	28	16		221	20	51308	116	0
	183	3	3	2	3		228	5	7	8	4	8	124	14	252	24	0						
	184	3	3	2	3		230	5	19	4	4		127	12	328	24	0						

$$4\bar{\Gamma}_2\bar{\Gamma}_2 + 4\bar{R}_3\bar{R}_3 + 4\bar{T}_3\bar{T}_3 + 4\bar{U}_3\bar{U}_3 + 4\bar{V}_3\bar{V}_3 + 4\bar{X}_3\bar{X}_3 + 4\bar{Y}_3\bar{Y}_3 + 4\bar{Z}_3\bar{Z}_3. \quad (20)$$

The subscript 2 (3) means that the corresponding Kramer pair is odd (even) under inversion. Because of the Fu-Kane formula [81], Eq. (19) is the double of a centrosymmetric weak TI with the index $(0;001)$. In Ref. [82], it has been shown that the double of a 2D centrosymmetric TI remains nontrivial since its entanglement spectrum is gapless. Equation (19) can be thought of as a stacking of centrosymmetric double 2D TIs in the 001 direction. On the other hand, Eq. (20) is 4 times a 3D centrosymmetric TI. In Refs. [32,35,43,44], it was shown that the double of a 3D centrosymmetric TI is an inversion-protected topological crystalline insulator HOTI. Equation (20) shows that the double of a HOTI is a fragile phase.

Second, we look at SG 183 ($P6mm$)—the SG of graphene. As discussed in Refs. [55–58], in the presence of C_2T symmetry $[(C_2T)^2 = 1]$, a two-band system can host a fragile topology, and the topological invariant is given as the two-band Wilson loop winding. References [55–57] have made use of TQC and similar methods to analyze the fragile phases in graphene. We relate the analysis of Refs. [55,56] to our classification in which SG 183 has only three EFP roots: $\bar{\Gamma}_7 + \bar{K}_6 + \bar{M}_5$, $\bar{\Gamma}_8 + \bar{K}_4 + \bar{K}_5 + \bar{M}_5$, and $\bar{\Gamma}_9 + \bar{K}_4 + \bar{K}_5 + \bar{M}_5$. Here, Γ, K, and M stand for the high symmetry momenta (0,0,0), $[(2\pi/3), (2\pi/3), 0]$, and $(\pi, 0, 0)$, respectively. Because of compatibility relations, the irreps in the $k_z = \pi$ plane are completely determined by the irreps in the $k_z = 0$ plane. The irreps are defined in Table II. For the first root, the C_3 representation matrices at Γ and K can be written as $-\sigma_0$ and $e^{-i(\pi/3)\sigma_z}$, respectively. And, for the second and third roots, the C_3 representation matrices at Γ and K can be written as $e^{-i(\pi/3)\sigma_z}$ and $-\sigma_0$, respectively. Because of the correspondence between C_3 eigenvalues and Wilson loop winding in Refs. [55,56], one can find that the Wilson loop winding in all three cases is $3n \pm 1$ for n some integer, showing the topological nature of the state.

TABLE II. Character tables of irreps at high symmetry momenta in SG *P6mm* (with TRS). The little co-groups at Γ, K, and M are C_{6v}, C_{3v}, and C_{2v} respectively. Here, C_6, C_3, C_2 represent the sixfold, threefold, and twofold rotations, and σ_d and σ_v represent the two classes of mirrors.

	$\bar{\Gamma}_7$	$\bar{\Gamma}_8$	$\bar{\Gamma}_9$		$\bar{K}_4$	$\bar{K}_5$	$\bar{K}_6$		$\bar{M}_5$
E	2	2	2	E	1	1	2	E	2
$2C_6$	0	$-\sqrt{3}$	$\sqrt{3}$	$2C_3$	−1	−1	1	C_2	0
$2C_3$	−2	1	1	$3\sigma_v$	$-i$	i	0	σ_d	0
C_2	0	0	0					σ_v	0
$3\sigma_d$	0	0	0						
$3\sigma_v$	0	0	0						

VI. MATERIALS

Armed with our new complete classification, we set out to discover examples of topological bands in existing materials. This task is particularly challenging, as one recent catalogue of high-throughput topological materials [46] searched and found that no materials are topologically fragile at the Fermi level due to the fact that there are usually enough occupied EBR to turn any fragile set of bands into trivial ones. Hence, we have to settle for finding fragile sets of *bands* hopefully close to the Fermi level. We have performed thousands of *ab initio* calculations and have produced a list of 100 good materials that exhibit fragile topological bands close to the Fermi level (Table III). We showcase some of them in Fig. 5: $CsAu_3S_2$,

TABLE III. Fragile bands in materials. In the first three columns, we tabulate the chemical formulas, the space group numbers, and the ICSD numbers of the materials. The fourth column gives the number of fragile branches in the band structure of the corresponding material. In the fifth to tenth columns, the information of the fragile branch closest to the Fermi level is tabulated. The column "Bands" gives the band indices of the fragile branch. Here, we refer to the highest occupied band as the zeroth band and the lowest empty band as the first band, etc. The column "Irreps" gives the irreps formed by the fragile bands at high symmetry momenta. The column Δ_l (Δ_u) is the indirect gap between the fragile bands and the lower (upper) bands, and Δ'_l (Δ'_u) is the direct gap between the fragile bands and the lower (upper) bands.

Formula	SG	ICSD	NF	Bands	Irreps	Δ_l (eV)	Δ_u (eV)	Δ'_l (eV)	Δ'_u (eV)
$Cs(Au_3S_2)$	164	82540	2	−3–0	$\bar{A}_4\bar{A}_5+\bar{A}_8+\bar{\Gamma}_4\bar{\Gamma}_5+\bar{\Gamma}_8+\bar{H}_4\bar{H}_5+\bar{H}_6+\bar{K}_4\bar{K}_5+\bar{K}_6+2\bar{L}_5\bar{L}_6+2\bar{M}_5\bar{M}_6$	0.0946	1.7424	0.0946	1.7424
$RbNiF_3$	194	15090	3	−3–4	$\bar{A}_4\bar{A}_5+\bar{A}_6+2\bar{\Gamma}_{10}+\bar{\Gamma}_{11}+\bar{\Gamma}_{12}+2\bar{H}_8+2\bar{H}_9+2\bar{K}_8+2\bar{K}_9+2\bar{L}_3\bar{L}_4+4\bar{M}_6$	0.1416	0.0121	0.2149	0.0336
$Rb_6Ni_6F_{18}$	194	410391	1	−3–4	$\bar{A}_4\bar{A}_5+\bar{A}_6+2\bar{\Gamma}_{10}+\bar{\Gamma}_{11}+\bar{\Gamma}_{12}+2\bar{H}_8+2\bar{H}_9+2\bar{K}_8+2\bar{K}_9+2\bar{L}_3\bar{L}_4+4\bar{M}_6$	0.1561	0.012	0.2329	0.0121
$Bi_2(Ru_2O_7)$	227	166566	2	−15–0	$\bar{\Gamma}_6+\bar{\Gamma}_7+3\bar{\Gamma}_{10}+4\bar{X}_5+3\bar{L}_6\bar{L}_7+5\bar{L}_9+2\bar{W}_3\bar{W}_4+2\bar{W}_5\bar{W}_6+4\bar{W}_7$	0.5048	0.0065	0.771	0.0865
Bi_2O_3	164	186365	1	1–2	$\bar{A}_8+\bar{\Gamma}_8+\bar{H}_4\bar{H}_5+\bar{K}_4\bar{K}_5+\bar{L}_3\bar{L}_4+\bar{M}_3\bar{M}_4$	0.4934	0.0	1.1165	0.2286
Pb_4Se_4	225	238502	1	−3–0	$\bar{\Gamma}_{11}+\bar{X}_8+\bar{X}_9+\bar{L}_4\bar{L}_5+\bar{L}_9+2\bar{W}_7$	0.0	0.3062	0.2209	0.3085
PbSe	225	248492	1	−3–0	$\bar{\Gamma}_{11}+\bar{X}_8+\bar{X}_9+\bar{L}_4\bar{L}_5+\bar{L}_9+2\bar{W}_7$	0.0	0.224	0.2056	0.224
PbSe	225	62195	1	−3–0	$\bar{\Gamma}_{11}+\bar{X}_8+\bar{X}_9+\bar{L}_6\bar{L}_7+\bar{L}_8+2\bar{W}_6$	0.0	0.1305	0.212	0.1305
$BiScO_3$	221	181115	1	−15–0	$\bar{\Gamma}_8+\bar{\Gamma}_9+3\bar{\Gamma}_{11}+2\bar{R}_9+3\bar{R}_{11}+3\bar{M}_6+3\bar{M}_7+2\bar{M}_8+3\bar{X}_6+3\bar{X}_7+\bar{X}_8+\bar{X}_9$	0.0	0.6693	0.1211	0.8368
Ge	227	44841	1	−3–4	$\bar{\Gamma}_8+\bar{\Gamma}_9+\bar{\Gamma}_{10}+2\bar{X}_5+\bar{L}_4\bar{L}_5+\bar{L}_8+2\bar{L}_9+\bar{W}_3\bar{W}_4+\bar{W}_5\bar{W}_6+2\bar{W}_7$	0.0	0.0	0.2548	0.0874
$MgCl_2$	166	26157	1	−3–0	$\bar{\Gamma}_6\bar{\Gamma}_7+\bar{\Gamma}_9+\bar{T}_6\bar{T}_7+\bar{T}_9+2\bar{F}_3\bar{F}_4+2\bar{L}_3\bar{L}_4$	0.0	5.9915	0.085	6.1919
LiCdAs	216	609966	2	−1–2	$\bar{\Gamma}_8+2\bar{X}_7+\bar{L}_4\bar{L}_5+\bar{L}_6+2\bar{W}_6+\bar{W}_7+\bar{W}_8$	0.0	0.0	0.1502	0.0849
$Bi_2(Ru_2O_7)$	227	161102	2	−15–0	$\bar{\Gamma}_6+\bar{\Gamma}_7+3\bar{\Gamma}_{10}+4\bar{X}_5+3\bar{L}_4\bar{L}_5+5\bar{L}_8+2\bar{W}_3\bar{W}_4+2\bar{W}_5\bar{W}_6+4\bar{W}_7$	0.5238	0.0	0.7923	0.0842
PbTe	225	648615	1	−3–0	$\bar{\Gamma}_{11}+\bar{X}_8+\bar{X}_9+\bar{L}_4\bar{L}_5+\bar{L}_9+2\bar{W}_7$	0.0	0.2613	0.0836	0.3544
$Bi(ScO_3)$	221	158759	1	−15–0	$\bar{\Gamma}_8+\bar{\Gamma}_9+3\bar{\Gamma}_{11}+2\bar{R}_6+3\bar{R}_{10}+3\bar{M}_6+3\bar{M}_7+2\bar{M}_9+\bar{X}_6+\bar{X}_7+3\bar{X}_8+3\bar{X}_9$	0.0	0.422	0.0765	0.6957
$AlSiTe_3$	147	75001	4	−1–0	$\bar{A}_7\bar{A}_7+\bar{\Gamma}_4\bar{\Gamma}_4+\bar{H}_5\bar{H}_6+\bar{K}_5\bar{K}_6+\bar{L}_2\bar{L}_2+\bar{M}_3\bar{M}_3$	0.0	0.6883	0.0669	0.8923
CuIn	194	180112	1	1–8	$\bar{A}_4\bar{A}_5+\bar{A}_6+\bar{\Gamma}_7+\bar{\Gamma}_8+\bar{\Gamma}_9+\bar{\Gamma}_{10}+2\bar{H}_6\bar{H}_7+2\bar{H}_8+2\bar{K}_7+\bar{K}_8+\bar{K}_9+2\bar{L}_3\bar{L}_4+3\bar{M}_5+\bar{M}_6$	0.0	0.0	0.131	0.0669
PtO_2	164	24922	4	1–2	$\bar{A}_4\bar{A}_5+\bar{\Gamma}_4\bar{\Gamma}_5+\bar{H}_6+\bar{K}_6+\bar{L}_3\bar{L}_4+\bar{M}_3\bar{M}_4$	1.5328	0.0	1.757	0.0619
$Hf_3Al_3C_5$	194	161587	3	−1–6	$\bar{A}_4\bar{A}_5+\bar{A}_6+2\bar{\Gamma}_7+\bar{\Gamma}_8+\bar{\Gamma}_9+\bar{H}_4\bar{H}_5+\bar{H}_6\bar{H}_7+\bar{H}_8+\bar{H}_9+2\bar{K}_7+\bar{K}_8+\bar{K}_9+2\bar{L}_3\bar{L}_4+4\bar{M}_6$	0.0	0.0	0.0594	0.1486

(Table continued)

TABLE III. *(Continued)*

Formula	SG	ICSD	NF	Bands	Irreps	Δ_l (eV)	Δ_u (eV)	Δ'_l (eV)	Δ'_u (eV)
$SrAl_2Si_2$	164	419886	3	−3–0	$\bar{A}_4\bar{A}_5+\bar{A}_8+\bar{\Gamma}_6\bar{\Gamma}_7+\bar{\Gamma}_9+\bar{H}_4\bar{H}_5+\bar{H}_6+\bar{K}_4\bar{K}_5+\bar{K}_6+2\bar{L}_5\bar{L}_6+2\bar{M}_3\bar{M}_4$	0.0	0.0	0.0559	0.3243
SnAs	225	611424	1	−2–1	$\bar{\Gamma}_{11}+\bar{X}_8+\bar{X}_9+\bar{L}_6\bar{L}_7+\bar{L}_8+2\bar{W}_6$	0.0	0.0	0.0518	0.1985
$Bi_2(Os_2O_7)$	227	161105	1	−15–0	$\bar{\Gamma}_6+\bar{\Gamma}_7+3\bar{\Gamma}_{10}+4\bar{X}_5+3\bar{L}_4\bar{L}_5+5\bar{L}_8+2\bar{W}_3\bar{W}_4+2\bar{W}_5\bar{W}_6+4\bar{W}_7$	0.8702	0.0	0.9833	0.0512
$BaZr(PO_4)_2$	164	173842	9	1–2	$\bar{A}_9+\bar{\Gamma}_8+\bar{H}_4\bar{H}_5+\bar{K}_4\bar{K}_5+\bar{L}_5\bar{L}_6+\bar{M}_3\bar{M}_4$	3.905	0.0	3.9474	0.0502
SnS	225	52107	1	−3–0	$\bar{\Gamma}_{11}+\bar{X}_8+\bar{X}_9+\bar{L}_6\bar{L}_7+\bar{L}_8+2\bar{W}_6$	0.0	0.1121	0.0484	0.1328
NbSbSi	129	646436	1	−5–2	$2\bar{A}_5+\bar{\Gamma}_8+3\bar{\Gamma}_9+2\bar{M}_5+\bar{Z}_8+3\bar{Z}_9+2\bar{R}_3\bar{R}_4+2\bar{X}_3\bar{X}_4$	0.0	0.0	0.0465	0.0639
$Na_2BaMgP_2O_8$	147	262716	10	1–2	$\bar{A}_8\bar{A}_9+\bar{\Gamma}_5\bar{\Gamma}_6+\bar{H}_4\bar{H}_4+\bar{K}_4\bar{K}_4+\bar{L}_2\bar{L}_2+\bar{M}_3\bar{M}_3$	5.2768	0.0	5.312	0.0458
BiTeI	156	79364	5	−1–0	$\bar{A}_4\bar{A}_5+\bar{\Gamma}_4\bar{\Gamma}_5+\bar{H}_5+\bar{H}_6+\bar{K}_5+\bar{K}_6+\bar{L}_3\bar{L}_4+\bar{M}_3\bar{M}_4$	0.0	0.0447	0.0879	0.0447
$Zr(MoO_4)_2$	164	59999	10	1–2	$\bar{A}_4\bar{A}_5+\bar{\Gamma}_4\bar{\Gamma}_5+\bar{H}_6+\bar{K}_6+\bar{L}_3\bar{L}_4+\bar{M}_3\bar{M}_4$	3.1215	0.0	3.135	0.0431
$MoGe_2$	139	76139	1	−3–2	$2\bar{\Gamma}_6+\bar{\Gamma}_9+\bar{M}_6+\bar{M}_7+\bar{M}_8+2\bar{P}_6+\bar{P}_7+2\bar{X}_5+\bar{X}_6+3\bar{N}_3\bar{N}_4$	0.0	0.0	0.0389	0.0832
$PbMg_2$	225	151361	1	−1–6	$\bar{\Gamma}_{10}+\bar{\Gamma}_{11}+\bar{X}_6+\bar{X}_7+\bar{X}_8+\bar{X}_9+\bar{L}_4\bar{L}_5+\bar{L}_6\bar{L}_7+2\bar{L}_8+3\bar{W}_6+\bar{W}_7$	0.0	0.0	0.1356	0.0338
$Ni(OH)_2$	164	28101	4	−1–0	$\bar{A}_4\bar{A}_5+\bar{\Gamma}_4\bar{\Gamma}_5+\bar{H}_6+\bar{K}_6+\bar{L}_3\bar{L}_4+\bar{M}_3\bar{M}_4$	0.4417	0.0	0.494	0.0336
$KSc(MoO_4)_2$	164	28019	7	1–2	$\bar{A}_4\bar{A}_5+\bar{\Gamma}_4\bar{\Gamma}_5+\bar{H}_6+\bar{K}_6+\bar{L}_3\bar{L}_4+\bar{M}_3\bar{M}_4$	2.9384	0.0	2.9384	0.0331
PbS	225	250762	1	−3–0	$\bar{\Gamma}_{11}+\bar{X}_8+\bar{X}_9+\bar{L}_4\bar{L}_5+\bar{L}_9+2\bar{W}_7$	0.0	0.1131	0.0328	0.1131
$SrSi_2Al_2$	164	609338	3	−3–0	$\bar{A}_4\bar{A}_5+\bar{A}_8+\bar{\Gamma}_6\bar{\Gamma}_7+\bar{\Gamma}_9+\bar{H}_4\bar{H}_5+\bar{H}_6+\bar{K}_4\bar{K}_5+\bar{K}_6+2\bar{L}_5\bar{L}_6+2\bar{M}_3\bar{M}_4$	0.0	0.0	0.0327	0.3753
PtB	194	615210	1	−1–10	$\bar{A}_4\bar{A}_5+2\bar{A}_6+\bar{\Gamma}_7+\bar{\Gamma}_8+\bar{\Gamma}_{10}+\bar{\Gamma}_{11}+2\bar{\Gamma}_{12}+\bar{H}_4\bar{H}_5+2\bar{H}_6\bar{H}_7+2\bar{H}_8+\bar{H}_9+3\bar{K}_7+\bar{K}_8+2\bar{K}_9+3\bar{L}_3\bar{L}_4+6\bar{M}_5$	0.0	0.0	0.0321	0.2012
CaGaGeH	156	173567	1	−1–0	$\bar{A}_4\bar{A}_5+\bar{\Gamma}_4\bar{\Gamma}_5+\bar{H}_4+\bar{H}_6+\bar{K}_4+\bar{K}_6+\bar{L}_3\bar{L}_4+\bar{M}_3\bar{M}_4$	0.0	0.4363	0.0314	0.7898
$MgCl_2$	164	17063	2	−3–0	$\bar{A}_6\bar{A}_7+\bar{A}_9+\bar{\Gamma}_6\bar{\Gamma}_7+\bar{\Gamma}_9+\bar{H}_4\bar{H}_5+\bar{H}_6+\bar{K}_4\bar{K}_5+\bar{K}_6+2\bar{L}_3\bar{L}_4+2\bar{M}_3\bar{M}_4$	0.0	5.5186	0.0299	5.5186
$Mg_2Al_2Se_5$	164	41928	7	−1–0	$\bar{A}_4\bar{A}_5+\bar{\Gamma}_6\bar{\Gamma}_7+\bar{H}_6+\bar{K}_6+\bar{L}_3\bar{L}_4+\bar{M}_5\bar{M}_6$	0.0	0.7281	0.0292	0.7281
$K_3V(VO_4)_2$	164	100782	7	−1–0	$\bar{A}_6\bar{A}_7+\bar{\Gamma}_4\bar{\Gamma}_5+\bar{H}_6+\bar{K}_6+\bar{L}_5\bar{L}_6+\bar{M}_3\bar{M}_4$	2.1516	0.0	2.1663	0.0289
PtS_2	164	41375	4	1–2	$\bar{A}_4\bar{A}_5+\bar{\Gamma}_4\bar{\Gamma}_5+\bar{H}_6+\bar{K}_6+\bar{L}_3\bar{L}_4+\bar{M}_3\bar{M}_4$	0.4445	0.0	1.1335	0.0278
PbS	225	62190	1	−3–0	$\bar{\Gamma}_{11}+\bar{X}_8+\bar{X}_9+\bar{L}_6\bar{L}_7+\bar{L}_8+2\bar{W}_6$	0.0	0.0277	0.0338	0.0277
$Cd(OH)_2$	164	165225	4	−1–0	$\bar{A}_8+\bar{\Gamma}_8+\bar{H}_4\bar{H}_5+\bar{K}_4\bar{K}_5+\bar{L}_3\bar{L}_4+\bar{M}_3\bar{M}_4$	0.0	1.747	0.0262	1.9915
Mg_2Pb	225	642745	1	−1–6	$\bar{\Gamma}_{10}+\bar{\Gamma}_{11}+\bar{X}_6+\bar{X}_7+\bar{X}_8+\bar{X}_9+\bar{L}_4\bar{L}_5+\bar{L}_6\bar{L}_7+2\bar{L}_8+3\bar{W}_6+\bar{W}_7$	0.0	0.0	0.2433	0.0259
$K(Ag(CN)_2)$	163	30275	2	−3–0	$\bar{A}_4\bar{A}_4+\bar{\Gamma}_4\bar{\Gamma}_5+\bar{\Gamma}_6\bar{\Gamma}_7+\bar{H}_4\bar{H}_5+\bar{H}_6+\bar{K}_4\bar{K}_5+\bar{K}_6+\bar{L}_2\bar{L}_2+\bar{M}_3\bar{M}_4+\bar{M}_5\bar{M}_6$	0.0	3.1161	0.0251	3.1161
SnP	225	77786	1	−2–1	$\bar{\Gamma}_{11}+\bar{X}_8+\bar{X}_9+\bar{L}_6\bar{L}_7+\bar{L}_8+2\bar{W}_6$	0.0	0.0	0.0251	0.2046
$Mg_2O(OH)_2$	164	95472	1	−1–0	$\bar{A}_6\bar{A}_7+\bar{\Gamma}_6\bar{\Gamma}_7+\bar{H}_6+\bar{K}_6+\bar{L}_5\bar{L}_6+\bar{M}_5\bar{M}_6$	0.0	3.6627	0.0242	3.6627
Cu_4O_3	141	100566	1	−7–0	$2\bar{\Gamma}_6+2\bar{\Gamma}_7+2\bar{M}_5+2\bar{P}_3\bar{P}_6+2\bar{P}_7+2\bar{X}_3\bar{X}_4+\bar{N}_3\bar{N}_4+3\bar{N}_5\bar{N}_6$	0.0	0.0	0.0466	0.0242
$BaSr_2Mg(SiO_4)_2$	164	247861	4	1–2	$\bar{A}_9+\bar{\Gamma}_8+\bar{H}_4\bar{H}_5+\bar{K}_4\bar{K}_5+\bar{L}_5\bar{L}_6+\bar{M}_3\bar{M}_4$	5.0528	0.0	5.1228	0.0236
CuI	156	84217	5	−1–0	$\bar{A}_4\bar{A}_5+\bar{\Gamma}_4\bar{\Gamma}_5+\bar{H}_4+\bar{H}_5+\bar{K}_4+\bar{K}_5+\bar{L}_3\bar{L}_4+\bar{M}_3\bar{M}_4$	0.0	1.367	0.0234	1.367
Ag_2O	164	20368	5	−1–0	$\bar{A}_6\bar{A}_7+\bar{\Gamma}_6\bar{\Gamma}_7+\bar{H}_6+\bar{K}_6+\bar{L}_5\bar{L}_6+\bar{M}_5\bar{M}_6$	0.0	0.0	0.0542	0.0233
Nb_3Au_2	139	54403	1	0–3	$\bar{\Gamma}_6+\bar{\Gamma}_9+\bar{M}_7+\bar{M}_8+2\bar{P}_7+\bar{X}_5+\bar{X}_6+2\bar{N}_5\bar{N}_6$	0.0	0.0	0.0212	0.0369
W_2Zr	227	653435	1	−15–4	$\bar{\Gamma}_7+\bar{\Gamma}_8+2\bar{\Gamma}_{10}+2\bar{\Gamma}_{11}+5\bar{X}_5+\bar{L}_4\bar{L}_5+3\bar{L}_6\bar{L}_7+2\bar{L}_8+4\bar{L}_9+3\bar{W}_3\bar{W}_4+2\bar{W}_5\bar{W}_6+5\bar{W}_7$	0.0	0.0	0.021	0.0702

(Table continued)

TABLE III. *(Continued)*

Formula	SG	ICSD	NF	Bands	Irreps	Δ_l (eV)	Δ_u (eV)	Δ'_l (eV)	Δ'_u (eV)
ZrW_2	227	151401	1	−15–4	$\bar{\Gamma}_7+\bar{\Gamma}_8+2\bar{\Gamma}_{10}+2\bar{\Gamma}_{11}+5\bar{X}_5+\bar{L}_4\bar{L}_5+3\bar{L}_6\bar{L}_7+2\bar{L}_8+4\bar{L}_9+3\bar{W}_3\bar{W}_4+2\bar{W}_5\bar{W}_6+5\bar{W}_7$	0.0	0.0	0.021	0.0702
$MgSiN_2$	166	186509	1	−3–0	$\bar{\Gamma}_6\bar{\Gamma}_7+\bar{\Gamma}_9+\bar{T}_4\bar{T}_5+\bar{T}_8+2\bar{F}_3\bar{F}_4+2\bar{L}_5\bar{L}_6$	0.0	4.2025	0.0206	5.0508
$Ba(Ag_2S_2)$	164	50183	5	1–2	$\bar{A}_8+\bar{\Gamma}_8+\bar{H}_4\bar{H}_5+\bar{K}_4\bar{K}_5+\bar{L}_3\bar{L}_4+\bar{M}_3\bar{M}_4$	0.9298	0.0	0.9298	0.0201
In_2Se_3	164	602266	5	1–2	$\bar{A}_8+\bar{\Gamma}_8+\bar{H}_4\bar{H}_5+\bar{K}_4\bar{K}_5+\bar{L}_3\bar{L}_4+\bar{M}_3\bar{M}_4$	0.0	0.0	0.4934	0.0199
PbTe	225	153711	1	−3–0	$\bar{\Gamma}_{11}+\bar{X}_8+\bar{X}_9+\bar{L}_6\bar{L}_7+\bar{L}_8+2\bar{W}_6$	0.0	0.0199	0.0597	0.0199
$RbYTe_2$	194	419996	3	−3–0	$\bar{A}_4\bar{A}_5+2\bar{\Gamma}_{10}+\bar{H}_8+\bar{H}_9+\bar{K}_8+\bar{K}_9+\bar{L}_3\bar{L}_4+2\bar{M}_6$	0.0	0.9207	0.0196	1.604
W_2Zr	227	106218	1	−15–4	$\bar{\Gamma}_7+\bar{\Gamma}_8+2\bar{\Gamma}_{10}+2\bar{\Gamma}_{11}+5\bar{X}_5+3\bar{L}_4\bar{L}_5+\bar{L}_6\bar{L}_7+4\bar{L}_8+2\bar{L}_9+2\bar{W}_3\bar{W}_4+3\bar{W}_5\bar{W}_6+5\bar{W}_7$	0.0	0.0	0.0191	0.0676
Li_2CuSn_2	141	426084	1	−1–6	$2\bar{\Gamma}_6+2\bar{\Gamma}_7+2\bar{M}_5+2\bar{P}_3\bar{P}_6+2\bar{P}_7+2\bar{X}_3\bar{X}_4+\bar{N}_3\bar{N}_4+3\bar{N}_5\bar{N}_6$	0.0	0.0	0.0182	0.0336
BaGaGeH	156	246820	1	−1–0	$\bar{A}_4\bar{A}_5+\bar{\Gamma}_4\bar{\Gamma}_5+\bar{H}_4+\bar{H}_5+\bar{K}_4+\bar{K}_5+\bar{L}_3\bar{L}_4+\bar{M}_3\bar{M}_4$	0.0	0.0179	0.0335	0.0179
$Ni_3Sn_2S_2$	166	646379	1	1–4	$\bar{\Gamma}_4\bar{\Gamma}_5+\bar{\Gamma}_8+\bar{T}_4\bar{T}_5+\bar{T}_8+2\bar{F}_5\bar{F}_6+2\bar{L}_5\bar{L}_6$	0.0	0.0	0.0175	0.0501
$CaBe_2P_2$	164	616191	1	−3–0	$\bar{A}_4\bar{A}_5+\bar{A}_8+\bar{\Gamma}_6\bar{\Gamma}_7+\bar{\Gamma}_9+\bar{H}_4\bar{H}_5+\bar{H}_6+\bar{K}_4\bar{K}_5+\bar{K}_6+2\bar{L}_5\bar{L}_6+2\bar{M}_3\bar{M}_4$	0.0	0.8824	0.0171	1.5635
$Ni_3Sn_2S_2$	166	402458	1	1–4	$\bar{\Gamma}_4\bar{\Gamma}_5+\bar{\Gamma}_8+\bar{T}_6\bar{T}_7+\bar{T}_9+2\bar{F}_5\bar{F}_6+2\bar{L}_3\bar{L}_4$	0.0	0.0	0.017	0.0496
Li_2NiO_2	164	71421	3	−1–0	$\bar{A}_4\bar{A}_5+\bar{\Gamma}_4\bar{\Gamma}_5+\bar{H}_6+\bar{K}_6+\bar{L}_3\bar{L}_4+\bar{M}_3\bar{M}_4$	0.5262	0.0	0.5298	0.0169
BaGaGeH	156	173573	1	−1–0	$\bar{A}_4\bar{A}_5+\bar{\Gamma}_4\bar{\Gamma}_5+\bar{H}_4+\bar{H}_6+\bar{K}_4+\bar{K}_6+\bar{L}_3\bar{L}_4+\bar{M}_3\bar{M}_4$	0.0	0.0186	0.0167	0.0186
Au_2Nb_3	139	58559	1	0–3	$\bar{\Gamma}_6+\bar{\Gamma}_9+\bar{M}_7+\bar{M}_8+2\bar{P}_7+\bar{X}_5+\bar{X}_6+2\bar{N}_5\bar{N}_6$	0.0	0.0	0.0152	0.0275
$BaSr(Fe_4O_8)$	162	1838	10	1–2	$\bar{A}_6\bar{A}_7+\bar{\Gamma}_6\bar{\Gamma}_7+\bar{H}_6+\bar{K}_6+\bar{L}_5\bar{L}_6+\bar{M}_5\bar{M}_6$	0.0	0.0	0.0152	0.0534
$CaAl_2Si_2$	164	20278	2	−3–0	$\bar{A}_4\bar{A}_5+\bar{A}_8+\bar{\Gamma}_6\bar{\Gamma}_7+\bar{\Gamma}_9+\bar{H}_4\bar{H}_5+\bar{H}_6+\bar{K}_4\bar{K}_5+\bar{K}_6+2\bar{L}_5\bar{L}_6+2\bar{M}_3\bar{M}_4$	0.0	0.0	0.0126	0.5233
Cr_2Ta	227	626854	1	−9–2	$\bar{\Gamma}_7+\bar{\Gamma}_8+\bar{\Gamma}_{10}+\bar{\Gamma}_{11}+3\bar{X}_5+2\bar{L}_4\bar{L}_5+3\bar{L}_8+\bar{L}_9+\bar{W}_3\bar{W}_4+2\bar{W}_5\bar{W}_6+3\bar{W}_7$	0.0	0.0	0.0125	0.0857
$CdTlTe_2$	164	620548	3	−4–1	$\bar{A}_4\bar{A}_5+\bar{A}_6\bar{A}_7+\bar{A}_9+\bar{\Gamma}_4\bar{\Gamma}_5+\bar{\Gamma}_6\bar{\Gamma}_7+\bar{\Gamma}_8+\bar{H}_4\bar{H}_5+2\bar{H}_6+\bar{K}_4\bar{K}_5+2\bar{K}_6+\bar{L}_3\bar{L}_4+2\bar{L}_5\bar{L}_6+2\bar{M}_3\bar{M}_4+\bar{M}_5\bar{M}_6$	0.0	0.0	0.0123	0.9159
$Ba(Sb_2O_6)$	162	74541	5	−1–0	$\bar{A}_6\bar{A}_7+\bar{\Gamma}_6\bar{\Gamma}_7+\bar{H}_6+\bar{K}_6+\bar{L}_5\bar{L}_6+\bar{M}_5\bar{M}_6$	0.0	3.3497	0.0119	3.4314
$Ca(Al_{12}Si_4O_{27})$	147	91233	6	1–2	$\bar{A}_5\bar{A}_6+\bar{\Gamma}_5\bar{\Gamma}_6+\bar{H}_4\bar{H}_4+\bar{K}_4\bar{K}_4+\bar{L}_3\bar{L}_3+\bar{M}_3\bar{M}_3$	5.4299	0.0	5.5036	0.0119
Au_3In_2	164	612019	2	0–1	$\bar{A}_9+\bar{\Gamma}_8+\bar{H}_4\bar{H}_5+\bar{K}_4\bar{K}_5+\bar{L}_5\bar{L}_6+\bar{M}_3\bar{M}_4$	0.0	0.0	0.0116	0.1515
$Tl(Mo_6O_{17})$	164	62699	9	0–1	$\bar{A}_8+\bar{\Gamma}_8+\bar{H}_4\bar{H}_5+\bar{K}_4\bar{K}_5+\bar{L}_3\bar{L}_4+\bar{M}_3\bar{M}_4$	0.0	0.0	0.0188	0.0115
$NbSe_2$	164	76576	6	0–1	$\bar{A}_4\bar{A}_5+\bar{\Gamma}_4\bar{\Gamma}_5+\bar{H}_6+\bar{K}_6+\bar{L}_3\bar{L}_4+\bar{M}_3\bar{M}_4$	0.0	0.0	0.011	0.0667
$CdLi_2Ge$	225	52803	2	−1–2	$\bar{\Gamma}_{11}+\bar{X}_8+\bar{X}_9+\bar{L}_6\bar{L}_7+\bar{L}_8+2\bar{W}_6$	0.0	0.0	0.0109	0.1314
$Sr(As_2O_6)$	162	420296	3	−1–0	$\bar{A}_6\bar{A}_7+\bar{\Gamma}_4\bar{\Gamma}_5+\bar{H}_6+\bar{K}_6+\bar{L}_5\bar{L}_6+\bar{M}_3\bar{M}_4$	0.0	3.9384	0.0106	4.2275
$Mg(Cr_2O_4)$	227	167459	1	−7–0	$\bar{\Gamma}_6+\bar{\Gamma}_7+\bar{\Gamma}_{10}+2\bar{X}_5+\bar{L}_6\bar{L}_7+\bar{L}_8+2\bar{L}_9+2\bar{W}_5\bar{W}_6+2\bar{W}_7$	0.0	0.0	0.0132	0.0101
YRe_2	194	150517	1	−15–0	$2\bar{A}_4\bar{A}_5+2\bar{A}_6+2\bar{\Gamma}_7+\bar{\Gamma}_8+2\bar{\Gamma}_{10}+\bar{\Gamma}_{11}+2\bar{\Gamma}_{12}+2\bar{H}_6\bar{H}_7+4\bar{H}_8+2\bar{H}_9+2\bar{K}_7+4\bar{K}_8+2\bar{K}_9+4\bar{L}_3\bar{L}_4+3\bar{M}_5+5\bar{M}_6$	0.0	0.0	0.0099	0.0238
$HfMo_2$	227	638607	1	−11–8	$\bar{\Gamma}_7+\bar{\Gamma}_8+2\bar{\Gamma}_{10}+2\bar{\Gamma}_{11}+5\bar{X}_5+3\bar{L}_4\bar{L}_5+\bar{L}_6\bar{L}_7+4\bar{L}_8+2\bar{L}_9+2\bar{W}_3\bar{W}_4+3\bar{W}_5\bar{W}_6+5\bar{W}_7$	0.0	0.0	0.0168	0.0097
$Ba_3Si_6O_{12}N_2$	147	421322	3	−1–0	$\bar{A}_8\bar{A}_9+\bar{\Gamma}_8\bar{\Gamma}_9+\bar{H}_4\bar{H}_4+\bar{K}_4\bar{K}_4+\bar{L}_2\bar{L}_2+\bar{M}_2\bar{M}_2$	0.0	4.766	0.0095	5.0373
$MgCr_2O_4$	227	290599	1	−7–0	$\bar{\Gamma}_6+\bar{\Gamma}_7+\bar{\Gamma}_{10}+2\bar{X}_5+\bar{L}_6\bar{L}_7+\bar{L}_8+2\bar{L}_9+2\bar{W}_5\bar{W}_6+2\bar{W}_7$	0.0	0.0	0.013	0.0095
Al_3Pd_2	164	58117	1	0–1	$\bar{A}_6\bar{A}_7+\bar{\Gamma}_4\bar{\Gamma}_5+\bar{H}_6+\bar{K}_6+\bar{L}_5\bar{L}_6+\bar{M}_3\bar{M}_4$	0.0	0.0	0.0093	0.1289

(Table continued)

TABLE III. *(Continued)*

Formula	SG	ICSD	NF	Bands	Irreps	Δ_l (eV)	Δ_u (eV)	Δ'_l (eV)	Δ'_u (eV)
$Zr_3Al_3C_5$	194	159412	2	−1–6	$\bar{A}_4\bar{A}_5+\bar{A}_6+2\bar{\Gamma}_7+\bar{\Gamma}_8+\bar{\Gamma}_9+\bar{H}_4\bar{H}_5+\bar{H}_6\bar{H}_7+\bar{H}_8+\bar{H}_9+2\bar{K}_7+\bar{K}_8+\bar{K}_9+2\bar{L}_3\bar{L}_4+4\bar{M}_6$	0.0	0.0	0.017	0.0093
$Ca(As_2O_6)$	162	81064	1	−1–0	$\bar{A}_6\bar{A}_7+\bar{\Gamma}_4\bar{\Gamma}_5+\bar{H}_6+\bar{K}_6+\bar{L}_5\bar{L}_6+\bar{M}_3\bar{M}_4$	0.0	3.9469	0.0093	4.2667
$CaSi_2$	166	248517	1	1–4	$\bar{\Gamma}_6\bar{\Gamma}_7+\bar{\Gamma}_9+\bar{T}_6\bar{T}_7+\bar{T}_9+2\bar{F}_3\bar{F}_4+2\bar{L}_3\bar{L}_4$	0.0	0.0	0.0153	0.0092
CuV_2S_4	227	628953	1	−5–6	$\bar{\Gamma}_7+\bar{\Gamma}_8+\bar{\Gamma}_{10}+\bar{\Gamma}_{11}+3\bar{X}_5+2\bar{L}_6\bar{L}_7+\bar{L}_8+3\bar{L}_9+2\bar{W}_3\bar{W}_4+\bar{W}_5\bar{W}_6+3\bar{W}_7$	0.0	0.0	0.0105	0.009
SiC	156	43827	10	−1–0	$\bar{A}_4\bar{A}_5+\bar{\Gamma}_4\bar{\Gamma}_5+\bar{H}_4+\bar{H}_6+\bar{K}_4+\bar{K}_6+\bar{L}_3\bar{L}_4+\bar{M}_3\bar{M}_4$	0.0	1.6239	0.0087	2.733
$CsSnI_3$	127	69995	1	1–12	$3\bar{A}_6\bar{A}_7+\bar{\Gamma}_6+3\bar{\Gamma}_7+\bar{\Gamma}_8+\bar{\Gamma}_9+3\bar{M}_8\bar{M}_9+2\bar{Z}_6+4\bar{Z}_7+3\bar{R}_3\bar{R}_4+3\bar{X}_3\bar{X}_4$	0.1877	0.0	0.1877	0.0086
$ZnCr_2S_4$	227	42019	2	−11–0	$\bar{\Gamma}_7+\bar{\Gamma}_8+\bar{\Gamma}_{10}+\bar{\Gamma}_{11}+3\bar{X}_5+2\bar{L}_6\bar{L}_7+\bar{L}_8+3\bar{L}_9+2\bar{W}_3\bar{W}_4+\bar{W}_5\bar{W}_6+3\bar{W}_7$	0.0	0.0	0.0083	0.0099
$LiSr(AlF_6)$	163	68905	1	1–4	$\bar{A}_5\bar{A}_6+2\bar{\Gamma}_8+\bar{H}_4\bar{H}_5+\bar{H}_6+\bar{K}_4\bar{K}_5+\bar{K}_6+\bar{L}_2\bar{L}_2+2\bar{M}_3\bar{M}_4$	7.6262	0.0	7.6405	0.0083
Ba_2NiOsO_6	164	16406	11	−1–0	$\bar{A}_6\bar{A}_7+\bar{\Gamma}_4\bar{\Gamma}_5+\bar{H}_6+\bar{K}_6+\bar{L}_5\bar{L}_6+\bar{M}_3\bar{M}_4$	0.0	0.0	0.0079	0.0096
$BaSrFe_4O_8$	162	37011	11	−1–0	$\bar{A}_9+\bar{\Gamma}_9+\bar{H}_4\bar{H}_5+\bar{K}_4\bar{K}_5+\bar{L}_5\bar{L}_6+\bar{M}_5\bar{M}_6$	0.0	0.0	0.0299	0.0079
SiC	156	107204	2	−1–0	$\bar{A}_4\bar{A}_5+\bar{\Gamma}_4\bar{\Gamma}_5+\bar{H}_5+\bar{H}_6+\bar{K}_5+\bar{K}_6+\bar{L}_3\bar{L}_4+\bar{M}_3\bar{M}_4$	0.0	1.7191	0.0079	2.8422
BC_7	156	181953	3	0–1	$\bar{A}_4\bar{A}_5+\bar{\Gamma}_4\bar{\Gamma}_5+\bar{H}_4+\bar{H}_6+\bar{K}_4+\bar{K}_6+\bar{L}_3\bar{L}_4+\bar{M}_3\bar{M}_4$	0.0	2.7989	0.0077	3.7572
$Sn_2(Ta_2O_7)$	227	27119	4	−11–0	$\bar{\Gamma}_7+\bar{\Gamma}_8+\bar{\Gamma}_{10}+\bar{\Gamma}_{11}+3\bar{X}_5+2\bar{L}_6\bar{L}_7+\bar{L}_8+3\bar{L}_9+2\bar{W}_3\bar{W}_4+\bar{W}_5\bar{W}_6+3\bar{W}_7$	0.0	0.8308	0.0077	0.8798
$Fe(Cr_2O_4)$	227	183963	2	1–8	$\bar{\Gamma}_6+\bar{\Gamma}_7+\bar{\Gamma}_{10}+2\bar{X}_5+\bar{L}_4\bar{L}_5+3\bar{L}_9+\bar{W}_3\bar{W}_4+\bar{W}_5\bar{W}_6+2\bar{W}_7$	0.0	0.0	0.0085	0.0075
$Zn(Cr_2S_4)$	227	166481	1	−11–0	$\bar{\Gamma}_7+\bar{\Gamma}_8+\bar{\Gamma}_{10}+\bar{\Gamma}_{11}+3\bar{X}_5+2\bar{L}_6\bar{L}_7+\bar{L}_8+3\bar{L}_9+2\bar{W}_3\bar{W}_4+\bar{W}_5\bar{W}_6+3\bar{W}_7$	0.0	0.0	0.0075	0.0141
BC_5	156	180770	3	0–1	$\bar{A}_4\bar{A}_5+\bar{\Gamma}_4\bar{\Gamma}_5+\bar{H}_5+\bar{H}_6+\bar{K}_5+\bar{K}_6+\bar{L}_3\bar{L}_4+\bar{M}_3\bar{M}_4$	0.0	2.9665	0.0074	4.2867

$Bi_2Ru_2O_7$, $RbNiF_3$, and $AlSiTe_3$ have a fragile band right at or immediately below the Fermi level, well separated in the whole k space sampled, from both the conduction and the valence bands. We compute our new fragile indices of these materials and confirm them to be topological. This study is the first time fragile topological bands have been predicted in crystalline systems. The (relatively) flat fragile bands in $RbNiF_3$ may have interesting interacting physics since the bandwidths are smaller than the on-site Hubbard interaction of Ni, which is usually 8–10 eV.

Fragile topological bands have in-gap boundary states (the "filling anomaly" [83]) if the boundary cuts through empty Wyckoff positions that have nonzero coefficients in the EBR decomposition. Here, we take $AlSiTe_3$ as an example to show such in-gap states. The SG 147 $P\bar{3}$ has four types of maximal Wyckoff positions—$1a(000)$, $1b(00\frac{1}{2})$, $3e(\frac{1}{2}00)\times(0\frac{1}{2}0)(\frac{1}{2}\frac{1}{2}0)$, $3f(\frac{1}{2}0\frac{1}{2})(0\frac{1}{2}\frac{1}{2})(\frac{1}{2}\frac{1}{2}\frac{1}{2})$—and three types of nonmaximal Wyckoff positions—$2c(0,0,z)(0,0,-z)$, $2d(\frac{1}{3},\frac{2}{3},z)(\frac{2}{3},\frac{1}{3},-z)$, $6g(x,y,z)(-y,x-y,z)(-x+y,-x,z)\times(-x,-y,-z)(y,-x+y,-z)(x-y,x,-z)$. The Al, Si, and Te atoms occupy the $2d$, $2c$, and $6g$ positions, respectively. The BZ of SG 147 $P\bar{3}$, as shown in Fig. 5(f), has six high symmetry momenta: Γ, K, M, A, H, and L. The irreps formed by the fragile band shown in Fig. 5(d) are

$$\bar{\Gamma}_4\bar{\Gamma}_4+\bar{K}_5\bar{K}_6+\bar{M}_3\bar{M}_3+\bar{A}_7\bar{A}_7+\bar{H}_5\bar{H}_6+\bar{L}_2\bar{L}_2. \quad (21)$$

These irreps decompose into EBRs as

$$({}^1\bar{E}_g{}^2\bar{E}_g)_b\uparrow\mathrm{SG}\oplus({}^1\bar{E}_u{}^2\bar{E}_u)_b\uparrow\mathrm{SG}\oplus(\bar{E}_u\bar{E}_u)_b\uparrow\mathrm{SG}\ominus({}^1\bar{E}^2\bar{E})_{2d}\uparrow\mathrm{SG}, \quad (22)$$

where $(\rho)_w\uparrow\mathrm{SG}$ represent the EBR induced from the irrep ρ of the site symmetry group of the Wyckoff position w. Therefore, the fragile band is equivalent (in terms of irreps) to a combination of three Wannier functions at the b position and "−1" Wannier functions at the $2d$ position. We have checked that the trivial bands below the fragile band do not cancel the Wannier functions at $1b$. Now, we consider a surface terminating at the b position [as shown in Fig. 5(f)]. Since the three Wannier states cannot be symmetrically

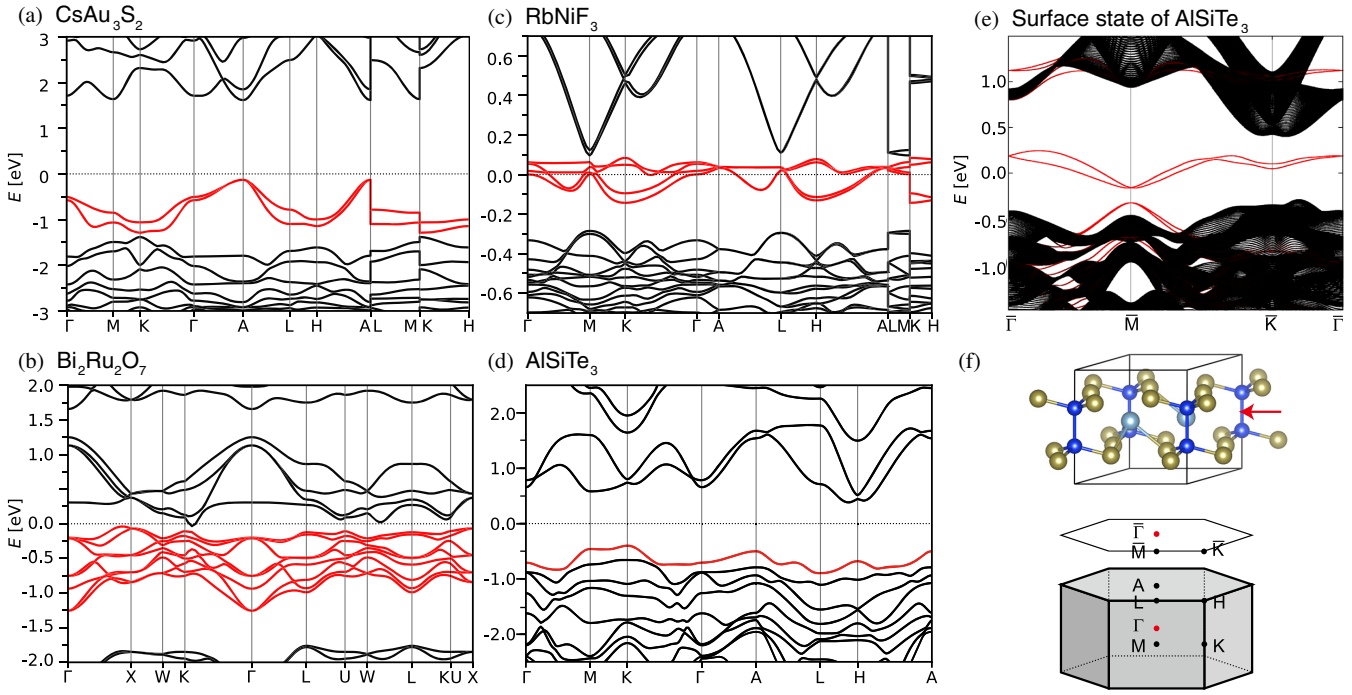

FIG. 5. Fragile bands in materials. (a) The band structure of $CsAu_3S_2$ (ICSD = 82540) in SG 164 ($P\bar{3}m1$). (b) $Bi_2Ru_2O_7$ (ICSD = 166566) in SG 227 ($Fd\bar{3}m$). (c) $RbNiF_3$ (ICSD = 15090) in SG 194 ($P6_3/mmc$). (d) $AlSiTe_2$ (ICSD = 75001) in SG 147 ($P\bar{3}$). (e) Top surface state of $AlSiTe_3$. (f) The crystal structure of $AlSiTe_3$ and the bulk or surface BZ. The red arrow shows the position of the surface termination. Here, the fragile bands are colored red, and the upper and lower bands are colored black; the Fermi levels are represented by the horizontal dotted lines. More information about the fragile bands, such as irreps and gaps from lower and upper bands as well as 100 more band structures with fragile topology, can be found in Ref. [74].

divided into the two sides, there must be in-gap states on the surface. We confirm the existence of such in-gap states by a first-principle calculation of a slab [Fig. 5(e)].

We hope new experiments and predictions of responses in fragile states will follow our exciting discovery of fragile bands.

VII. DISCUSSION

In this section, we discuss two examples related to our classification. The first is the TBG [55,58,59,69,70], and the second is Fu's topological crystalline insulator [24]. TBG can be successfully diagnosed through our framework, while Fu's model is beyond the symmetry eigenvalue classification. Nevertheless, we develop a generalized symmetry eigenvalue criterion for Fu's state.

A. Twisted bilayer graphene

TBG has an approximate valley-U(1) symmetry [63], and the single-valley Hamiltonian has the magnetic SG $P6'2'2$ (#177.151 in BNS notation). The irreps of $P6'2'2$ are tabulated in Table IV. The nearly flat bands around the Fermi level form the irreps [55]

$$\Gamma_1 + \Gamma_2 + \mathrm{M}_1 + \mathrm{M}_2 + \mathrm{K}_2\mathrm{K}_3. \tag{23}$$

Reference [55] found that these irreps cannot be obtained as a difference of EBRs and proved that bands having these irreps have C_2T-protected Wilson loop winding, with the winding number $3n \pm 1$ ($n \in \mathbb{Z}$). Another EFP having Wilson loop winding given in the supplemental material of Ref. [55] is

$$\Gamma_3 + \mathrm{M}_1 + \mathrm{M}_2 + 2\mathrm{K}_1. \tag{24}$$

We apply the polyhedron method (Sec. IV) to the magnetic SG $P6'2'2$ and obtain the complete eigenvalue criteria for the EFPs. The details of the calculations are

TABLE IV. Character table of irreps at high symmetry momenta in magnetic space group $P6'2'2$ (#177.151 in BNS settings) [51]. For the little group of Γ, E, C_3, and C_2' represent the conjugation classes generated from identity, C_{3z}, and C_{2x}, respectively. The number before each conjugate class represents the number of operations in this class. Conjugate class symbols at M and K are defined in similar ways.

	Γ_1	Γ_2	Γ_3		M_1	M_2		K_1	$\mathrm{K}_2\mathrm{K}_3$
E	1	1	2	E	1	1	E	1	2
$2C_3$	1	1	−1	C_2'	1	−1	C_3	1	−1
$3C_2'$	1	−1	0				C_3^{-1}	1	−1

given in Appendix D. Here, we briefly describe the results. We obtain a single inequality-type criterion

$$2m(\mathrm{K}_2\mathrm{K}_3) < m(\Gamma_3) \tag{25}$$

and a single $\mathbb{Z}_2$-type criterion

$$\begin{aligned} &m(\Gamma_1) + m(\Gamma_2) + 2m(\Gamma_3) - 2m(\mathrm{K}_2\mathrm{K}_3) = 0, \\ &m(\Gamma_2) = 1 \mod 2. \end{aligned} \tag{26}$$

The EFP (23) is diagnosed by the $\mathbb{Z}_2$-type criterion, and the other EFP (24) is diagnosed by the inequality-type criterion. We emphasize that Eqs. (25) and (26) go beyond the two-band eigenvalue criteria derived in Ref. [55] because they apply to many-band systems. Applying the method introduced in Sec. V, we find that $P6'2'2$ has only two EFP roots, and the two roots are just Eqs. (23) and (24).

B. Fu's topological crystalline insulator and a generalized symmetry eigenvalue criterion

Fu's state is spinless and is protected by C_4 rotation and TRS. The topological invariant is well defined only if the Hilbert space is restricted to $p_{x,y}$ orbitals. Correspondingly, the topological surface state is stable only if the model consists of $p_{x,y}$ orbitals. Therefore, this state has the defining character of fragile topology. Recently, Alexandradinata *et al.* proved that the topology of Fu's model is indeed fragile [84].

This model has an accidental inversion symmetry. In Appendix E 1, we show that the fragile topology cannot be diagnosed through the C_4 and inversion eigenvalues. Nevertheless, we develop a "generalized symmetry eigenvalue criterion" for this state (Appendix E 3). Usually, the diagnosis of topology involves additional symmetries. For example, diagnosis of a strong topological insulator, which is protected by TRS, involves inversion symmetry. We find that the additional symmetries diagnosing Fu's state are inversion and C_{2x} rotation. With these additional symmetries, a $\mathbb{Z}_2$ invariant can be defined in terms of the symmetry eigenvalues. However, the $\mathbb{Z}_2$ nontrivial phase is indeed a topological nodal ring semimetal, where the nodal rings are stabilized by inversion (and/or M_z). After the inversion is broken, the nodal rings are gapped. If the inversion symmetry is broken in such a way that no gap closing happens at the high symmetry points, the insulating phase obtained has the topology of Fu's model. Since the additional symmetries for diagnosis enforce the topological state to be a semimetal, we call this eigenvalue criterion "generalized."

VIII. SUMMARY

In this paper, we have obtained three major goals in the field of topological phases. For the first time, we have entirely mathematically classified the fragile topological states indicated by symmetry eigenvalues—EFPs. We found an extremely rich structure of these phases, linked to the mathematical classification of affine monoids, which surpasses the richness of stable topological phases. Then, for the first time, we have provided examples of fragile bands in more than 100 realistic materials, showcasing some of the best, well-separated sets of bands. Our work finishes an important subfield of topological states of matter. It would be remarkably interesting to find a clear experimental consequence of the well-separated fragile sets of bands we have discovered. One such fragile band is the wonder material of twisted bilayer graphene.

ACKNOWLEDGMENTS

We acknowledge Maia G. Vergniory, Zhijun Wang, and Claudia Felser for collaboration on previous related works. Z. S. and B. B. are supported by the Department of Energy Grant No. desc-0016239; the National Science Foundation EAGER Grant No. DMR 1643312; Simons Investigator Grants No. 404513, No. ONR N00014-14-1-0330, and No. NSF-MRSECDMR DMR 1420541; the Packard Foundation No. 2016-65128; and the Schmidt Fund for Development of Majorama Fermions funded by the Eric and Wendy Schmidt Transformative Technology Fund. L. E. is supported by the Government of the Basque Country (Project No. IT779-13), the Spanish Ministry of Economy and Competitiveness (MINECO), and the European Fund for Economic and Regional Development (FEDER; Project No. MAT2015-66441-P). We are mostly grateful to the MPG computing center for allowing us access to the Cobra and Draco Supercomputers. This research also used resources of the National Energy Research Scientific Computing Center (NERSC), a U.S. Department of Energy Office of Science User Facility operated under Contract No. DE-AC02-05CH11231. The mathematical analysis of this work is supported by the Department of Energy.

APPENDIX A: DIAGNOSIS FOR FRAGILE PHASES: THE INEQUALITY METHOD

Fragile topological states [37,42,57], also referred to as fragile phases in this paper, are defined to be non-Wannierizable insulating states, where the Wannier obstruction can be removed by coupling the state to a particular set of trivial (Wannierizable) bands. (A band structure is Wannierizable if a set of *symmetric* Wannier functions can be constructed from the bands.) In other words, if the number of Wannier functions is fixed to be the number of bands, the fragile phase is not Wannierizable; however, if more Wannier functions are allowed, the fragile bands can be realized as a subset of the bands constructed from all the Wannier functions; the bands outside of this subset are completely trivial (Wannierizable). Physically, the bands outside the subset correspond to the trivial bands that are added to remove the Wannier obstruction. In this

paper, we restrict ourselves to the fragile phases that can be diagnosed from symmetry eigenvalues. These fragile phases cannot be diagnosed from the indicators introduced in Refs. [38,43–45], but they can be written in terms of EBRs [37,54,55,57–59].

Thus, we need a new framework to understand the symmetry data vector (B) of fragile phases. Generally speaking, if the symmetry eigenvalues have the following property,

$$\exists\, p \in \mathbb{Z}^{N_{\mathrm{EBR}}}, \text{s.t.} B = \mathrm{EBR}\cdot p \quad \text{and} \quad \forall\, p \in \mathbb{N}^{N_{\mathrm{EBR}}}, B \neq \mathrm{EBR}\cdot p, \tag{A1}$$

then we say that the corresponding band structure has at least a fragile topology diagnosable by the symmetry eigenvalues or EBRs. (It could also have robust or strong topology undiagnosable by symmetry eigenvalues.) In other words, the symmetry data vector B of a fragile phase cannot be written as a sum of EBRs but only as a difference of two sums of EBRs, i.e., $B = \sum_i p_i EBR_i - \sum_i q_j EBR_j$, where $p_i, q_j \geq 0$ and $p_i q_i = 0$ for all i. Hereafter, we use A_i to represent the ith column of the matrix A. Then, adding the BR written as $\sum_i q_i EBR_i$ to the fragile phase makes the total symmetry data vector completely trivial.

1. An example: SG 150

To familiarize ourselves with the symmetry data of fragile phases, here we take an example SG 150 ($P321$) in the presence of SOC and TRS. The EBR matrix is given by

$$\mathrm{EBR} = \begin{pmatrix} 0&1&2&0\\ 1&0&0&2\\ 0&1&2&0\\ 1&0&0&2\\ 0&1&0&1\\ 0&1&0&1\\ 1&0&2&1\\ 0&1&0&1\\ 0&1&0&1\\ 1&0&2&1\\ 0&1&0&1\\ 0&1&0&1\\ 1&0&2&1\\ 0&1&0&1\\ 0&1&0&1\\ 1&0&2&1\\ 1&1&2&2\\ 1&1&2&2 \end{pmatrix} = \begin{pmatrix} 1&0&-1&0&0&0&1&0&0&0&0&0&0&0&0&0&0&0\\ 0&0&1&0&0&0&0&1&0&0&0&0&0&0&0&0&0&0\\ 1&0&-1&0&0&0&0&0&0&0&0&0&0&0&0&0&0&0\\ 0&0&1&0&0&1&0&0&0&0&0&0&0&0&0&0&0&0\\ 1&-1&0&0&0&0&0&0&1&0&0&0&0&0&0&0&0&0\\ 1&-1&0&0&0&0&0&0&0&1&0&0&0&0&0&0&0&0\\ 0&1&0&0&0&0&0&0&0&0&1&0&0&0&0&0&0&0\\ 1&-1&0&0&0&0&0&0&0&0&0&1&0&0&0&0&0&0\\ 1&-1&0&0&0&0&0&0&0&0&0&0&1&0&0&0&0&0\\ 0&1&0&0&0&0&0&0&0&0&0&0&0&1&0&0&0&0\\ 1&-1&0&0&0&0&0&0&0&0&0&0&0&0&1&0&0&0\\ 1&-1&0&0&0&0&0&0&0&0&0&0&0&0&0&1&0&0\\ 0&1&0&0&0&0&0&0&0&0&0&0&0&0&0&0&1&0\\ 1&-1&0&0&0&0&0&0&0&0&0&0&0&0&0&0&0&1\\ 1&-1&0&0&0&0&0&0&0&0&0&0&0&0&0&0&0&0\\ 0&1&0&0&1&0&0&0&0&0&0&0&0&0&0&0&0&0\\ 1&0&0&0&0&0&0&0&0&0&0&0&0&0&0&0&0&0\\ 1&0&0&1&0&0&0&0&0&0&0&0&0&0&0&0&0&0 \end{pmatrix} \begin{pmatrix} 1&0&0&0\\ 0&1&0&0\\ 0&0&1&0\\ 0&0&0&0\\ 0&0&0&0\\ 0&0&0&0\\ 0&0&0&0\\ 0&0&0&0\\ 0&0&0&0\\ 0&0&0&0\\ 0&0&0&0\\ 0&0&0&0\\ 0&0&0&0\\ 0&0&0&0\\ 0&0&0&0\\ 0&0&0&0 \end{pmatrix} \times \begin{pmatrix} 1&1&2&2\\ 1&0&2&1\\ 1&0&0&2\\ 0&0&-1&0 \end{pmatrix}, \tag{A2}$$

where the Smith decomposition $L\Lambda R$ is given after the second equal sign. Here, each column of the matrix EBR represents an EBR, and the irreps represented by the rows of the EBR matrix are $\bar{A}_4\bar{A}_5$, $\bar{A}_6$, $\bar{\Gamma}_4\bar{\Gamma}_5$, $\bar{\Gamma}_6$, $\bar{H}_4$, $\bar{H}_5$, $\bar{H}_6$, $\overline{HA}_4$, $\overline{HA}_5$, $\overline{HA}_6$, $\bar{K}_4$, $\bar{K}_5$, $\bar{K}_6$, $\overline{KA}_4$, $\overline{KA}_5$, $\overline{KA}_6$, $\bar{L}_3\bar{L}_4$, $\bar{M}_3\bar{M}_4$, in the notation of the Bilbao Crystallographic Server (BCS) [40,51]. (One can find the definitions of these irreps through the Irreducible representations of the Double Space Groups tool of the BCS [40].) Since the diagonal elements of Λ are either 1 or 0, there is no indicator in this SG. As described in Refs. [37,38,40,73], the space of compatibility-relation-allowed symmetry data can be generated from the first r columns of the L matrix, with r the rank of Λ (here, $r = 3$). In other words, we can

always write the symmetry data vector as $B = \mathrm{EBR} \cdot p = L\Lambda R \cdot p$. Thus, we can introduce the parameter's $y_i = (Rp)_i$ $(i = 1, 2 \cdots r)$ and write the symmetry data as

$$B = \sum_{i=1}^{3} (L\Lambda)_i y_i = (y_1 - y_3, y_3, y_1 - y_3, y_3, y_1 - y_2, y_1 - y_2, y_2, y_1 - y_2, y_1 - y_2, y_2, y_1 - y_2, y_1 - y_2, y_2, y_1 - y_2, y_2, y_1, y_1)^T. \tag{A3}$$

For the number of irreps to be non-negative, i.e., $B \geq 0$, the following inequalities should be satisfied

$$y_1 \geq y_3 \geq 0, \qquad y_1 \geq y_2 \geq 0. \tag{A4}$$

Therefore, only the y's that satisfy Eq. (A4) correspond to physical band structures. In the following, we use y to represent the band structures.

Now, we decompose the symmetry data vector in Eq. (A3) as a combination of EBRs, i.e., $B = \sum_i p_i EBR_i$ [Eq. (A1)]. On one hand, as $y_i = (R \cdot p)_i$ $(i = 1, 2, 3)$ and $\Lambda = \mathrm{diag}(1110)$ [Eq. (A2)], we can always write p as $p = y_1 R_1^{-1} + y_2 R_2^{-1} + y_3 R_3^{-1}$. ($R_i^{-1}$ is the ith column of the matrix R^{-1}.) On the other hand, if p is a solution of $y_i = (Rp)_i$ $(i = 1, 2, 3)$, $p + kR_4^{-1}$ is also a solution, where k is a free parameter, because $(RR_4^{-1})_{1,2,3} = 0$. Therefore, the general solution of the equation $B = \mathrm{EBR} \cdot p$ or $y_i = (\Lambda R p)_i$ $(i = 1, 2, 3)$ takes the form of

$$p = y_1 R_1^{-1} + y_2 R_2^{-1} + y_3 R_3^{-1} + kR_4^{-1}. \tag{A5}$$

Substituting the R matrix into Eq. (A5), we obtain

$$p = (2y_2 - y_3 - 4k, y_1 - y_3 - 2k, k, -y_2 + y_3 + 2k)^T. \tag{A6}$$

For p to be an integer, the vector k needs to be an integer because $p_3 = k$. For a given y vector, if there exists some integer k such that each element of p is non-negative, then the corresponding symmetry data vector can be written as a sum of positive EBRs, so it can be a trivial phase; otherwise, the corresponding band structure necessarily has a fragile topology. Therefore, we conclude that the equivalent condition for symmetry data associated with y to be trivial is

$$\exists\, k \in \mathbb{Z}, \quad \text{s.t.} \quad 2y_2 - y_3 - 4k \geq 0, \quad y_1 - y_3 - 2k \geq 0, \quad k \geq 0, \quad -y_2 + y_3 + 2k \geq 0. \tag{A7}$$

Solving the inequalities in Eq. (A7), we rewrite the trivial condition as

$$\exists\, k \in \mathbb{Z}, \quad \text{s.t.} \quad \max\left(0, \frac{1}{2}y_2 - \frac{1}{2}y_3\right) \leq k \leq \min\left(\frac{1}{2}y_2 - \frac{1}{4}y_3, \frac{1}{2}y_1 - \frac{1}{2}y_3\right). \tag{A8}$$

There are two possible cases where Eq. (A8) has no solution: In case I, Eq. (A8) has no solution even where k is allowed to be a rational number; in case II, Eq. (A8) has rational solutions but no integer solution. The two cases correspond to the inequality-type index and the $\mathbb{Z}_2$-type index defined in the main text, respectively. Here, we first consider case I. We directly see that case I happens when any of the following four inequalities is satisfied: (A) $0 > \frac{1}{2}y_2 - \frac{1}{4}y_3$, (B) $\frac{1}{2}y_2 - \frac{1}{2}y_3 > \frac{1}{2}y_2 - \frac{1}{4}y_3$, (C) $0 > \frac{1}{2}y_1 - \frac{1}{2}y_3$, or (D) $\frac{1}{2}y_2 - \frac{1}{2}y_3 > \frac{1}{2}y_1 - \frac{1}{2}y_3$. For example, if $0 > \frac{1}{2}y_2 - \frac{1}{4}y_3$ (A), Eq. (A8) implies $0 \leq k < 0$, which has no solution. Actually, inequalities (B), (C), and (D) cannot be satisfied by real band structures because they conflict with $B \geq 0$ [Eq. (A4)]. Therefore, the only possibility left is (A), for which we get the fragile criterion

$$y_3 - 2y_2 > 0. \tag{A9}$$

In this paper, we refer to $y_3 - 2y_2$ as an inequality-type fragile index. A key difference between the inequality-type index for a fragile phase and the symmetry-based indicator for a stable or strong phase is that the latter can become trivial upon stacking whereas the former cannot. For example, the double of the generator state of a $\mathbb{Z}_2$ indicator becomes a trivial state, whereas stacking of any positive number of the inequality-type fragile phase, for example, the $y_3 - 2y_2 = 1$ state, is still a fragile phase because the inequality is still satisfied.

Now, we consider case II, where Eq. (A8) has solutions only if k is allowed to be a rational number. Case II happens if the interval set by Eq. (A8) is nonzero but does not contain any integer. We notice that the solution of Eq. (A8) can be written as the intersection of the following three intervals:

$$0 \leq k \leq \min\left(\frac{1}{2}y_2 - \frac{1}{4}y_3, \frac{1}{2}y_1 - \frac{1}{2}y_3\right), \tag{A10}$$

$$\frac{1}{2}y_2 - \frac{1}{2}y_3 \leq k \leq \frac{1}{2}y_2 - \frac{1}{4}y_3, \tag{A11}$$

$$\frac{1}{2}y_2 - \frac{1}{2}y_3 \leq k \leq \frac{1}{2}y_1 - \frac{1}{2}y_3. \tag{A12}$$

If Eq. (A10) has solutions, the solutions must include the lower bound 0, which violates our request that the interval does not contain integers. Thus, Eq. (A10) does not produce new indices. Therefore, we only need to consider the case where Eq. (A11) or (A12) has fractional solutions but no integer solution. In order for Eq. (A11) not to have

an integer solution, we set $y_2 - y_3$ to be an odd integer such that the lower bound $\frac{1}{2}y_2 - \frac{1}{2}y_3$ is fractional, and, at the same time, we set the interval to be smaller than $\frac{1}{2}$, i.e., $0 \le \frac{1}{2}y_2 - \frac{1}{4}y_3 - (\frac{1}{2}y_2 - \frac{1}{2}y_3) < \frac{1}{2}$. Considering that y's are integers, this condition can be realized when (A) $y_2 - y_3 = 1 \mod 2$ and $\frac{1}{2}y_2 - \frac{1}{4}y_3 - (\frac{1}{2}y_2 - \frac{1}{2}y_3) = 0$, or (B) $y_2 - y_3 = 1 \mod 2$ and $\frac{1}{2}y_2 - \frac{1}{4}y_3 - (\frac{1}{2}y_2 - \frac{1}{2}y_3) = \frac{1}{4}$. In order for Eq. (A12) not to have an integer solution, we set $y_2 - y_3$ to be an odd integer such that the lower bound $\frac{1}{2}y_2 - \frac{1}{2}y_3$ is fractional, and, at the same time, we set the interval to be smaller than $\frac{1}{2}$, i.e., $0 \le \frac{1}{2}y_1 - \frac{1}{2}y_3 - (\frac{1}{2}y_2 - \frac{1}{2}y_3) < \frac{1}{2}$. Considering that y's are integers, this condition can be realized when (C) $y_2 - y_3 = 1 \mod 2$ and $\frac{1}{2}y_1 - \frac{1}{2}y_3 - (\frac{1}{2}y_2 - \frac{1}{2}y_3) = 0$. Since all three cases—A, B, and C—are not inconsistent with Eq. (A4), all of them can be realized by some physical band structures. Therefore, we obtain fragile criteria for the three cases as

$$y_3 = 0 \quad \text{and} \quad \delta_1 = y_2 - y_3 = 1 \mod 2, \tag{A13}$$

$$y_3 = 1 \quad \text{and} \quad \delta_2 = y_2 - y_3 = 1 \mod 2, \tag{A14}$$

$$y_1 - y_2 = 0 \quad \text{and} \quad \delta_3 = y_2 - y_3 = 1 \mod 2. \tag{A15}$$

In this paper, we refer to $\delta_{1,2,3}$ as $\mathbb{Z}_2$-type fragile indices, which are similar to the symmetry-based indicators in the sense that they will also become trivial upon stacking. For example, the double of the state $y = (1, 1, 0)$, where $y_3 = 0$ and $\delta_1 = 1$, is a trivial state because it reads $2y = (2, 2, 0)$ and has trivial indices.

2. Inequality method to get the fragile criteria

The above method can be generalized to any SG. In this paper, we refer to this method as the inequality method. Here, we present a summary of the inequality method. First, making use of the Smith decomposition of the EBR matrix (EBR $= L\Lambda R$), we parametrize the symmetry data as $B = \sum_{i=1}^{r}(L\Lambda)_i y_i$, with r the rank of Λ and $y = (y_1 \cdots y_r)^T$ an integer vector, such that B has vanishing indicators. For the numbers of irreps to be non-negative, we need

$$B = \sum_{i=1}^{r}(L\Lambda)_i y_i \ge 0. \tag{A16}$$

Second, we decompose the symmetry data vector associated with y as a combination of EBRs, i.e., $B = \mathrm{EBR} \cdot p$ or $y_i = (Rp)_i$ $(i = 1 \cdots r)$, where $p = (p_1 \cdots p_{N_{\mathrm{EBR}}})^T$ is the combination coefficient. Clearly, the decomposition

$$B = \sum_{i=1}^{r}(L\Lambda)_i y_i + \sum_{i=1}^{N_{\mathrm{EBR}}-r}(L\Lambda)_{r+i} k_i, \tag{A17}$$

where k_i's are free (integer) parameters, gives the same symmetry data vector as Eq. (A16) because $\Lambda_i = 0$ for $i > r$. Thus, the general solution of $B = \mathrm{EBR} \cdot p$ can be written as $p = R^{-1}\begin{pmatrix} y \\ k \end{pmatrix}$. As both R and R^{-1} are integer matrices, p is an integer vector iff k is an integer vector. Therefore, the condition for the symmetry data to be trivial is equivalent to the existence of integer solutions of k for the inequalities $p \ge 0$ subject to the constraints $B \ge 0$ [Eq. (A16)]: If there exists k such that $p \ge 0$, then the symmetry data can be written as a sum of EBRs. Now, we describe the solution of $p \ge 0$. At the first step, we consider k_1 as a variable and $k_2 \cdots k_{N_{\mathrm{EBR}}-1}$ and y as fixed parameters. Then, the solution of $p \ge 0$ takes the form

$$\begin{aligned} &\max\left[f_1^{(-1)}(k_2 \cdots y_r), f_1^{(-2)}(k_2 \cdots y_r), \cdots\right] \le k_1 \\ &\le \min\left[f_1^{(1)}(k_2 \cdots y_r), f_1^{(2)}(k_2 \cdots y_r), \cdots\right]. \end{aligned} \tag{A18}$$

Here, f's are linear functions of k and y with rational coefficients. In the second step, by requiring $f_1^{(i)} \le f_1^{(j)}$, where $i < 0$ and $j > 0$, such that k_1 has a nontrivial solution, we obtain a set of constraints about $k_2 \cdots k_{N_{\mathrm{EBR}}-r}$ and y. Solving these constraints by regarding k_2 as the variable and $k_3 \cdots k_{N_{\mathrm{EBR}}-1}$ and y as fixed parameters, we obtain the solution

$$\begin{aligned} &\max\left[f_2^{(-1)}(k_3 \cdots y_r), f_2^{(-2)}(k_3 \cdots y_r), \cdots\right] \le k_2 \\ &\le \min\left[f_2^{(1)}(k_3 \cdots y_r), f_2^{(2)}(k_3 \cdots y_r), \cdots\right]. \end{aligned} \tag{A19}$$

At the $(N_{\mathrm{EBR}} - r)$th step, solving the constraints that guarantee $k_{N_{\mathrm{EBR}}-r-1}$ to have a nontrivial solution by considering $k_{N_{\mathrm{EBR}}-r}$ as a variable and y as a fixed parameter, we obtain the solution

$$\begin{aligned} &\max\left[h_0^{(-1)}(y_1 \cdots y_r), h_0^{(-2)}(y_1 \cdots y_r), \cdots\right] \le k_{N_{\mathrm{EBR}}-r} \\ &\le \min\left[h_0^{(1)}(y_1 \cdots y_r), h_0^{(2)}(y_1 \cdots y_r), \cdots\right]. \end{aligned} \tag{A20}$$

Here, h's are linear functions of y with rational coefficients. In the next step, we regard y_1 as the variable and $y_2 \cdots y_r$ as fixed parameters. By requiring $k_{N_{\mathrm{EBR}}-r}$ to have a nontrivial solution, we obtain the constraints satisfied by y_1 as

$$\begin{aligned} &\max\left[h_1^{(-1)}(y_2 \cdots y_r), h_1^{(-2)}(y_2 \cdots y_r), \cdots\right] \le y_1 \\ &\le \min\left[h_1^{(1)}(y_2 \cdots y_r), h_1^{(2)}(y_2 \cdots y_r), \cdots\right]. \end{aligned} \tag{A21}$$

Following the procedure, we can successfully obtain the constraints satisfied by $y_2 \cdots y_r$ as

$$\max\left[h_2^{(-1)}(y_3\cdots y_r), h_2^{(-2)}(y_3\cdots y_r),\cdots\right] \le y_2 \le \min\left[h_2^{(1)}(y_3\cdots y_r), h_2^{(2)}(y_3\cdots y_r),\cdots\right], \tag{A22}$$

$$\max\left[h_{r-1}^{(-1)}(y_r), h_{r-1}^{(-2)}(y_r),\cdots\right] \le y_{r-1} \le \min\left[h_{r-1}^{(1)}(y_r), h_{r-1}^{(2)}(y_r),\cdots\right]. \tag{A23}$$

Equations (A18)–(A23) can be thought of as an algorithm, where the $(n+1)$th step is obtained by requiring that the nth step has a nontrivial (rational) solution. Therefore, to ensure that $k_1\cdots k_{N_{\mathrm{EBR}}}$ has a nontrivial (rational) solution, we need only the constraints in Eqs. (A21)–(A23) to be satisfied. In other words, if $h_l^{(i)} > h_l^{(j)}$ for any $i<0$, $j>0$ $(l=0,1\cdots r)$, the constraints Eqs. (A21)–(A23) are violated; this result would imply the nonexistence of k satisfying Eqs. (A18)–(A20). Hence, we can define the inequality-type indices as $h_l^{(i)} - h_l^{(j)}$ $(i<0,$ $j>0,$ $l=0,1\cdots r)$, the positive values of which imply that Eqs. (A18)–(A20) do not have a solution and hence $k_1\cdots k_{N_{\mathrm{EBR}}-r}$ does not have a solution; hence, they imply a fragile topology. In practice, we need to check whether $h_l^{(i)} - h_l^{(j)} > 0$ is consistent with the positivity of B [Eq. A16]. If not, then there is no need to introduce such an index, as it cannot be realized by a real band structure. As discussed in the paragraph below Eq. (A8), in the example of SG 150, $h_l^{(i)}$ and $h_l^{(j)}$ pairs set four possible inequality-type indices, but only one of them is consistent with Eq. (A16). By this method, we can obtain all the inequality-type fragile indices, in principle. However, we emphasize that the computational time of solving $p \ge 0$ in the form of Eqs. (A18)–(A21) and (A23) increases exponentially with the number of variables. Therefore, it is very hard to solve SGs where r is very large using the inequality method; several of these groups are solved in Ref. [73].

Finding $\mathbb{Z}_{n=2,3\cdots}$-type fragile indices is more complicated: One needs to check whether the solution of k contains integer points. For simplicity, let us first check whether the $k_{N_{\mathrm{EBR}}-r}$ component has integer solutions. For a given $y=(y_1\cdots y_r)^T$, if there exist fractional $h_0^{(i)}$ and $h_0^{(j)}$ $(i<0,\ j>0)$, then the conditions for $k_{N_{\mathrm{EBR}}-r}$ to have no integer solutions are (i) $h_0^{(i)} \in \mathbb{Q}-\mathbb{Z}$ (noninteger rational) and (ii) $h_0^{(j)} < \lceil h_0^{(i)} \rceil$ such that $h_0^{(i)} \le k_{N_{\mathrm{EBR}}-r} \le h_0^{(j)} < \lceil h_0^{(i)} \rceil$ has no integer solution sitting between a noninteger rational and the smallest integer larger than or equal to this noninteger rational. Here, $\lceil x \rceil$ represents the smallest integer larger than or equal to x. Now, let us write the conditions (i) and (ii) more explicitly to get the $\mathbb{Z}_n$-type indices. As $h_0^{(i)}$ is a rational linear function of y, there exists a minimal integer κ such that $\kappa h_0^{(i)} \in \mathbb{Z}$ for arbitrary $y \in \mathbb{Z}^r$. Therefore, for given y, condition (i) is equivalent to

$$\delta = \kappa h_0^{(i)}(y) \neq 0 \mod \kappa. \tag{A24}$$

When Eq. (A24) is satisfied, $\lceil h_0^{(i)} \rceil$ can be written as $h_0^{(i)} + 1 - \frac{1}{\kappa}(\kappa h_0^{(i)} \bmod \kappa)$, and thus condition (ii) is equivalent to

$$h_0^{(j)} - h_0^{(i)} < 1 - \frac{1}{\kappa}(\kappa h_0^{(i)} \bmod \kappa). \tag{A25}$$

In the example of SG 150, picking $h_0^{(i)}$ as $\frac{1}{2}y_2 - \frac{1}{2}y_3$, $h_0^{(j)}$ as $\frac{1}{2}y_2 - \frac{1}{4}y_3$, and $\kappa = 2$, Eqs. (A24) and (A25) are given as $\delta = y_2 - y_3 = 1 \bmod 2$ and $\frac{1}{4}y_3 < \frac{1}{2}$, respectively, which implies Eqs. (A13) and (A14).

So far, we have derived the $\mathbb{Z}_n$-type fragile indices given by the $k_{N_{\mathrm{EBR}}-r}$ component. Now, we consider the $\mathbb{Z}_n$-type fragile indices given by the $k_{N_{\mathrm{EBR}}-r-1}$ component. We can rederive Eqs. (A18)–(A20) in a different order of k components, where the last-solved component is $k_{N_{\mathrm{EBR}}-r-1}$. Then, following Eqs. (A24) and (A25), we can derive the $\mathbb{Z}_n$-type fragile criteria given by $k_{N_{\mathrm{EBR}}-r-1}$. In Appendix A 3, we present an example of interchanging the order of $k_{N_{\mathrm{EBR}}-r}$ and $k_{N_{\mathrm{EBR}}-r-1}$. By setting each k_i as the last-solved component, we can get all the $\mathbb{Z}_n$-type fragile criteria given by *individual* k components. We present a case-by-case study of this method in Ref. [73].

3. Another example: SG 143

Here, we present the calculation of fragile indices in SG 143 ($P3$) as a nontrivial example of the $\mathbb{Z}_n$-type indices. The Smith decomposition of the EBR matrix is given by

$$\mathrm{EBR} = \begin{pmatrix}
1 & 0 & 0 & -1 & 0 & 0 & 0 & 0 & 1 & 0 & 0 & 0 & 0 & 0 & 0 & 0 & 0 & 0 \\
0 & 0 & 0 & 1 & 0 & 0 & 0 & 0 & 0 & 1 & 0 & 0 & 0 & 0 & 0 & 0 & 0 & 0 \\
1 & 0 & 0 & -1 & 0 & 0 & 0 & 0 & 0 & 0 & 0 & 0 & 0 & 0 & 0 & 0 & 0 & 0 \\
0 & 0 & 0 & 1 & 0 & 0 & 0 & 1 & 0 & 0 & 0 & 0 & 0 & 0 & 0 & 0 & 0 & 0 \\
2 & -1 & -1 & 0 & 0 & 0 & 0 & 0 & 0 & 0 & 1 & 0 & 0 & 0 & 0 & 0 & 0 & 0 \\
0 & 0 & 1 & 0 & 0 & 0 & 0 & 0 & 0 & 0 & 0 & 1 & 0 & 0 & 0 & 0 & 0 & 0 \\
0 & 1 & 0 & 0 & 0 & 0 & 0 & 0 & 0 & 0 & 0 & 0 & 1 & 0 & 0 & 0 & 0 & 0 \\
2 & -1 & -1 & 0 & 0 & 0 & 0 & 0 & 0 & 0 & 0 & 0 & 0 & 1 & 0 & 0 & 0 & 0 \\
0 & 0 & 1 & 0 & 0 & 0 & 0 & 0 & 0 & 0 & 0 & 0 & 0 & 0 & 1 & 0 & 0 & 0 \\
0 & 1 & 0 & 0 & 0 & 0 & 0 & 0 & 0 & 0 & 0 & 0 & 0 & 0 & 0 & 1 & 0 & 0 \\
2 & -1 & -1 & 0 & 0 & 0 & 0 & 0 & 0 & 0 & 0 & 0 & 0 & 0 & 0 & 0 & 1 & 0 \\
0 & 0 & 1 & 0 & 0 & 0 & 0 & 0 & 0 & 0 & 0 & 0 & 0 & 0 & 0 & 0 & 0 & 1 \\
0 & 1 & 0 & 0 & 0 & 0 & 0 & 0 & 0 & 0 & 0 & 0 & 0 & 0 & 0 & 0 & 0 & 0 \\
2 & -1 & -1 & 0 & 0 & 0 & 0 & 0 & 0 & 0 & 0 & 0 & 0 & 0 & 0 & 0 & 0 & 0 \\
0 & 0 & 1 & 0 & 0 & 0 & 1 & 0 & 0 & 0 & 0 & 0 & 0 & 0 & 0 & 0 & 0 & 0 \\
0 & 1 & 0 & 0 & 0 & 1 & 0 & 0 & 0 & 0 & 0 & 0 & 0 & 0 & 0 & 0 & 0 & 0 \\
1 & 0 & 0 & 0 & 0 & 0 & 0 & 0 & 0 & 0 & 0 & 0 & 0 & 0 & 0 & 0 & 0 & 0 \\
1 & 0 & 0 & 0 & 1 & 0 & 0 & 0 & 0 & 0 & 0 & 0 & 0 & 0 & 0 & 0 & 0 & 0
\end{pmatrix}
\begin{pmatrix}
1 & 0 & 0 & 0 & 0 & 0 \\
0 & 1 & 0 & 0 & 0 & 0 \\
0 & 0 & 1 & 0 & 0 & 0 \\
0 & 0 & 0 & 1 & 0 & 0 \\
0 & 0 & 0 & 0 & 0 & 0 \\
0 & 0 & 0 & 0 & 0 & 0 \\
0 & 0 & 0 & 0 & 0 & 0 \\
0 & 0 & 0 & 0 & 0 & 0 \\
0 & 0 & 0 & 0 & 0 & 0 \\
0 & 0 & 0 & 0 & 0 & 0 \\
0 & 0 & 0 & 0 & 0 & 0 \\
0 & 0 & 0 & 0 & 0 & 0 \\
0 & 0 & 0 & 0 & 0 & 0 \\
0 & 0 & 0 & 0 & 0 & 0 \\
0 & 0 & 0 & 0 & 0 & 0 \\
0 & 0 & 0 & 0 & 0 & 0
\end{pmatrix}
\times
\begin{pmatrix}
1 & 1 & 1 & 1 & 1 & 1 \\
2 & 0 & 0 & 0 & 1 & 1 \\
0 & 2 & 0 & 1 & 0 & 1 \\
0 & 0 & 0 & 1 & 1 & 1 \\
-1 & -1 & 0 & 0 & 0 & 0 \\
1 & 0 & 0 & 0 & 0 & 0
\end{pmatrix}, \tag{A26}$$

where the order of irreps is $\bar{A}_4\bar{A}_4$, $\bar{A}_5\bar{A}_6$, $\bar{\Gamma}_4\bar{\Gamma}_4$, $\bar{\Gamma}_5\bar{\Gamma}_6$, $\bar{H}_4$, $\bar{H}_5$, $\bar{H}_6$, $\overline{HA}_4$, $\overline{HA}_5$, $\overline{HA}_6$, $\bar{K}_4$, $\bar{K}_5$, $\bar{K}_6$, $\overline{KA}_4$, $\overline{KA}_5$, $\overline{KA}_6$, $\bar{L}_2\bar{L}_2$, and $\bar{M}_2\bar{M}_2$, in the BCS notation [40,51]. The rank of the EBR matrix is $r = 4$, and the number of EBRs is $N_{\mathrm{EBR}} = 6$; thus, y has four components, and k has two components. From Eq. (A26), we can directly see that the solution of $B = \sum_{i=1}^{r}(L\Lambda)_i y_i \geq 0$ is

$$y_1 \geq y_4 \geq 0, \qquad y_2 \geq 0, \quad y_3 \geq 0, \quad 2y_1 - y_2 - y_3 \geq 0. \tag{A27}$$

Relying on the discussion in Appendix A 2, we can write the p vector as

$$p = R^{-1}\begin{pmatrix} y \\ k \end{pmatrix} = \begin{pmatrix} k_2 \\ -k_1 - k_2 \\ y_1 - y_4 + k_1 \\ -y_2 + y_4 + 2k_2 \\ -y_3 + y_4 - 2k_1 - 2k_2 \\ y_2 + y_3 - y_4 + 2k_1 \end{pmatrix}. \tag{A28}$$

Now, we solve the inequality by the method described in Eqs. (A18)–(A23). In the first step, we take k_1 as the variable,; then, $p \geq 0$ gives

$$\begin{aligned} &-k_1 - k_2 \geq 0, \qquad y_1 - y_4 + k_1 \geq 0, \\ &-y_3 + y_4 - 2k_1 - 2k_2 \geq 0, \quad y_2 + y_3 - y_4 + 2k_1 \geq 0. \end{aligned} \tag{A29}$$

(For now, we temporarily omit the first and fourth components of p, i.e., k_2 and $-y_2 + y_4 + 2k_2$, where k_1 is not involved.) The four constraints in Eq. (A29) should be satisfied at the same time, so we obtain

$$\begin{aligned} &\max\left(-\frac{1}{2}y_2 - \frac{1}{2}y_3 + \frac{1}{2}y_4, -y_1 + y_4\right) \leq k_1 \\ &\leq \min\left(-k_2, -k_2 - \frac{1}{2}y_3 + \frac{1}{2}y_4\right). \end{aligned} \tag{A30}$$

In the second step, we regard k_2 as the variable and find the constraints satisfied by k_2 that guarantee (i) $p_1 \geq 0$, $p_4 \geq 0$,

and (ii) k_1 has a nontrivial solution. On one hand, for p_1 and p_4 to be non-negative, we have

$$k_2 \geq 0, \qquad -y_2 + y_4 + 2k_2 \geq 0. \tag{A31}$$

On the other hand, for k_1 to have nontrivial solutions, we should satisfy the inequalities

$$\begin{aligned} &-\frac{1}{2}y_2 - \frac{1}{2}y_3 + \frac{1}{2}y_4 \leq -k_2 \\ &-\frac{1}{2}y_2 - \frac{1}{2}y_3 + \frac{1}{2}y_4 \leq -k_2 - \frac{1}{2}y_3 + \frac{1}{2}y_4 \\ &-y_1 + y_4 \leq -k_2 \\ &-y_1 + y_4 \leq -k_2 - \frac{1}{2}y_3 + \frac{1}{2}y_4. \end{aligned} \tag{A32}$$

Regarding k_2 as the variable, the constraints in Eqs. (A31) and (A32) can be equivalently written as

$$\begin{aligned} &\max\left(0, \frac{1}{2}y_2 - \frac{1}{2}y_4\right) \leq k_2 \\ &\leq \min\left(\frac{1}{2}y_2, \frac{1}{2}y_2 + \frac{1}{2}y_3 - \frac{1}{2}y_4, y_1 - \frac{1}{2}y_3 - \frac{1}{2}y_4, y_1 - y_4\right). \end{aligned} \tag{A33}$$

Equation (A33) guarantees that (i) $p_{1,4}$ are non-negative, and (ii) Eq. (A30) has a nontrivial solution, which guarantees that $p_{2,3,5,6}$ are non-negative. Thus, the sufficient and necessary condition for p to be non-negative is that Eq. (A33) has nontrivial solutions. And, Eq. (A33) has nontrivial solutions if and only if the two lower bounds are smaller than the four upper bounds, i.e., the eight inequalities

$$\begin{aligned} &y_2 \geq 0, \quad y_2 + y_3 - y_4 \geq 0, \quad 2y_1 - y_3 - y_4 \geq 0, \quad y_1 - y_4 \geq 0, \\ &y_4 \geq 0, \quad y_3 \geq 0, \quad 2y_1 - y_2 - y_3 \geq 0, \quad 2y_1 - y_2 - y_4 \geq 0. \end{aligned} \tag{A34}$$

Now, we are ready to work out the fragile indices. First, we look at the inequality type. We notice that the first, fourth, fifth, sixth, and seventh inequalities in Eq. (A34) are identical to the inequalities in Eq. (A27) obtained from $B \geq 0$ and hence do not bring any new index. But the second, third, and last inequalities are not included in Eq. (A27). Therefore, we get three inequality-type fragile criteria as the second, third, and last inequalities in Eq. (A27) (for which k_2 solutions do not exist),

$$y_4 - y_2 - y_3 > 0, \tag{A35}$$

$$y_3 + y_4 - 2y_1 > 0, \tag{A36}$$

$$y_2 + y_4 - 2y_1 > 0. \tag{A37}$$

Now, we look at the $\mathbb{Z}_n$-type indices. First, let us derive the condition for k_2 to have fractional solutions but no integer solution. Equation (A33) can be thought of as the intersection of the following five equations:

$$\begin{aligned} &0 \leq k_2 \leq \min \\ &\times \left(\frac{1}{2}y_2, \frac{1}{2}y_2 + \frac{1}{2}y_3 - \frac{1}{2}y_4, y_1 - \frac{1}{2}y_3 - \frac{1}{2}y_4, y_1 - y_4\right), \end{aligned} \tag{A39}$$

$$\frac{1}{2}y_2 - \frac{1}{2}y_4 \leq k_2 \leq \frac{1}{2}y_2, \tag{A40}$$

$$\frac{1}{2}y_2 - \frac{1}{2}y_4 \leq k_2 \leq \frac{1}{2}y_2 + \frac{1}{2}y_3 - \frac{1}{2}y_4, \tag{A41}$$

$$\frac{1}{2}y_2 - \frac{1}{2}y_4 \leq k_2 \leq y_1 - \frac{1}{2}y_3 - \frac{1}{2}y_4, \tag{A42}$$

$$\frac{1}{2}y_2 - \frac{1}{2}y_4 \leq k_2 \leq y_1 - y_4. \tag{A43}$$

If Eq. (A39) has solutions, the solutions must contain the integer 0, which would *not* be a fractional solution of k_2 but an integer solution. Similarly, if Eq. (A43) has solutions, the solutions must contain the integer $y_1 - y_4$. Thus, neither Eq. (A39) nor Eq. (A43) can bring new indices since the bounds of these equations are integers, and we are looking for the case where no integer solution exists. Therefore, we only need to consider the cases where Eq. (A40), Eq. (A41), or Eq. (A42) has only fractional solutions but no integer solution. For Eq. (A40) to have no integer solution, we set the lower bound as a half integer and set the interval to be smaller than $\frac{1}{2}$, i.e., $y_2 - y_4 = 1 \mod 2$ and $0 \leq \frac{1}{2}y_2 - (\frac{1}{2}y_2 - \frac{1}{2}y_4) < \frac{1}{2}$. Considering that y's are integers, we can rewrite this condition as (A):

$$y_2 - y_4 = 1 \mod 2, \qquad y_4 = 0. \tag{A44}$$

Similarly, for Eqs. (A41) and (A42) to have no integer solution, we get (B),

$$y_2 - y_4 = 1 \mod 2, \qquad y_3 = 0, \tag{A45}$$

and (C),

$$y_2 - y_4 = 1 \mod 2, \qquad 2y_1 - y_2 - y_3 = 0, \tag{A46}$$

respectively. Then, we consider the case where k_2 can be an integer but k_1 cannot. The solution in Eq. (A30) can be thought of as the intersection of the following three solutions:

$$-\frac{1}{2}y_2-\frac{1}{2}y_3+\frac{1}{2}y_4\le k_1\le -k_2, \tag{A47}$$

$$-\frac{1}{2}y_2-\frac{1}{2}y_3+\frac{1}{2}y_4\le k_1\le -k_2-\frac{1}{2}y_3+\frac{1}{2}y_4, \tag{A48}$$

$$-y_1+y_4\le k_1\le \min\left(-k_2,-k_2-\frac{1}{2}y_3+\frac{1}{2}y_4\right). \tag{A49}$$

Since we are looking for noninteger solutions, Eqs. (A47) and (A49) cannot bring new indices because, if they have solutions, they must have integer solutions. (If there is an integer solution, then there is always at least one way of writing B as a sum of EBRs with non-negative coefficients.) For example, when Eq. (A47) has solutions, $-k_2$ must be a solution; when Eq. (A49) has solutions, $-y_1+y_4$ must be a solution. Thus, we only need to consider the case where Eq. (A48) has no integer solution. We set the lower bound of Eq. (A48) as half integer, i.e., $-y_2-y_3+y_4=1 \mod 2$, and set the interval to be smaller than $\frac{1}{2}$, i.e., $-k_2-\frac{1}{2}y_3+\frac{1}{2}y_4-(-\frac{1}{2}y_2-\frac{1}{2}y_3+\frac{1}{2}y_4)=-k_2+\frac{1}{2}y_2<\frac{1}{2}$ for an arbitrary integer k_2 allowed by Eq. (A33). The interval smaller than $\frac{1}{2}$ condition can be equivalently written as $\frac{1}{2}y_2-\frac{1}{2}<\min(k_2)$.

Because of Eq. (A33), $\min(k_2)$ can be either 0 or $\lceil(y_2-y_4)/2\rceil$. Because of Eq. (A33), $\min(k_2)$ can be either 0 or $\lceil(y_2-y_4)/2\rceil$: (D) If $y_2-y_4\le 0$, then $\min(k_2)=0$, (E) if $y_2-y_4\ge 0$ and $y_2-y_4=0 \mod 2$, then $\min(k_2)=\frac{1}{2}(y_2-y_4)$, and (F) if $y_2-y_4\ge 0$ and $y_2-y_4=1 \mod 2$, then $\min(k_2)=\frac{1}{2}(y_2-y_4)+\frac{1}{2}$. Case (D) with the condition $\frac{1}{2}y_2-\frac{1}{2}<\min(k_2)$ implies $y_2<1$ and $y_4\ge 0$ ($y_4\ge 0$ is already contained in Eq. (A27). Since $y_2\ge 0$ [Eq. (A27)], we have $y_2=0$ and the fragile criterion

$$-y_2-y_3+y_4=1 \mod 2, \qquad y_2=0. \tag{A50}$$

Case (E) with the condition $\frac{1}{2}y_2-\frac{1}{2}<\min(k_2)$ implies $y_4<1$ and $y_2\ge y_4$. Since $y_4\ge 0$ [Eq. (A27)], we have $y_4=0$ and $y_2\ge 0$ [$y_2\ge 0$ is already contained in Eq. (A27)]. Thus, the fragile criterion is

$$\begin{aligned}-y_2-y_3+y_4&=1 \mod 2,\\ y_2-y_4&=0 \mod 2, \qquad y_4=0.\end{aligned} \tag{A51}$$

Case (F) with the condition $\frac{1}{2}y_2-\frac{1}{2}<\min(k_2)$ implies $y_4<2$ and $y_2\ge y_4$. Since $y_4\ge 0$ [Eq. (A27)], we have $y_4=0$, 1. For $y_4=0$, we have $y_2\ge 0$, and the fragile criterion is

$$\begin{aligned}-y_2-y_3+y_4&=1 \mod 2,\\ y_2-y_4&=1 \mod 2, \qquad y_4=0.\end{aligned} \tag{A52}$$

For $y_4=1$, we have $y_2\ge 1$, and the fragile criterion is

$$\begin{aligned}-y_2-y_3+y_4&=1 \mod 2,\\ y_2-y_4&=1 \mod 2, \qquad y_4=1.\end{aligned} \tag{A53}$$

Therefore, Eqs. (A44)–(A46) and (A50)–(A53) are all the $\mathbb{Z}_2$-type criteria in SG 143.

APPENDIX B: FRAGILE PHASES AS AFFINE MONOIDS

1. Examples of Y and X

Here, we take Y of SG 150 as an example to show the two representations of the polyhedral cone. Because of Eq. (A4), the H-representation of Y can be written as

$$Y=\{y\in\mathbb{R}^3 | y_1\ge y_2, y_1\ge y_3, y_2\ge 0, y_3\ge 0\}. \tag{B1}$$

As shown in Fig. 6, the two-dimensional faces of the polyhedral cone are the subsets of Y where a single inequality is saturated, and the one-dimensional faces, or the rays, of the polyhedral cone are where two of the inequalities are saturated. To be specific, for the six pairs of the four inequalities in Eq. (B1), we set (i) $y_1=y_2=y_3$ and $y_1\ge 0$, (ii) $y_1=y_2=0$ and $0\ge y_3\ge 0$ (or $y_3=0$), (iii) $y_1=y_2$ and $y_3=0$ and $y_2\ge 0$, (iv) $y_1=y_3$ and $y_2=0$ and $y_1\ge 0$, (v) $y_1=y_3=0$ and $0\ge y_2\ge 0$, and

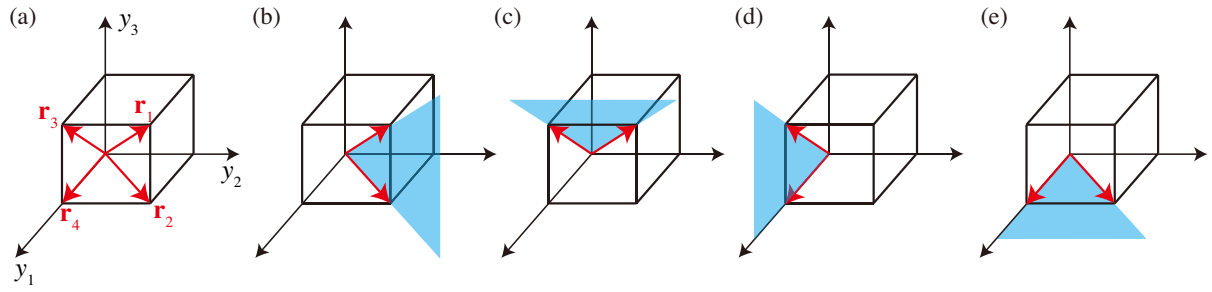

FIG. 6. The rays and boundary planes in the polyhedral cone Y in SG 150. (a) $\mathbf{r}_1=(1,1,1)^T$, $\mathbf{r}_2=(1,1,0)^T$, $\mathbf{r}_3=(1,0,1)^T$, $\mathbf{r}_4=(1,0,0)^T$. (b) The $y_1-y_2=0$ plane; (c) the $y_1-y_3=0$ plane; (d) the $y_2=0$ plane; and (e) the $y_3=0$ plane.

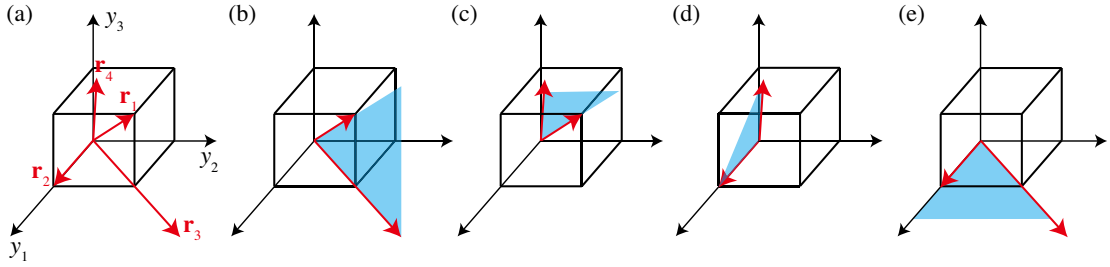

FIG. 7. The rays and boundary planes in the polyhedral cone X in SG 150. (a) $\mathbf{r}_1 = (1,1,1)^T$, $\mathbf{r}_2 = (1,0,0)^T$, $\mathbf{r}_3 = (2,2,0)^T$, $\mathbf{r}_4 = (2,1,2)^T$. (b) The $y_1 - y_2 = 0$ plane; (c) the $y_1 - y_3 = 0$ plane; (d) the $2y_2 - y_3 = 0$ plane; and (e) the $y_3 = 0$ plane.

(vi) $y_2 = y_3 = 0$ and $y_1 \geq 0$; we find that (i), (iii), (iv), and (vi) are rays, and (ii) and (v) are points. Therefore, the ray matrix in the V-representation of Y is given by

$$\text{Ray} = \begin{pmatrix} 1 & 1 & 1 & 1 \\ 1 & 1 & 0 & 0 \\ 1 & 0 & 1 & 0 \end{pmatrix}. \tag{B2}$$

Here, we take X in SG 150 as another example to show the two representations of the polyhedral cone. The rays of X are given by the first r rows of each column of the R matrix in Eq. (A2), as shown in Fig. 7(a). Because of Theorem 4, there will be an H-representation of X. Let us work out the H-representation. As $R_{1:r,:}$ is a 3×4 matrix [Eq. (A2)], X has four rays, where each pair sets a plane: (i) The first two rays set the plane $y_2 - y_3 = 0$, (ii) the first and the third set $y_1 - y_2 = 0$ [Fig. 7(b)], (iii) the first and the last set $y_1 - y_3 = 0$ [Fig. 7(c)], (iv) the second and the third set $y_3 = 0$ [Fig. 7(d)], (v) the second and the last set $2y_2 - y_3 = 0$ [Fig. 7(e)], and (vi) the last two set $2y_1 - 2y_2 + y_3 = 0$. We can directly verify that (ii)–(v) are boundaries of X, whereas (i) and (vi) are not. For example, all points (except the origin) on the third ray and the fourth ray satisfy $y_2 - y_3 > 0$ and $y_2 - y_3 < 0$, respectively; because the points on the rays are on different sides of the $y_2 - y_3 = 0$, $y_2 - y_3 = 0$ is not a boundary. On the other hand, all the rays satisfy $y_1 - y_2 \geq 0$; thus, $y_1 - y_2 = 0$ is a boundary. Therefore, we obtain

$$X = \{y \in \mathbb{R}^3 | y_1 \geq y_2, y_1 \geq y_3, 2y_2 - y_3 \geq 0, y_3 \geq 0\}. \tag{B3}$$

2. Hilbert bases of $\bar{Y}$ and EFP roots

An affine monoid M is called *positive* if $\forall\, a, b \in M - \{0\} \Rightarrow a + b \neq 0$. Theorem 7 in Appendix F tells us that the intersection of a pointed polyhedral cone and the integer lattice is a positive monoid. Therefore, $\bar{Y}$ is indeed a positive affine monoid. Since $\bar{X}$ is a subset of $\bar{Y}$, $\bar{X}$ is also a positive affine monoid.

Because of Theorem 6, any positive affine monoid has a unique minimal set of generators, called the Hilbert bases. All the elements in the monoid can be written as a sum of the Hilbert bases with positive coefficients. It should be noticed that none of the Hilbert basis can be written as a sum of other nonzero elements in the positive affine monoid with positive coefficients. As shown in the following examples, in some cases, the vectors of the Hilbert bases are linearly dependent on each other, but writing any one of them as a linear combination of others will involve negative coefficients. Here, we divide the Hilbert bases into two parts: the fragile phase bases and the trivial bases. The trivial bases actually correspond to EBRs because they are trivial (BR) and cannot be written as a sum of other elements with positive coefficients (elementary basis). We call the fragile phase bases EFP roots. From the aspect of symmetry data, the fragile roots are the "representative" phases of EFPs, as any EFP can be obtained by either stacking the roots or stacking the roots with EBRs (trivial bands).

Example.—We take Y in SG 150 as an example to derive the Hilbert bases. The Y polyhedron is given in Eq. (B1). To derive the Hilbert bases, we further divide the points in $\bar{Y}$ into two cases: (i) $0 \leq y_3 \leq y_2 \leq y_1$, (ii) $0 \leq y_2 \leq y_3 \leq y_1$. For case (i), we can rewrite the y vector as

$$y = \begin{pmatrix} y_1 \\ y_2 \\ y_3 \end{pmatrix} = y_3 \begin{pmatrix} 1 \\ 1 \\ 1 \end{pmatrix} + (y_2 - y_3) \begin{pmatrix} 1 \\ 1 \\ 0 \end{pmatrix} + (y_1 - y_2) \begin{pmatrix} 1 \\ 0 \\ 0 \end{pmatrix}. \tag{B4}$$

For case (ii), we can rewrite the y vector as

$$y = \begin{pmatrix} y_1 \\ y_2 \\ y_3 \end{pmatrix} = y_2 \begin{pmatrix} 1 \\ 1 \\ 1 \end{pmatrix} + (y_3 - y_2) \begin{pmatrix} 1 \\ 0 \\ 1 \end{pmatrix} + (y_1 - y_3) \begin{pmatrix} 1 \\ 0 \\ 0 \end{pmatrix}. \tag{B5}$$

Therefore, there are four Hilbert bases:

$$b_1 = \begin{pmatrix} 1 \\ 1 \\ 1 \end{pmatrix}, \quad b_2 = \begin{pmatrix} 1 \\ 0 \\ 0 \end{pmatrix}, \quad b_3 = \begin{pmatrix} 1 \\ 1 \\ 0 \end{pmatrix}, \quad b_4 = \begin{pmatrix} 1 \\ 0 \\ 1 \end{pmatrix}, \tag{B6}$$

where b_1, b_2, b_3, b_4 are also the rays of the polyhedral cone Y [Eq. (B2)]. The four bases are linearly dependent, but they are not redundant for the monoid as none of them can be written as a sum of the other three with positive coefficients. To be specific, $b_1 = b_3 + b_4 - b_2$, $b_2 = b_3 + b_4 - b_1$, $b_3 = b_1 + b_2 - b_4$, $b_4 = b_1 + b_2 - b_3$. Applying the fragile criteria of SG 150, i.e., Eqs. (A9) and (A13)–(A15) to be four bases, we find that b_1 and b_2 are trivial, b_3 satisfies the $\mathbb{Z}_2$-type criterion in Eq. (A13), and b_4 satisfies the inequality-type criterion in Eq. (A9). In fact, b_1 and b_3 are the first and second columns of the right transformation matrix R (the first three rows) in the Smith decomposition of the EBR matrix [Eq. (A2)], respectively, and thus present two EBRs of SG 150. Therefore, SG 150 has only two EFP roots: b_3 and b_4.

There are two commonly used algorithms to calculate the Hilbert bases of a positive affine monoid, i.e., the Normaliz algorithm [79] and the Hemmecke algorithm [80], which are available in the Normaliz package and the 4ti2 package, respectively. In this work, we mainly use the 4ti2 package to solve the Hilbert bases. Applying this algorithm for each $\bar{Y}$, we are able to calculate all the fragile roots in all SGs, as tabulated in Table S3 of Ref. [74]. In Table 1 in the main text, we summarized the numbers of fragile roots in all the SGs.

3. Hilbert bases of $\mathbb{Z}^r \cap X$

As introduced in Sec. IV A, $\bar{X} = \{y \in \mathbb{Z}^r | y_i = (Rp)_i, p \in \mathbb{N}^{N_{\mathrm{EBR}}}\}$ represent all the trivial points in Y. Thus, the fragile phases are represented by points in $\bar{Y} - \bar{X}$. For convenience, we introduce the auxiliary polyhedral cone $X = \{y \in \mathbb{R}^r | y_i = (Rp)_i, p \in \mathbb{R}^{N_{\mathrm{EBR}}}\}$ and divide the points in $\bar{Y} - \bar{X}$ into $\bar{Y} - \mathbb{Z}^r \cap X$ and $\mathbb{Z}^r \cap X - \bar{X}$. Here, we discuss a special issue of the Hilbert bases of $\mathbb{Z}^r \cap X$, which will be used in deriving the fragile indices in Appendix C 2. A basis $b_l \in \mathrm{Hil}(\mathbb{Z}^r \cap X)$ is either trivial ($\in \bar{X}$) or nontrivial ($\notin \bar{X}$), depending on whether it can be written as a sum of columns of $R_{1:r,:}$, i.e., $\exists q_l \in \mathbb{N}^{N_{\mathrm{EBR}}}$ s.t. $b_l = R_{1:r,:} q_l$. Now, we define the order of b_l as the smallest positive integer κ_l that makes $\kappa_l b_l \in \bar{X}$. We first consider the solutions of the equation $b_l = R_{1:r,:} q_l$, where q_l is a vector with N_{EBR} components. The general solution of $b_l = R_{1:r,:} q_l$ is given as $q_l = \sum_i^r (b_l)_i R_i^{-1} + \sum_{j=1}^{N_{\mathrm{EBR}}-r} k_j R_{j+r}^{-1}$, where R_i^{-1} is the ith column of R^{-1}, r is the rank of the EBR matrix, and k's are free parameters. For convenience, we introduce the auxiliary polyhedron

$$K_l = \left\{ k \in \mathbb{Q}^{N_{\mathrm{EBR}}} | \sum_i^r (b_l)_i R_i^{-1} + \sum_{j=1}^{N_{\mathrm{EBR}}-r} k_j R_{j+r}^{-1} \geq 0 \right\}. \tag{B7}$$

Notice that R is a unimodular matrix; thus, $q_l \in \mathbb{N}^r \Leftrightarrow k \in \mathbb{Z}^{N_{\mathrm{EBR}}-r}$. If K_l contains integer points, we can take an integer point in it, k, such that the corresponding $q_l \in \mathbb{N}^r$, and hence $b_l = R_{1:r,:} q_l$, is a combination with non-negative coefficients of columns in $R_{1:r,:}$. If K_l contains only fractional points but no integer point, the corresponding q_l's are non-negative but fractional, and hence b_l can only be written as a combination with non-negative fractional coefficients of columns in $R_{1:r,:}$. For this second case, we can introduce a (minimal) positive integer κ_l such that $\kappa_l K_l$, i.e.,

$$\kappa_l K_l = \{\kappa_l k | k \in K_l\}, \tag{B8}$$

contains at least one integer point. Such a κ_l always exists: Suppose k is a fractional vector in K_l; then, we can take κ_l as the least common multiplier of the denominators of the components of k such that $\kappa_l k$ is an integer vector. We always choose κ_l as the minimal integer such that $\kappa_l K_l$ contains at least one integer point. Here, κ_l can be thought of as the "order" of a nontrivial Hilbert basis because $\kappa_l b_l$ can be written as a combination with non-negative integer coefficients of columns in $R_{1:r,:}$ and hence belongs to $\bar{X}$.

Example.—Now, we derive the Hilbert bases of $\mathbb{Z}^3 \cap X$ in SG 150. Note that X is shown in Fig. 7, and its H-representation is derived in Eq. (B3). To derive the Hilbert bases, we further divide the points in $\mathbb{Z}^3 \cap X$ into two cases: (i) $y_2 - y_3 \geq 0$ and (ii) $y_2 - y_3 \leq 0$. For case (i), we can rewrite the y vector as

$$y = \begin{pmatrix} y_1 \\ y_2 \\ y_3 \end{pmatrix} = y_3 \begin{pmatrix} 1 \\ 1 \\ 1 \end{pmatrix} + (y_2 - y_3) \begin{pmatrix} 1 \\ 1 \\ 0 \end{pmatrix} + (y_1 - y_2) \begin{pmatrix} 1 \\ 0 \\ 0 \end{pmatrix}. \tag{B9}$$

The three bases in case (i) are the same as the bases in case (i) of $\bar{Y}$ [Eq. (B4)]. For case (ii), where $y_2 - y_3 \leq 0$, we can rewrite the y vector as

$$y = \begin{pmatrix} y_1 \\ y_2 \\ y_3 \end{pmatrix} = (y_1 - y_3) \begin{pmatrix} 1 \\ 1 \\ 1 \end{pmatrix} + (2y_2 - y_3) \begin{pmatrix} 1 \\ 0 \\ 0 \end{pmatrix} + (y_3 - y_2) \begin{pmatrix} 2 \\ 1 \\ 2 \end{pmatrix}. \tag{B10}$$

The three bases in case (ii), where $y_2 - y_3 \leq 0$, are different than the bases in case (ii) of $\bar{Y}$ [Eq. (B5)] because here we cannot decompose y into $(1,0,1)^T$ since $(1,0,1)^T \notin \bar{X}$. Therefore, there are four Hilbert bases:

$$b_1 = \begin{pmatrix} 1 \\ 1 \\ 1 \end{pmatrix}, \quad b_2 = \begin{pmatrix} 1 \\ 0 \\ 0 \end{pmatrix}, \quad b_3 = \begin{pmatrix} 1 \\ 1 \\ 0 \end{pmatrix}, \quad b_4 = \begin{pmatrix} 2 \\ 1 \\ 2 \end{pmatrix}, \tag{B11}$$

where b_1, b_2, and b_4 are the (first three rows of the) columns of R [Eq. (A2)] and hence are trivial. On the other hand, b_3 is half of the (first three rows of the) third column in R. Thus, we obtain $\kappa_1 = \kappa_2 = \kappa_4 = 1$ and $\kappa_3 = 2$. To check, we calculate κ_3 using the algorithm described in the last paragraph. The inverse of the R matrix [Eq. (A2)] is

$$R^{-1} = \begin{pmatrix} 0 & 2 & -1 & 4 \\ 1 & 0 & -1 & 2 \\ 0 & 0 & 0 & -1 \\ 0 & -1 & 1 & -2 \end{pmatrix}, \tag{B12}$$

and hence, because of Eq. (B7), we obtain

$$K_3 = \{k \in \mathbb{Q} | 2 + 4k \geq 0, 1 + 2k \geq 0, -k \geq 0, -1 - 2k \geq 0\} = \left\{-\frac{1}{2}\right\}. \tag{B13}$$

Therefore, $\kappa_3 = 2$ is the minimal integer that makes $\kappa_3 K_3$ have an integer point.

APPENDIX C: FRAGILE INDICES

1. Removing unallowed inequality-type indices

In Sec. IV B, we have introduced the general method to derive inequality-type criteria in the form of $ay < 0$. Here, we describe how to judge whether $ay < 0$ is allowed. For a given row a in A, we define $Y' = \{y \in \mathbb{R}^r | L\Lambda_{:,1:r} y \geq 0 \text{ and } ay < 0\}$. Notice that Y' is an open set (due to the condition $ay < 0$). (A set is open if it does not contain any of its boundary points.) Clearly, $Y' = \varnothing$ implies that $ay < 0$ is not allowed in Y. However, we do not use Y' in practical calculations because it is complicated to store and process an open set in our group calculations; instead, we make use of the closed extension of Y', i.e., $Y'' = \{y \in \mathbb{R}^r | \binom{L\Lambda_{:,1:r}}{-a} y \geq 0\}$. Since Y'' is a superset of Y', obviously, $Y'' = \varnothing \Rightarrow Y' = \varnothing$. Thus, $Y'' = \varnothing$ implies $ay < 0$ is forbidden by the $B \geq 0$ condition. Now, we show how to detect the case $Y' = \varnothing$ but $Y'' \neq \varnothing$. We notice that $Y' = \varnothing$ implies that $Y'' = Y'' - Y' = \{y \in \mathbb{R}^r | L\Lambda_{:,1:r} y \geq 0 \text{ and } ay = 0\} \neq \varnothing$. The presence of equation $ay = 0$ will reduce the dimension of the polyhedron. Thus, this case can be diagnosed by $\dim(Y'') < r$.

Example.—In the paragraphs above, we have described a general algorithm to derive the inequality-type fragile criteria. As an example, here we rederive the inequality-type fragile criteria of SG 150 using the polyhedron method. The polyhedral cone Y is given by Eq. (B1), and the polyhedral cone X is given by Eq. (B3). We rewrite Eq. (B3) in terms of the A matrix as

$$X = \{y \in \mathbb{R}^3 | Ay \geq 0\}, \qquad A = \begin{pmatrix} 1 & -1 & 0 \\ 1 & 0 & -1 \\ 0 & 2 & -1 \\ 0 & 0 & 1 \end{pmatrix}. \tag{C1}$$

The four rows in A correspond to four possible inequality-type fragile indices, i.e., $y_2 - y_1$, $y_3 - y_1$, $y_3 - 2y_2$, and $-y_3$, the positive values of which imply fragile phases. However, the first, second, and last inequalities are not allowed in Y. For the first index $y_2 - y_1$, the auxiliary polyhedral cone $Y'' = \{y_1 \geq y_2, y_1 \geq y_3, y_2 \geq 0, y_3 \geq 0, y_2 - y_1 \geq 0\} = \{y_1 = y_2, y_1 \geq y_3, y_2 \geq 0, y_3 \geq 0\}$ has a dimension 2 (<3), implying $y_2 - y_1 > 0$ is not allowed in Y. For the second index $y_3 - y_1$, the auxiliary polyhedral cone $Y'' = \{y_1 \geq y_2, y_1 = y_3, y_2 \geq 0, y_3 \geq 0\}$ has a dimension 2 (<3), implying $y_3 - y_1 > 0$ is not allowed in Y. For the last index $-y_3$, the auxiliary polyhedral cone $Y'' = \{y_1 \geq y_2, y_1 \geq y_3, y_2 \geq 0, y_3 = 0\}$ has a dimension 2 (<3), implying $-y_3 > 0$ is not allowed in Y, so the corresponding fragile index is not necessary. Therefore, the only inequality-type index is $y_3 - 2y_2$, consistent with the result [Eq. (A9)] in Appendix A 1.

2. $\mathbb{Z}_2$-type fragile indices

In this subsection, we consider the type-II fragile phases, i.e., symmetry data vectors represented by points in $\mathbb{Z}^r \cap X - \bar{X}$, and derive the corresponding $\mathbb{Z}_n$-type fragile criteria. It turns out that all the $\mathbb{Z}_n$-type criteria are of $\mathbb{Z}_2$ type.

a. $\mathbb{Z}^r \cap X - \bar{X}$ is close to the boundary of X

A key property allowing us to derive the general $\mathbb{Z}_n$ indices is that the points in $\mathbb{Z}^r \cap X - \bar{X}$ are all close to the boundaries of X, as will be explained more clearly below. Here, we present a heuristic description of this conclusion and leave the proof for the following paragraphs. As we will prove, there always exists a finite integer vector $\Delta y \in \bar{X}$ such that for $\forall\, y \in \mathbb{Z}^r \cap X - \bar{X}$, $y + \Delta y \in \bar{X}$. In other words, the shifted monoid $\Delta y + \mathbb{Z}^r \cap X = \{y + \Delta y | y \in \mathbb{Z}^r \cap X\}$ is a subset of $\bar{X}$ and hence

$$\Delta y + \mathbb{Z}^r \cap X \subset \bar{X} \Rightarrow \mathbb{Z}^r \cap X - \bar{X} \subset \mathbb{Z}^r \cap X - (\Delta y + \mathbb{Z}^r \cap X) = \mathbb{Z}^r \cap (X - (\Delta y + X)); \tag{C2}$$

i.e., $X - (\Delta y + X)$ is a superset of $\mathbb{Z}^r \cap X - \bar{X}$. We show that $X - (\Delta y + X)$ is close to the boundary of X. We assume that X has the H-representation $X = \{y \in \mathbb{R}^r | Ay \geq 0\}$; then, if $x \in \Delta y + X$, we have $x - \Delta y \in X$ and hence $A(x - \Delta y) \geq 0$. Thus, we obtain the H-representation of $\Delta y + X$,

$$\Delta y + X = \{y \in \mathbb{R}^r | A(y - \Delta y) \geq 0\}, \tag{C3}$$

and hence obtain $X - (\Delta y + X)$ as

$$X - (\Delta y + X) = \{y \in \mathbb{R}^r | Ay \geq 0, \quad \text{and} \quad \exists\, i, \text{s.t.} (Ay)_i < (A\Delta y)_i\}. \tag{C4}$$

Since the ith boundary of X is given by $(Ay)_i = 0$, for a given point y, $(Ay)_i$ can be thought of as the distance from y to the ith boundary of X. Equation (C4) means that for $\forall\, y \in X - (\Delta y + X)$, there always exists some boundary of X such that the distance from y to this boundary is smaller than the distance from Δy (the existence of which we will prove) to this boundary. Thus, the point $X - (\Delta y + X)$ is close to the boundary of X.

Before proving the existence of Δy, here we first study the property of points in $\mathbb{Z}^r \cap X$. Note that $\mathbb{Z}^r \cap X$ is generated from the so-called Hilbert bases, denoted as $\text{Hil}(\mathbb{Z}^r \cap X)$ (Theorem 6 in Appendix F). To be specific, we can rewrite $\mathbb{Z}^r \cap X$ as

$$\mathbb{Z}^r \cap X = \{y = b_1 p_1 + b_2 p_2 + \cdots + b_{N_H} p_{N_H} | b_1, \; b_2 \cdots b_{N_H} \in \text{Hil}(\mathbb{Z}^r \cap X), p_1, p_2 \cdots p_{N_H} \in \mathbb{N}\}, \tag{C5}$$

where N_H is the number of Hilbert bases. As shown in Appendix B 3, for each basis b_l, there is a positive integer κ_l—the order of b_l—such that $\kappa_l b_l \in \bar{X}$ (a trivial point). With the concept of order κ_l of the Hilbert basis, we can decompose a general point in $\mathbb{Z}^r \cap X$ in Eq. (C5) into two parts:

$$y = \sum_l (p_l \bmod \kappa_l) b_l + \sum_l \lfloor p_l/\kappa_l \rfloor \kappa_l b_l, \tag{C6}$$

where $\lfloor a \rfloor$ is the largest integer equal to or smaller than a. The second part in this decomposition belongs to $\bar{X}$, by construction, since $\kappa_l b_l \in \bar{X}$ and $\lfloor p_l/\kappa_l \rfloor \in \mathbb{N}$. Therefore, to shift y to $\bar{X}$, we only need to shift the first part to $\bar{X}$.

Now, we prove the existence of Δy. As shown in Eq. (C6), the nontrivial part of any point in $\mathbb{Z}^r \cap X - \bar{X}$ is of the form $\sum_l (p_l \bmod \kappa_l) b_l$; thus, to shift it to $\bar{X}$, we only need Δy to satisfy

$$\forall\, p \in \mathbb{N}^{N_H}, \qquad \Delta y + \sum_l (p_l \bmod \kappa_l) b_l \in \bar{X}. \tag{C7}$$

As b_l represents either a trivial state (EBR) or an EFP, both of which can be written as an integer combination of EBRs, we can write b_l as $b_l = R_{1:r,:} q_l$ for some $q_l \in \mathbb{Z}^{N_H}$. If $b_l \in \bar{X}$, q_l can be a non-negative vector, whereas if $b_l \notin \bar{X}$, at least one component of q_l is negative. The choice of q_l is not unique. In general, q_l can be written as $\sum_{i=1}^{r} R_i^{-1} (b_l)_i + \sum_{j=1}^{N_{\text{EBR}}-r} R_j^{-1} k_j$, where R_i^{-1} is the ith column of the R^{-1} matrix, and k's are free parameters. For now, for each b_l, we just pick a specific q_l. We decompose q_l into two parts: the non-negative part q_l^+ and the negative part q_l^-, i.e.,

$$(q_l^+)_i = \begin{cases} (q_l)_i & \text{if } (q_l)_i \geq 0 \\ 0 & \text{if } (q_l)_i < 0, \end{cases} \qquad (q_l^-)_i = \begin{cases} 0 & \text{if } (q_l)_i \geq 0 \\ (q_l)_i & \text{if } (q_l)_i < 0. \end{cases} \tag{C8}$$

Then, we have

$$\Delta y + \sum_l (p_l \bmod \kappa_l) b_l = \Delta y + \sum_l (p_l \bmod \kappa_l) R_{1:r,:} q_l^+ + \sum_l (p_l \bmod \kappa_l) R_{1:r,:} q_l^-. \tag{C9}$$

Notice that p_l is a number, and q_l, q_l^+, and q_l^- are vectors. The second term in the right-hand side of Eq. (C9) is already in $\bar{X}$ as it is a non-negative integer combination of columns of $R_{1:r,:}$. Hence, Δy only needs to shift the third term in Eq. (C9) to $\bar{X}$. We can choose Δy as

$$\Delta y = -\sum_l (\kappa_l - 1) R_{1:r,:} q_l^- \tag{C10}$$

such that

$$\Delta y + \sum_l (p_l \bmod \kappa_l) R_{1:r,:} q_l^- = \sum_l ((p_l \bmod \kappa_l) - \kappa_l + 1) R_{1:r,:} q_l^- \tag{C11}$$

is always a non-negative integer combination of columns of $R_{1:r,:}$ because $(p_l \bmod \kappa_l) - \kappa_l + 1 \leq 0$ and hence $((p_l \bmod \kappa_l) - \kappa_l + 1) q_l^- \geq 0$. Therefore, Δy defined in Eq. (C10) satisfies the condition in Eq. (C7).

Example.—Here, we take SG 199 as an example to show how to determine Δy. As discussed in the main text [Eq. (8)] and shown in Fig. 8, $\bar{X}$ is given as

$$\bar{X} = \{p_1 (0,2)^T + p_2 (1,2)^T + p_3 (1,3)^T | p_{1,2,3} \in \mathbb{N}\} = \{R_{1:r,:} p | p \in \mathbb{N}^3\}, \tag{C12}$$

where $R_{1:r,:}$ is given by [Eq. (4) in the main text]

$$R_{1:r,:} = \begin{pmatrix} 0 & 1 & 1 \\ 2 & 2 & 3 \end{pmatrix}. \tag{C13}$$

On the other hand, the polyhedron cone X, which is identical to Y [Eq. (6) in the main text], is given as

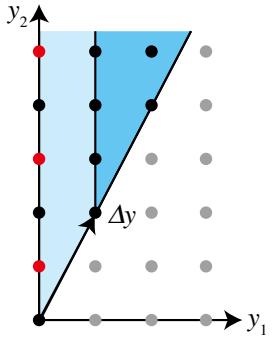

FIG. 8. The shift vector Δy in SG 199. Points in $\bar{X}$ are represented by the black dots, the polyhedral cone X is shaded light blue, the shifted polyhedral cone $\Delta y + X$ is shaded blue, and points in $\mathbb{Z}^2 \cap X - \bar{X}$ are represented by red dots. All the points in $\mathbb{Z}^2 \cap X - \bar{X}$ are in $X - (\Delta y + X)$ and are close to the boundary of X.

$$X = \{y \in \mathbb{R}^2 | y_2 \geq 2y_1 \geq 0\}. \tag{C14}$$

The inequality $y_1 \geq 0$ can be rewritten as $(1,0)y \geq 0$, and the inequality $y_2 \geq 2y_1$ can be rewritten as $(-2,1)y \geq 0$. Thus, X can be rewritten as

$$X = \{y \in \mathbb{R}^2 | Ay \geq 0\}, \qquad A = \begin{pmatrix} 1 & 0 \\ -2 & 1 \end{pmatrix}. \tag{C15}$$

For any point y in $\mathbb{Z}^2 \cap X$, we can decompose it as $y = y_1(1,2)^T + (y_2 - 2y_1)(0,1)^T$. Thus, the Hilbert bases of $\mathbb{Z}^2 \cap X$ are $b_1 = (0,1)^T$ and $b_2 = (1,2)^T$, and the monoid $\mathbb{Z}^r \cap X$ is

$$\mathbb{Z} \cap X = \{p_1(0,1)^T + p_2(1,2)^T | p_{1,2} \in \mathbb{N}\}. \tag{C16}$$

On the other hand, $\bar{X}$ can be obtained by adding the (first two rows of the) columns of R in Eq. (C13), i.e., $\bar{X} = \{p_1(0,2)^T + p_2(1,2)^T + p_3(1,3)^T | p_{1,2,3} \in \mathbb{N}\}$ (Fig. 8). As shown in Fig. 8 and proved in the main text [around Eq. (9)], the set $\mathbb{Z}^r \cap X - \bar{X}$ is given as

$$\begin{aligned} \mathbb{Z}^r \cap X - \bar{X} &= \{(0, 2p+1)^T | p \in \mathbb{N}\} \\ &= \{(0,1)^T, (0,3)^T, (0,5)^T \cdots\}. \end{aligned} \tag{C17}$$

One can immediately observe that the vector $\Delta y = (1,2)^T$ shifts all the points in $\mathbb{Z}^r \cap X - \bar{X}$ to $\bar{X}$, e.g., $(0,1) \to (1,3)^T$, $(0,3) \to (1,5)^T$, $(0,5) \to (1,7)^T$, etc.

Now, let us pretend that we do not know Δy and use the algorithm described in the last paragraph to determine Δy. Twice b_1 belongs to $\bar{X}$ [Eq. (C12)], and hence $\kappa_1 = 2$; b_2 is already in $\bar{X}$, and hence $\kappa_2 = 1$. To obtain the q_l^+ and q_l^- [Eq. (C8)], which will be used to determine Δy, we write b_1, b_2 in terms of columns of $R_{1:r,:}$ with integer coefficients as

$$\begin{aligned} b_1 &= (1,3)^T - (1,2)^T = R_{1:r,1}(0,-1,1)^T, \\ b_2 &= (1,2)^T = R_{1:r,1}(0,1,0)^T, \end{aligned} \tag{C18}$$

i.e., $q_1 = (0,-1,1)^T$ and $q_2 = (0,1,0)^T$. Because of Eq. (C8), $q_1^- = (0,-1,0)^T$, $q_2^- = 0$. Then, according to Eq. (C9), we obtain

$$\Delta y = -(\kappa_1 - 1) R_{1:r,:} q_1^- = (1,2)^T, \tag{C19}$$

which is identical to direct observation. Finally, let us verify Eq. (C4). The distances from Δy to the first and second boundaries are $(A\Delta y)_1 = 1$ and $(A\Delta y)_2 = 0$, respectively. Thus, Eq. (C4) can be written as $X - (\Delta y + X) = \{y \in \mathbb{R}^4 | Ay \geq 0, (Ay)_1 < 1\} = \{y \in \mathbb{R}^4 | 0 \leq y_1 < 1, -2y_1 + y_2 \geq 0\}$, which is consistent with Fig. 8.

Example.—We take SG 150 as a nontrivial example to show how to determine Δy. The $R_{1:r,:}$ matrix can be directly read from Eq. (A2). Thus, we can write $\bar{X}$ as

$$\bar{X} = \{R_{1:r,:} p | p \in \mathbb{N}^4\}, \qquad R_{1:r,:} = \begin{pmatrix} 1 & 1 & 2 & 2 \\ 1 & 0 & 2 & 1 \\ 1 & 0 & 0 & 2 \end{pmatrix}. \tag{C20}$$

On the other hand, from the example analyses in Secs. IV A and IV B and Appendix B 3, we obtain the H-representation of X as Eqs. (B3) and (C1), and the four Hilbert bases of $\mathbb{Z}^3 \cap X$ as $b_1 = (1,1,1)^T$, $b_2 = (1,0,0)$, $b_3 = (1,1,0)^T$, and $b_4 = (2,1,2)^T$ [Eq. (B11)], respectively. Note that b_1, b_2, b_4 are the first, second, and fourth columns of $R_{1:r,:}$ shown in Eq. (C20) and hence belong to $\bar{X}$. Thus, we have the order $\kappa_1 = \kappa_2 = \kappa_4 = 1$. Here, b_3 is half of the second column of $R_{1:r,:}$ and thus the order $\kappa_3 = 2$. To obtain q_3^+ and q_3^- [Eq. (C8)], which will be used to determine Δy, we write b_3 as an integer combination of the columns of $R_{1:r,:}$ as

$$b_3 = 2\begin{pmatrix} 1 \\ 1 \\ 1 \end{pmatrix} + \begin{pmatrix} 1 \\ 0 \\ 0 \end{pmatrix} - \begin{pmatrix} 2 \\ 1 \\ 2 \end{pmatrix} = R_{1:r,:} q_3, \tag{C21}$$

with

$$q_3 = (2,1,0,-1)^T. \tag{C22}$$

Because of Eq. (C8), we have $q_3^- = (0,0,0-1)^T$. According to Eq. (C10), we have

$$\Delta y = -(\kappa_3 - 1) R_{1:r,:} q_3^- = (2,1,2)^T. \tag{C23}$$

Now, we calculate the distances from Δy to the boundaries of X. Using the A matrix in Eq. (C1), we obtain that (i) distance from Δy to the boundary $y_1 - y_2 = 0$ is

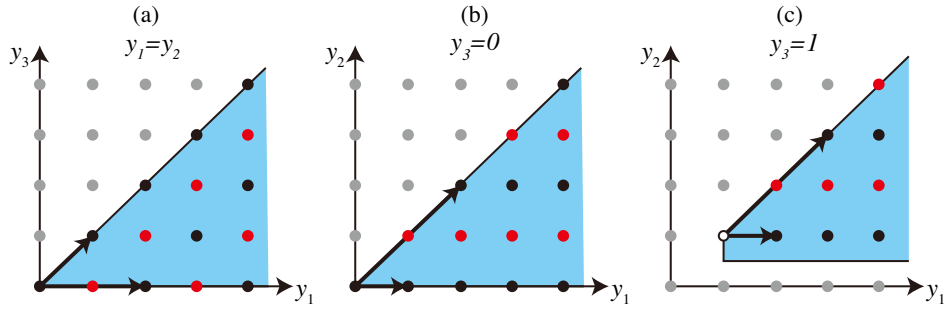

FIG. 9. $W^{(i,d)}$'s in SG 150. (a) $W^{(1,0)}$ in the $y_1 = y_2$ plane. (b) $W^{(4,0)}$ in the $y_3 = 0$ plane. In panels (a) and (b), the polyhedral cone $W^{(i,0)}$ is represented by the shaded area, the generators of $\bar{W}^{(i,0)}$ are represented by the bold black arrows, the points in $\bar{W}^{(i,0)}$ are represented by black dots, and the points in $\mathbb{Z}^3 \cap W^{(i,0)} - \bar{W}^{(i,0)}$ are represented by red dots. (c) $W^{(4,1)}$ in the $y_3 = 1$ plane. The polyhedron $W^{(4,1)}$ is represented by the shaded area, the points (only one) in the set $\bar{V}^{(4,1)}$ are represented by the hollow circle, the points in $\bar{W}^{(4,1)}$ are represented by black dots, and the points in $\mathbb{Z}^3 \cap W^{(4,1)} - \bar{W}^{(4,1)}$ are represented by red dots.

$(Ay)_1 = 2 - 1 = 1$, (ii) distance from Δy to the boundary $y_1 - y_3 = 0$ is $(Ay)_2 = 2 - 2 = 0$, (iii) distance from Δy to the boundary $2y_2 - y_3 = 0$ is $(Ay)_3 = 2 - 2 = 0$, and (iv) distance from Δy to the boundary $y_3 = 0$ is $(Ay)_4 = 2$. This means the points in $\mathbb{Z}^r \cap X - \bar{X}$ satisfy either $y_1 - y_2 = 0$ or $y_3 = 0,\ 1$, which is consistent with Eqs. (A13)–(A15).

b. Determining the $\mathbb{Z}_2$-type indices

We emphasize that, in general, $X - (\Delta y + X)$ defined in Eq. (C4) is *not* a polyhedron because Eq. (C4) does not match the definition of the polyhedron in Theorem 3. For example, if we take X as $X = \{y \in \mathbb{R}^2 | y_1 \geq 0, y_2 \geq 0\}$ and $\Delta y = (1, 1)$, then $X - (\Delta y + X) = \{y \in \mathbb{R}^2 | 0 \leq y_1 \leq 1, y_2 \geq 0\} + \{y \in \mathbb{R}^2 | 0 \leq y_2 \leq 1, y_1 \geq 0\}$ is obviously not a polyhedron. Nevertheless, the integer points in $X - (\Delta y + X)$ belong to some lower-dimensional polyhedra, i.e.,

$$\mathbb{Z}^r \cap (X - (\Delta y + X)) = \bigoplus_i \bigoplus_{d=0}^{(A\Delta y)_i - 1} \mathbb{Z}^r \cap W^{(i,d)}, \tag{C24}$$

with

$$W^{(i,d)} = \{x \in \mathbb{R}^r | (Ax)_i = d \text{ and } Ax \geq 0\} \tag{C25}$$

a $(r-1)$-dimensional polyhedron. Since Δy shifts all the points in $\mathbb{Z}^r \cap X$ into $\bar{X}$, Eq. (C24) sums over all the lower-dimensional polyhedra close to the boundaries with distances up to the distances from Δy to the boundaries. By definition (Theorem 4 in Appendix F), the H-representation of a polyhedral cone consists of a set of inequalities and a set of homogeneous equations, i.e., $P = \{x \in \mathbb{R}^r | Ax \geq 0, Cx = 0\}$, with A some $n \times r$ matrix and C some $m \times r$ matrix for some n and m. Thus, $W^{(i,0)}$ is a polyhedral cone in the $d = 0$ subspace, but, in general, $W^{(i,d)}$ $(d > 0)$ is neither a polyhedral cone nor a shifted polyhedral cone, i.e., $v + P = \{A(x - v) \geq 0, C(x - v) = 0\}$. Here, $W^{(i,d)}$ is a shifted polyhedral cone only if we can find some $v \in \mathbb{R}^r$ such that $(Av)_j = \delta_{ij} d$, and hence $W^{(i,d)}$ can be written as $\{(A(x - v))_i = 0 \text{ and } A(x - v) \geq 0\}$. However, such a v does not exist in the general case where $d > 0$. For example, if $A_{j,:}$ $(j = 1 \cdots, i-1, i+1, \cdots r+1)$ are all linearly independent, then $v = 0$ due to $(Av)_j = 0$ $(j \neq i)$, which is in contradiction with the condition $(Av)_i = d$. In the example discussed at the end of this section, as shown in Fig. 9(c), $W^{(4,1)}$ is not a shifted polyhedral cone.

The trivial integer points in $W^{(i,d)}$ are given by

$$\begin{aligned}\bar{W}^{(i,d)} = \bar{X} \cap W^{(i,d)} = \{R_{1:r,:} p | p \in \mathbb{N}^{N_{\mathrm{EBR}}} \text{ and } (AR_{1:r,:} p)_i \\ = d \text{ and } AR_{1:r,:} p \geq 0\}.\end{aligned} \tag{C26}$$

As each column in $R_{1:r,:}$ represents a point in X and hence certainly satisfies the inequalities of X, i.e., $\forall\, j, AR_{1:r,j} \geq 0$, and $AR_{1:r,:} p \geq 0$ is redundant, we can rewrite $\bar{W}^{(i,d)}$ as

$$\bar{W}^{(i,d)} = \{R_{1:r,:} p | p \in \mathbb{N}^{N_{\mathrm{EBR}}} \text{ and } (AR_{1:r,:} p)_i = d\}. \tag{C27}$$

In the following, we derive the criterion for a point $x \in \mathbb{Z}^r \cap W^{(i,d)}$ not to belong to $\bar{W}^{(i,d)}$ (such that x represents a fragile state). We first consider the case $d = 0$. Because of Eq. (C27), the monoid $\bar{W}^{(i,0)}$ is generated from the columns of $R_{1:r,:}$ that satisfy $(Ax)_i = 0$. We denote the columns of $R_{1:r,:}$ satisfying $(Ac)_i = 0$ columns as $\{C_1^{(i)}, C_2^{(i)}, \cdots\}$. In principle, there are two kinds of points in $\mathbb{Z}^r \cap W^{(i,0)} - \bar{W}^{(i,0)}$, which include the points representing EFPs: (i) points that cannot be written as any integer combinations of $\{C_1^{(i)}, C_2^{(i)}, \cdots\}$ but can only be written as fractional combinations of $\{C_1^{(i)}, C_2^{(i)}, \cdots\}$, and (ii) points that can be written as some integer combinations of $\{C_1^{(i)}, C_2^{(i)}, \cdots\}$ but cannot be written as non-negative

integer combinations of $\{C_1^{(i)}, C_2^{(i)}, \cdots\}$. However, as will be explained in Appendix *C 3, case (ii) does not exist in practice. Thus, we only need to consider case (i). We denote the matrix consisting of the columns $\{C_1^{(i)}, C_2^{(i)}, \cdots\}$ as $C^{(i)}$, i.e., $C^{(i)} = (C_1^{(i)}, C_2^{(i)}, \cdots)$. Then, a point $x \in \mathbb{Z}^r \cap W^{(i,0)}$ belongs to case (i) only if $x = C^{(i)}p$ has *no* integer solution, where p is regarded as the variable. To see whether such integer solutions exist, here we apply the Smith decomposition technique again. We write $C^{(i)}$ as $C^{(i)} = L^{(i)}\Lambda^{(i)}R^{(i)}$, where $L^{(i)}$, $R^{(i)}$ are unimodular integer matrices, and $\Lambda^{(i)}$ is a diagonal integer matrix. Here, we assume the rank of C is $r^{(i)}$, and thus the first $r^{(i)}$ diagonal elements of $\Lambda^{(i)}$ are nonzero. (The Smith decomposition matrices of $C^{(i)}$ are indexed by i. One should not confuse them with the Smith decomposition matrices of the EBR matrix, i.e., $L\Lambda R$.) Then, the equation $x = C^{(i)}p$ has integer solutions only if

$$(L^{(i)-1}x)_j = 0 \mod \Lambda_{jj}^{(i)}, \quad \text{for } j \le r^{(i)} \tag{C28}$$

because, when Eq. (C28) is true, we can write the integer solution as

$$p_j = \sum_{k=1}^{r^{(i)}} R_{jk}^{(i)-1} \frac{1}{\Lambda_{kk}^{(i)}} (L^{(i)-1}x)_k. \tag{C29}$$

Therefore, we conclude that the fragile criterion to diagnose points in $\mathbb{Z}^r \cap W^{(i,0)} - \bar{W}^{(i,0)}$ is

$$(Ax)_i = 0, \quad \text{and} \quad \delta^{(i)}(x) \neq 0 \quad (\text{for } \Lambda_{jj}^{(i)} > 0), \tag{C30}$$

where $\delta^{(i)}(x)$ is a vector consisting of the $\mathbb{Z}_n$-type fragile indices

$$\delta_j^{(i)}(x) = (L^{(i)-1}x)_j \mod \Lambda_{jj}^{(i)}. \tag{C31}$$

As the components where the corresponding $\Lambda_{jj}^{(i)} = 1$ always vanish ($0 \bmod 1 = 0$, $1 \bmod 1 = 0$), in the following, we only keep the components where the corresponding $\Lambda_{jj}^{(i)} > 1$. In practice, $\Lambda_{jj}^{(i)} = 2$ is the only case where $\Lambda_{jj}^{(i)} > 1$. Thus, all the $\mathbb{Z}_n$-type indices are $\mathbb{Z}_2$-type indices.

Example.—Here, we take SG 199 as an example to show the algorithm described above. First, as discussed in the example in Appendix C 2 a and shown in Fig. 8, Δy is $(1,2)^T$. Its distance to the first boundary $y_1 = 0$ is $(A\Delta y)_1 = 1$, and its distance to the second boundary $y_2 - 2y_1 = 0$ is $(A\Delta y)_2 = 0$, where A is given in Eq. (C15). Because of Eq. (C24), we only need to consider the subpolyhedron $W^{(1,0)} = \{y \in \mathbb{R}^2 | (Ay)_1 = 0, (Ay)_2 \ge 0\}$, which, because of A in Eqs. (C15) and (C25), is given as

$$W^{(1,0)} = \{y \in \mathbb{R}^2 | y_1 = 0, y_2 \ge 0\}. \tag{C32}$$

It contains the integer points

$$\mathbb{Z}^2 \cap W^{(1,0)} = \{(0,0), (0,1), (0,2), \cdots\}. \tag{C33}$$

Among the three columns of $R_{1:r,:}$ [Eq. (C13)], only the first column satisfies $(Ac)_1 = 0$. Thus, due to Eq. (C27), $\bar{W}^{(1,0)}$, which represents trivial points in $W^{(1,0)}$, is given as

$$\bar{W}^{(1,0)} = \{p(0,2)^T | p \in \mathbb{N}\}, \tag{C34}$$

and the $C^{(1)}$ matrix is given as $C^{(1)} = (0,2)^T$. Following the algorithm described in last paragraph, we calculate the Smith decomposition of $C^{(1)}$,

$$C^{(1)} = L^{(1)}\Lambda^{(1)}R^{(1)} = \begin{pmatrix} 0 & 1 \\ 1 & 0 \end{pmatrix} \begin{pmatrix} 2 \\ 0 \end{pmatrix} (1). \tag{C35}$$

Substituting $L^{(1)}$, $\Lambda^{(1)}$, and Eq. (C15) into Eqs. (C30) and (C31), we obtain the fragile criterion

$$y_1 = 0, \quad \text{and} \quad \delta^{(1)}(y) = y_2 \neq 0 \mod 2, \tag{C36}$$

which is identical to Eq. (9) in the main text.

Example.—We take SG 150 as another example to show the criteria to diagnose points in $\mathbb{Z}^r \cap W^{(i,0)} - \bar{W}^{(i,0)}$. According to Eq. (C24), we only need to analyze the $W^{(i,d)}$'s with $(A\Delta y)_i - 1 \ge d$. As discussed in the example in Appendix C 2 a, the shift vector is $\Delta y = (2,1,2)^T$ [Eq. (C23)], and its distances to the four boundaries defined by A in Eq. (C1) [Figs. 7(b)–7(e)] are $(A\Delta y)_1 = 1$, $(A\Delta y)_2 = 0$, $(A\Delta y)_3 = 0$, and $(A\Delta y)_4 = 2$, respectively. Thus, we only need to consider the subpolyhedra $W^{(1,0)}$, $W^{(4,0)}$, and $W^{(4,1)}$. Here, we only calculate the criteria in $W^{(1,0)}$ and $W^{(4,0)}$. Because of the A matrix for SG 150 in Eq. (C1), $(Ay)_1 = 0$ gives the equation $y_1 = y_2$, and $(Ay)_4 = 0$ gives the condition $y_3 = 0$. Then, following the definition of $W^{(i,d)}$ in Eq. (C25), we obtain

$$W^{(1,0)} = \{y \in \mathbb{R}^3 | y_1 = y_2, y_1 \ge y_3, y_3 \ge 0\}, \tag{C37}$$

$$W^{(4,0)} = \{y \in \mathbb{R}^3 | y_3 = 0, y_1 \ge y_2, y_2 \ge 0\}. \tag{C38}$$

Now, let us determine the trivial point monoids $\bar{W}^{(1,0)}$ and $\bar{W}^{(4,0)}$ from Eq. (C27). For $\bar{W}^{(1,0)}$, among the four columns of $R_{1:r,:}$ [Eq. (C20)], only the first $(1,1,1)^T$ and third $(2,2,0)^T$ satisfy $(Ac)_1 = 0$. For $\bar{W}^{(4,0)}$, among the four columns of $R_{1:r,:}$, only the second $(1,0,0)^T$ and third $(2,2,0)^T$ satisfy $(Ac)_4 = 0$. Thus,

$$\bar{W}^{(1,0)} = \{p_1(1,1,1)^T + p_2(2,2,0)^T | p_1, p_2 \in \mathbb{N}\}, \tag{C39}$$

$$\bar{W}^{(4,0)} = \{p_1(1,0,0)^T + p_2(2,2,0)^T | p_1, p_2 \in \mathbb{N}\}. \tag{C40}$$

From Fig. 9(a), where $W^{(1,0)}$ and $\bar{W}^{(1,0)}$ are plotted, one can conclude the criterion in $W^{(1,0)}$ is $y_1 = y_2$ and $y_1 - y_3 = 1 \bmod 2$, which is identical to Eq. (A15). Similarly, from Fig. 9(b), where $W^{(4,0)}$ and $\bar{W}^{(4,0)}$ are plotted, we can conclude the criterion in $W^{(4,0)}$ is $y_3 = 0$ and $y_2 = 1 \bmod 2$, which is identical to Eq. (A13). In the following, we show how to get these criteria by following the algorithm from Eqs. (C27)–(C30). For $W^{(1,0)}$, the $C^{(1)}$ matrix and its Smith decomposition are

$$C^{(1)} = \begin{pmatrix} 1 & 2 \\ 1 & 2 \\ 1 & 0 \end{pmatrix} = \begin{pmatrix} 1 & 1 & 0 \\ 1 & 1 & 1 \\ 1 & 0 & 0 \end{pmatrix} \begin{pmatrix} 1 & 0 \\ 0 & 2 \end{pmatrix} \begin{pmatrix} 1 & 0 \\ 0 & 1 \end{pmatrix}. \tag{C41}$$

The inversion of $L^{(1)}$ is

$$L^{(1)-1} = \begin{pmatrix} 0 & 0 & 1 \\ 1 & 0 & -1 \\ -1 & 1 & 0 \end{pmatrix}. \tag{C42}$$

Substituting $L^{(1)-1}$ and $\Lambda^{(1)}$ into Eqs. (C30) and (C31), we obtain

$$y_1 - y_2 = 0, \quad \text{and} \quad \delta^{(1)}(y) = y_1 - y_3 \neq 0 \mod 2. \tag{C43}$$

For $W^{(4,0)}$, the $C^{(4)}$ matrix and its Smith decomposition are

$$C^{(4)} = \begin{pmatrix} 1 & 2 \\ 1 & 2 \\ 1 & 0 \end{pmatrix} = \begin{pmatrix} 1 & 0 & 0 \\ 0 & 1 & 0 \\ 0 & 0 & 1 \end{pmatrix} \begin{pmatrix} 1 & 0 \\ 0 & 2 \end{pmatrix} \begin{pmatrix} 1 & 2 \\ 0 & 1 \end{pmatrix}. \tag{C44}$$

The inversion of $L^{(4)}$ is

$$L^{(4)-1} = \begin{pmatrix} 1 & 0 & 0 \\ 0 & 1 & 0 \\ 0 & 0 & 1 \end{pmatrix}. \tag{C45}$$

Substituting $L^{(4)-1}$ and $\Lambda^{(4)}$ into Eqs. (C30) and (C31), we obtain

$$y_3 = 0, \quad \text{and} \quad \delta^{(4)}(y) = y_2 \neq 0 \mod 2. \tag{C46}$$

Now, we consider the remaining part: the points in $\mathbb{Z}^r \cap W^{(i,d)} - \bar{W}^{(i,d)}$ for $d > 0$. In general, a point $x \in \mathbb{Z}^r \cap W^{(i,d)}$ decomposes into two parts, $x' + x''$: the first part is generated from $\{C_1^{(i)}, C_2^{(i)}, \cdots\}$ such that $(Ax')_i = 0$, and the second part is generated by the other columns of $R_{1:r,:}$ and $(Ax'')_i = d$. We denote the columns of $R_{1:r,:}$ that satisfy $(Ax)_i > 0$ as $\{D_1^{(i)}, D_2^{(i)}, \cdots\}$ and the matrix consisting of these columns as $D^{(i)} = (D_1^{(i)}, D_2^{(i)}, \cdots)$. (This decomposition is, in general, not unique because of the possible linear dependencies between columns of $R_{1:r,:}$. For example, if $C_1^{(i)} = D_1^{(i)} - D_2^{(i)}$, then $x = D_1^{(i)}$ has at least two different decompositions: $x' = 0$, $x'' = D_1^{(i)}$ or $x' = C_1^{(i)}$, $x'' = D_2^{(i)}$.) Then, we can rewrite $\bar{W}^{(i,d)}$ as

$$\bar{W}^{(i,d)} = \{x = x' + x'' | x' \in \bar{W}^{(i,0)}, x'' \in \bar{V}^{(i,d)}\}, \tag{C47}$$

where

$$\bar{V}^{(i,d)} = \{v | v = p_1 D_1^{(i)} + p_2 D_2^{(i)} + \cdots, p_{1,2\ldots} \in \mathbb{N} \text{ and } (Av)_i = d\}. \tag{C48}$$

Since all the columns in $D^{(i)}$ satisfy $(AD_j^{(i)}) > 0$ and the combination coefficients p_j's are non-negative integers and $(Av)_i = d$ is finite, $\bar{V}^{(i,d)}$ is always finite. Particularly, $\bar{V}^{(i,0)} = \{0\}$. By this construction, $\bar{W}^{(i,d)}$ can be thought of as a sum of $\bar{W}^{(i,0)}$'s shifted by vectors in $\bar{V}^{(i,d)}$, i.e.,

$$\bar{W}^{(i,d)} = \bigoplus_{v \in \bar{V}^{(i,d)}} v + W^{(i,0)}, \tag{C49}$$

where $v + W^{(i,0)} = \{v + y | y \in \bar{W}^{(i,0)}\}$. The sum in Eq. (C49) is finite because $\bar{V}^{(i,d)}$ is a finite set. A point x belongs to $v + \bar{W}^{(i,0)}$ only if $x - v$ belongs to $\bar{W}^{(i,0)}$. For $x - v$ to belong to $\bar{W}^{(i,0)}$, first it should belong to the polyhedral cone $W^{(i,0)}$, i.e., $A(x - v) \geq 0$, and second it should have vanishing Z_n-type indices such that it is a trivial point in $\mathbb{Z}^r \cap W^{(i,0)}$. Thus, for a point $x \in W^{(i,d)}$, we have

$$x \in v + \bar{W}^{(i,0)} \Leftrightarrow A(x - v) \geq 0, \quad \text{and} \quad \delta^{(i)}(x - v) = 0, \tag{C50}$$

where $\delta^{(i)}(x)$ is defined in Eq. (C31), and $\delta^{(i)}(x - v) = 0$ means $\delta_j^{(i)}(x - v) = 0$ for *all* j. As the $\mathbb{Z}_n$-type fragile indices are additive [Eq. (C31)], this condition can be equivalently written as

$$x \in v + \bar{W}^{(i,0)} \Leftrightarrow A(x - v) \geq 0, \quad \text{and} \quad \delta^{(i)}(x) = \delta^{(i)}(v). \tag{C51}$$

For a point $x \in \mathbb{Z}^r \cap W^{(i,d)}$ to be outside $\bar{W}^{(i,d)}$, which is a sum of some shifted $\bar{W}^{(i,0)}$ [Eq. (C49)], x needs to be outside of all of the shifted $\bar{W}^{(i,0)}$'s. In other words, for a point x outside $\bar{W}^{(i,d)}$, the condition in Eq. (C51) is violated for any $W^{(i,0)}$. Mathematically, the condition for $x \notin \bar{W}^{(i,d)}$ is

$$x \notin \bar{W}^{(i,d)} \Leftrightarrow \forall\ v \in \bar{V}^{(i,d)} \quad \text{either} \quad \exists j \text{s.t.} (A(x-v))_j < 0 \quad \text{or} \quad \delta^{(i)}(x) \neq \delta^{(i)}(v). \tag{C52}$$

For simplicity, here we consider a sufficient condition (which will also be shown to be necessary later) for $x \in W^{(i,d)}$ not to belong to $x \notin \bar{W}^{(i,d)}$,

$$x \notin \bar{W}^{(i,d)} \Leftarrow \forall\ v \in \bar{V}^{(i,d)} \delta^{(i)}(x) \neq \delta^{(i)}(v). \tag{C53}$$

This condition is obtained by abandoning the $\exists j \text{s.t.} (A(x-v))_j < 0$ condition in Eq. (C52). A point with the indices $(\delta^{(i)})$ that cannot be realized by any $v \in \bar{V}^{(i,d)}$ fulfills Eq. (C53). Thus, we rewrite it as

$$\delta^{(i)}(x) \notin \{\delta^{(i)}(v) | v \in \bar{V}^{(i,d)}\}. \tag{C54}$$

In principle, the criterion in Eq. (C54) will miss some cases, where $\delta^{(i)}(x)$ equals $\delta^{(i)}(v)$ for some v in $\bar{V}^{(i,d)}$, but x does not satisfy $A(x-v) \geq 0$. However, as will be discussed in Appendix C 3, such cases never appear in practical calculations with TRS and SOC. Therefore, we treat Eq. (C54) as the fragile criterion in $W^{(i,d)}$ for $d > 0$.

Example.—We take SG 150 as an example to show how the algorithm described above works. As discussed from Eqs. (C37)–(C46), points in $\mathbb{Z}^r \cap X - \bar{X}$ are included in (at least) one of the three subpolyhedra $W^{(1,0)}$, $W^{(4,0)}$, and $W^{(4,1)}$. The fragile criteria in $W^{(1,0)}$ and $W^{(4,0)}$ are shown in Eqs. (C43) and (C46), respectively. Now, we work out the fragile criterion in $W^{(4,1)}$. First, because of the A matrix in Eq. (C1) and the $W^{(i,d)}$ definition in Eq. (C25), we obtain

$$W^{(4,1)} = \left\{ y \in \mathbb{R}^3 | y_3 = 1, y_1 \geq y_2, y_1 \geq 1, y_2 \geq \frac{1}{2} \right\}. \tag{C55}$$

Second, we need to determine the set $\bar{V}^{(4,1)}$ and $\bar{W}^{(4,1)}$. Among the four columns in $R_{1:r,:}$ [Eq. (C20)], only the first $(1,1,1)^T$ and the fourth $(2,1,2)^T$ satisfy $(Ax)_4 > 0$. To be specific, the first gives $(Ax)_4 = 1$, and the fourth gives $(Ax)_4 = 2$. Then, because of Eq. (C48), we obtain

$$V^{(4,1)} = \{(1,1,1)^T\}, \tag{C56}$$

and from Eqs. (C40) and (C49), we obtain

$$\bar{W}^{(4,1)} = \{(1,1,1)^T + p_1(1,0,0)^T + p_2(2,2,0)^T | p_1, p_2 \in \mathbb{N}\}. \tag{C57}$$

In Fig. 9(c), we plot the $W^{(4,1)}$ and $\bar{W}^{(4,1)}$. From Fig. 9(c), we can see that the points with odd y_2 can always be reached by adding $(1,0,0)^T$ and $(2,2,0)^T$ to $(1,1,1)^T$, while the points with even y_2 cannot. Thus, we conclude that the criterion to diagnose the points in $\mathbb{Z}^3 \cap W^{(4,1)} - \bar{W}^{(4,1)}$ is $y_3 = 1$ and $y_2 = 0 \mod 2$, which is identical to Eq. (A14). Now, we apply the algorithm described in the last paragraph to rederive Eq. (A14). As we already have $V^{(4,1)}$, to get Eq. (C54), we only need to calculate the $\mathbb{Z}_2$ indices of the points in $V^{(4,1)}$. Because of Eq. (C56) and $\delta^{(4)}(y)$ shown in Eq. (C46), we obtain $\delta^{(4)}(v) = (v_2 \mod 2) = 1$. Then, Eq. (C54) gives the criterion $\delta^{(4)}(y) = (y_2 \mod 2) \notin \{1\}$, which can be equivalently written as

$$y_3 = 1, \qquad y_2 = 0 \mod 2. \tag{C58}$$

3. Two observations about the results

In this subsection, we discuss two observations about the results obtained from applying our algorithm for every SG. These observations have been used to support some conclusions in Appendix C 2. As discussed in Appendix C 2 b, the type-II nontrivial points, i.e., $\mathbb{Z}^r \cap X - \bar{X}$, are close to the boundary of X and hence belong to some lower-dimensional subpolyhedron of X [Eq. (C24)]. In each of the subpolyhedron $W^{(i,d)}$ [Eq. (C25)], the trivial points are denoted as $\bar{W}^{(i,d)}$ [Eq. (C27)]. First, we focus on the $d = 0$ case. Note that $\bar{W}^{(i,0)}$ is generated from the columns of $R_{1:r,:}$ that are exactly on the ith boundary of X $[d = (Ac)_i = 0]$. We denote these columns as $\{C_1^{(i)}, C_2^{(i)}, \cdots\}$. In general, there are two kinds of nontrivial points in $\mathbb{Z}^r \cap W^{(i,0)}$: (i) the points that cannot be written as any integer combination of $\{C_1^{(i)}, C_2^{(i)}, \cdots\}$ and (ii) the points that can be written as an integer combination $\{C_1^{(i)}, C_2^{(i)}, \cdots\}$ but with at least one of the coefficients necessarily negative. However, we found, by exhaustive computation, that case (ii) does not exist in practical calculation with TRS and SOC. Now, we prove this statement based on an observation about the $\{C_1^{(i)}, C_2^{(i)}, \cdots\}$. Let us assume there is a point x belonging to case (ii). On one hand, as said above, x can be written as an integer combination $\{C_1^{(i)}, C_2^{(i)}, \cdots\}$, but at least one of the coefficients is negative. On the other hand, as x belongs to $W^{(i,0)}$, x can be written as a linear combination of the columns of $\{C_1^{(i)}, C_2^{(i)}, \cdots\}$ where the coefficients are positive and rational. In principle, x can have two different decompositions because $\{C_1^{(i)}, C_2^{(i)}, \cdots\}$ are not linearly independent. Now, let us see whether the linear dependencies can change positive and rational coefficients into integer coefficients where at least one is negative. We enumerate all the linear dependencies of $\{C_1^{(i)}, C_2^{(i)}, \cdots\}$ in all SGs, and we find there are only two kinds of dependencies: (A) $c_1 + c_2 = c_3 + c_4$ and (B) $\frac{1}{2}c_1 + \frac{1}{2}c_2 = c_3$, where $c_{1,2,3,4}$ represent different vectors in $\{C_1^{(i)}, C_2^{(i)}, \cdots\}$.

In addition, we find that for each $W^{(i,0)}$, different linear dependence equations involve completely different sets of vectors; i.e., no $C_j^{(i)}$ is contained in two or more linear dependence equations. For example, in SG 188 ($P\bar{6}c2$), for a particular $\bar{W}^{(i,0)}$, there are two linear dependencies: $\frac{1}{2}C_1^{(i)}+\frac{1}{2}C_2^{(i)}=C_3^{(i)}$ and $\frac{1}{2}C_4^{(i)}+\frac{1}{2}C_5^{(i)}=C_6^{(i)}$. Thus, we only need to deal with the linear dependencies separately. Obviously, $c_1+c_2=c_3+c_4$ can only change an integer coefficient to another integer coefficient. Then, we consider the linear dependence $\frac{1}{2}c_1+\frac{1}{2}c_2=c_3$, which, in principle, could change rational coefficients to integer coefficients. Now, we prove that this is not the case. Let x be a fragile phase spanned by three columns having dependence $\frac{1}{2}c_1+\frac{1}{2}c_2=c_3$. We notice that only the coefficients of c_1 and c_2 are fractions ($\frac{1}{2}$), and thus, we consider three cases:

$$x=\frac{1}{2}c_1+p_1c_1+p_2c_2+p_3c_3, \tag{C59}$$

$$x=\frac{1}{2}c_2+p_1c_1+p_2c_2+p_3c_3, \tag{C60}$$

and

$$x=\frac{1}{2}c_1+\frac{1}{2}c_2+p_1c_1+p_2c_2+p_3c_3, \tag{C61}$$

where $p_{1,2,3}\in\mathbb{N}$. Because of $\frac{1}{2}c_1+\frac{1}{2}c_2=c_3$, the first case can be equivalently written as

$$\begin{aligned}x&=p_1c_1+\left(p_2-\frac{1}{2}\right)c_2+(p_3-1)c_3\\&=\left(p_1-\frac{1}{2}\right)c_1+(p_2-1)c_2+(p_3-2)c_3=\cdots,\end{aligned} \tag{C62}$$

none of which is an integer combination. Similarly, the second case cannot be written as an integer combination. The third case is a trivial point, and it can be written as

$$x=p_1c_1+p_2c_2+(p_3+1)c_3. \tag{C63}$$

Therefore, we conclude that the linear dependencies cannot change positive and rational coefficients into integer coefficients where at least one is negative. In other words, the points in $\mathbb{Z}^r\cap W^{(i,0)}-\bar{W}^{(i,0)}$ can never be written as an integer combination $\{C_1^{(i)},C_2^{(i)},\cdots\}$ with at least one negative coefficient.

Now, we consider the $d>0$ case. In the last section, we derive a sufficient condition [Eq. (C54)] for a point in $\mathbb{Z}^r\cap W^{(i,d)}$ to be nontrivial ($\notin\bar{W}^{(i,d)}$). Here, we show that this condition is necessary. As discussed in Appendix C 2, Δy sets the upper bound of d. We find that in most SGs, the maximal d determined by Δy is 0, and only for nine exceptions—i.e., SGs 150 ($P321$), 157 ($P31m$), 185 ($P6_3cm$), 143 ($P3$), 149 ($P312$), 156 ($P3m1$), 158 ($P3c1$), 165 ($P\bar{3}c1$), and 188 ($P\bar{6}c2$)—the maximal d is 1. No higher value is found. Hence, we only need to check the $d=1$ subpolyhedra in the nine SGs. Because of the proof in Appendix C 4, SGs 157 and 185 are equivalent to SG 150, and SGs 149, 156, and 158 are equivalent to SG 143. Here, "equivalent" means that there is a one-to-one mapping between the fragile criteria in equivalent SGs [73]. Thus, in fact, we only need to check the four inequivalent SGs 150, 143, 165, and 188. In Appendixes A 1 and A 3, we have derived all the fragile criteria in SG 150 and 143 by hand, which are all included in the polyhedron-method-based criteria, as shown in Table S2 of Ref. [74]. Therefore, the only cases left to be checked are SGs 165 and 188. Because of the high-rank—ranks of SG 165 and SG 188 are 6 and 7, respectively—we did not derive all the criteria by hand. Instead, we apply numerical checks: We enumerate all the fragile phases up to a number of bands and then check whether they can be diagnosed by Eq. (C54). We use a very large number of bands—6 times the largest number of bands of band structures represented by the Hilbert bases of $\bar{Y}$—and find no fragile phase is missed by Eq. (C54). Here, the symmetry data vector generators are the B vectors corresponding to the Hilbert bases of $\bar{Y}$.

4. Equivalent SGs

In this subsection, we denote the $\bar{Y}$ ($\bar{X}$) monoid for a given SG G as $\bar{Y}_G$ ($\bar{X}_G$). The definition for two SGs to be equivalent is given as follows:

Definition 1.—For two given SGs G and H, if there exists an isomorphism between $\bar{Y}_G$ and $\bar{Y}_H$, *i.e.*, a linear one-to-one mapping $f:\bar{Y}_H\to\bar{Y}_G$ (Theorem 8), such that f is also an isomorphism between $\bar{X}_H$ and $\bar{X}_G$, then we say G and H are equivalent SGs.

If G and H are equivalent, then there is a one-to-one mapping between the fragile phases in $\bar{Y}_G-\bar{X}_G$ and $\bar{Y}_H-\bar{X}_H$. Now, we derive the equivalence condition. First, we rewrite $\bar{Y}_G$ and $\bar{Y}_H$ as $\mathbb{Z}^r\cap Y_G$ and $\mathbb{Z}^r\cap Y_H$, respectively, where $Y_G=\{\mathrm{Ray}\cdot p|p\in\mathbb{R}_+^n\}\subset\mathbb{R}^r$ and $Y_H=\{\mathrm{Ray}'\cdot p|p\in\mathbb{R}_+^n\}\subset\mathbb{R}^r$ are two polyhedral cones. Here, we assume both Ray and Ray$'$ are $r\times n$ matrices, and $\mathrm{rank}(\mathrm{Ray})=\mathrm{rank}(\mathrm{Ray}')=r$. (If Ray and Ray$'$ have different shapes or ranks, G and H cannot be equivalent.) If $\bar{Y}_G$ and $\bar{Y}_H$ are isomorphic, we can represent the isomorphism map f by an $r\times r$ unimodular matrix F, the inverse of which is also an integer matrix, such that each column of $F\cdot\mathrm{Ray}'$ gives a different column of Ray, and every column of Ray is given by some column of $F\cdot\mathrm{Ray}'$. In other words, the columns of $F\cdot\mathrm{Ray}'$ are given by a rearrangement of the columns of Ray. Mathematically, there exists an $n\times n$ permutation matrix S such that $\mathrm{Ray}\cdot S=F\cdot\mathrm{Ray}'$. Given a

point $y' = \mathrm{Ray}' \cdot p' \in \bar{Y}_H$, F maps it to $y = Fy' = \mathrm{Ray} \cdot (Sp') \in \bar{Y}_G$; given a point $y = \mathrm{Ray} \cdot p \in \bar{Y}_G$, F^{-1} maps it to $y' = S^{-1}y = \mathrm{Ray}' \cdot (S^{-1})p \in \bar{Y}_H$. If there does not exist such F and S, $\bar{Y}_G$ and $\bar{Y}_H$ cannot be isomorphic. Let us assume we have found the matrices F and S. Then, we need to check whether F maps $\bar{X}_H$ to $\bar{X}_G$. The condition for $\bar{X}_G$ to $\bar{X}_H$ to be isomorphic under F is that the Hilbert bases of $\bar{X}_G$ and $\bar{X}_H$ transform to each other under F.

In practice, given two SGs, with Ray and Ray$'$ being two $r \times n$ matrices, we enumerate all the $n \times n$ permutation matrices, and for each permutation matrix S, we try to solve the matrix equation $\mathrm{Ray} \cdot S = F \cdot \mathrm{Ray}'$. To solve this matrix equation, we write the Smith decomposition of Ray$'$ as $\mathrm{Ray}' = L(\Lambda 0_{r\times(n-r)})R$, where Λ is an r-by-r diagonal integer matrix. (One should not confuse this with the Smith decomposition of the EBR matrix.) All the r diagonal elements in Λ are nonzero because the rank of Ray is r, which is true because the polyhedral cone Y_H spanned by Ray$'$ has dimension r. We can define the right inverse of Ray$'$ as $\overline{\mathrm{Ray}'} = R^{-1}\binom{\Lambda^{-1}}{0_{(n-r)\times r}}L^{-1}$ such that $\mathrm{Ray}' \cdot \overline{\mathrm{Ray}'} = \mathbb{1}_{r\times r}$. Then, a necessary condition of $\mathrm{Ray} \cdot S = F \cdot \mathrm{Ray}'$ is that

$$\begin{aligned}\mathrm{Ray} \cdot S = F \cdot \mathrm{Ray}' &\Rightarrow F = \mathrm{Ray} \cdot S \cdot \overline{\mathrm{Ray}'} \\ &= \mathrm{Ray} \cdot S \cdot R^{-1}\begin{pmatrix}\Lambda^{-1}\\ 0_{(n-r)\times r}\end{pmatrix}L^{-1}. \end{aligned} \tag{C64}$$

When $\mathrm{Ray} \cdot S \cdot \overline{\mathrm{Ray}'} \cdot \mathrm{Ray}' = \mathrm{Ray} \cdot S$, the right side of Eq. (C64) becomes sufficient,

$$\begin{aligned}\mathrm{Ray} \cdot S \cdot \overline{\mathrm{Ray}'} \cdot \mathrm{Ray}' = \mathrm{Ray} \cdot S \quad \text{and} \quad F = \mathrm{Ray} \cdot S \cdot \overline{\mathrm{Ray}'} \\ \Rightarrow \mathrm{Ray} \cdot S = F \cdot \mathrm{Ray}'. \end{aligned} \tag{C65}$$

However, this is not true, in general, since we usually have $\overline{\mathrm{Ray}'} \cdot \mathrm{Ray}' \neq \mathbb{1}_{n\times n}$. Therefore, the equation $\mathrm{Ray} \cdot S = F \cdot \mathrm{Ray}'$ has either no solution (when $\mathrm{Ray} \cdot S \cdot \overline{\mathrm{Ray}'} \cdot \mathrm{Ray}' \neq \mathrm{Ray} \cdot S$) or a unique solution (when $\mathrm{Ray} \cdot S \cdot \overline{\mathrm{Ray}'} \cdot \mathrm{Ray}' = \mathrm{Ray} \cdot S$). On the other hand, even if F in Eq. (C64) is a solution of $\mathrm{Ray} \cdot S = F \cdot \mathrm{Ray}'$, we still need to check whether F is an isomorphism between $\bar{X}_H$ and $\bar{X}_G$. We change to a different permutation matrix S until $\mathrm{Ray} \cdot S \cdot \overline{\mathrm{Ray}'} \cdot \mathrm{Ray}' = \mathrm{Ray} \cdot S$ and F in Eq. (C64) become an isomorphism between $\mathrm{Hil}(\bar{X}_H)$ and $\mathrm{Hil}(\bar{X}_G)$. As there are $n!$ distinct permutation matrices, this brute force algorithm takes a factorially long time as the n increases. We have to stop at some finite step. Therefore, for a given pair of SGs, with finite steps, we cannot guarantee that we will successfully find the possible equivalent relation.

Example.—We take the equivalent SGs 199 and 208 as examples to show the algorithm. As shown in Fig. 10, the Ray matrices of Y_{199} and Y_{208} are

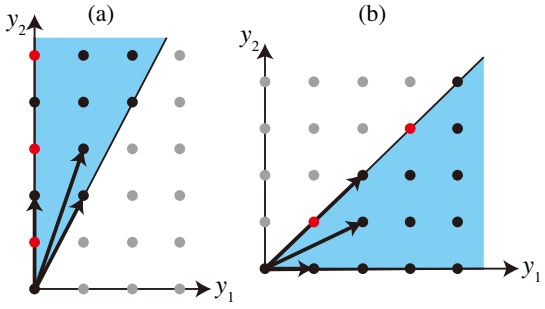

FIG. 10. Example of equivalent SGs. (a) SG 199. (b) SG 208. The polyhedral cone Y's are represented by the shaded area, the generators of $\bar{X}$ are represented by the bold black arrows, the points in $\mathbb{Z}^2 \cap Y$ are represented by black dots, and the points in $\mathbb{Z}^2 \cap Y - \bar{X}$ are represented by red dots. The transformation $F = \binom{1\ -1}{2\ -1}$ transforms Y and $\bar{X}$ in SG 208 to the Y and $\bar{X}$ in SG 199.

$$\mathrm{Ray} = \begin{pmatrix}0 & 1\\ 1 & 2\end{pmatrix}, \qquad \mathrm{Ray}' = \begin{pmatrix}1 & 1\\ 0 & 1\end{pmatrix}, \tag{C66}$$

respectively. On the other hand, the generators of $\bar{X}_{199}$ and $\bar{X}_{208}$ are

$$b_1 = (0,2)^T, \qquad b_2 = (1,2)^T, \qquad b_3 = (1,3)^T, \tag{C67}$$

and

$$b_1' = (2,2)^T, \qquad b_2' = (1,0)^T, \qquad b_3' = (2,1)^T, \tag{C68}$$

respectively. We first choose the permutation matrix as $\binom{1\ 0}{0\ 1}$ and, because of Eq. (C64), obtain the trial solution

$$F = \begin{pmatrix}0 & 1\\ 1 & 1\end{pmatrix}. \tag{C69}$$

This solution maps Ray$'$ to $\mathrm{Ray} \cdot S$. However, here F is not an isomorphism between $\bar{X}_{199}$ and $\bar{X}_{208}$; for example, $Fb_1' = (2,4)^T$ is not a generator of $\bar{X}_{199}$. Second, we choose the permutation matrix as $\binom{0\ 1}{1\ 0}$ and obtain the trial solution

$$F = \begin{pmatrix}1 & -1\\ 2 & -1\end{pmatrix}. \tag{C70}$$

This solution maps Ray$'$ to $\mathrm{Ray} \cdot S$ and is an isomorphism between $\bar{X}_{199}$ and $\bar{X}_{208}$. To be specific, we have $Fb_1' = b_1$, $Fb_2' = b_2$, $Fb_3' = b_3$. Therefore, SG 199 and 208 are equivalent.

In the following are the equivalences found by the brute force algorithm (each line is a class of equivalent SGs):

(1) 1, 3, 4, 5, 6, 7, 8, 9, 16, 17, 18, 19, 20, 21, 22, 23, 24, 25, 26, 27, 28, 29, 30, 31, 32, 33, 34, 35, 36, 37, 38, 39, 40, 41, 42, 43, 44, 45, 46, 76, 77, 78, 80, 91, 92, 93, 94, 95, 96, 98, 101, 102, 105, 106, 109, 110, 144,

145, 151, 152, 153, 154, 169, 170, 171, 172, 178, 179, 180, 181
(2) 79, 97, 104, 107, 146, 155, 160, 161, 195, 196, 197, 198, 212, 213
(3) 90, 100, 108
(4) 199, 208, 214, 210
(5) 48, 50, 59, 68
(6) 52, 54, 56, 57, 60, 62, 73, 112, 113, 116, 117, 118, 120
(7) 61, 75, 89, 99, 103, 114, 122
(8) 133, 142
(9) 150, 157, 185
(10) 159, 173, 182, 186
(11) 209, 211
(12) 63, 72
(13) 135, 138
(14) 143, 149, 156, 158
(15) 168, 177, 183, 184
(16) 218, 219
(17) 11, 13, 49, 51, 67
(18) 14, 53, 55, 58, 81, 82, 111, 115, 119
(19) 15, 66
(20) 86, 134
(21) 85, 125, 129
(22) 12, 65
(23) 2, 10, 47
(24) 162, 164

Notice that the SGs equivalent to SG 1 are all the rank-1 SGs. Thus, none of the rank-1 SGs has EFPs. This case will be explained in more detail in Ref. [73].

APPENDIX D: TWISTED BILAYER GRAPHENE

In this section, we apply our scheme to twisted bilayer graphene (TBG). The single-valley Hamiltonian of TBG has the magnetic SG $P6'2'2$ [55]. The irreps of $P6'2'2$ are given in Table IV. We define the symmetry data vector as

$$B = (m(\Gamma_1), m(\Gamma_2), m(\Gamma_3), m(\mathrm{K}_1), m(\mathrm{K}_2\mathrm{K}_3), m(\mathrm{M}_1), m(\mathrm{M}_2))^T. \tag{D1}$$

The EBRs of $P6'2'2$ can be found in Table 1 in the supplemental material of Ref. [55]. From the EBRs, we construct the EBR matrix as

$$\mathrm{EBR} = \begin{pmatrix} 1 & 0 & 0 & 2 & 0 & 0 \\ 0 & 1 & 0 & 0 & 2 & 0 \\ 0 & 0 & 1 & 0 & 0 & 2 \\ 1 & 1 & 0 & 0 & 0 & 2 \\ 0 & 0 & 1 & 1 & 1 & 1 \\ 1 & 0 & 1 & 2 & 0 & 2 \\ 0 & 1 & 1 & 0 & 2 & 2 \end{pmatrix}. \tag{D2}$$

Following the method introduced in Appendix A, we can parametrize the symmetry data vector as

$$B = (y_1 - y_4, y_2 - y_4, y_4, y_1 + y_2 - 2y_3, y_3, y_1, y_2)^T, \tag{D3}$$

where $y_{1,2,3,4}$ are

$$y_1 = m(\Gamma_1) + m(\Gamma_3), \qquad y_2 = m(\Gamma_2) + m(\Gamma_3),$$
$$y_3 = m(\mathrm{K}_2\mathrm{K}_3), \qquad y_4 = m(\Gamma_3). \tag{D4}$$

Following the machinery of the polyhedron method introduced in Appendix C, we obtain two criteria:

$$2y_3 - y_4 < 0, \tag{D5}$$

$$y_1 + y_2 - 2y_3 = 0, \qquad y_2 - y_4 = 1 \mod 2. \tag{D6}$$

Following the algorithm in Appendix B 2, we obtain two EFP roots,

$$b_1 = (1, 1, 0, 1)^T, \qquad b_2 = (1, 1, 1, 0)^T. \tag{D7}$$

APPENDIX E: FU'S TOPOLOGICAL CRYSTALLINE INSULATOR STATE AND A GENERALIZED SYMMETRY EIGENVALUE CRITERION

1. Symmetry eigenvalues of Fu's state

Here, we explain why Fu's model cannot be diagnosed through the usual symmetry eigenvalue analysis. Fu's model is

$$\begin{aligned} H = {} & \tau_z\sigma_0(\cos k_x + \cos k_y + \cos k_x \cos k_y) \\ & + \tau_z\sigma_z(\cos k_x - \cos k_y) + \tau_z\sigma_x \sin k_x \sin k_y \\ & + \tau_x\sigma_0\left(\frac{5}{2} + \cos k_x + \cos k_y\right) \\ & + t'(\tau_x\sigma_0 \cos k_z + \tau_y\sigma_0 \sin k_z). \end{aligned} \tag{E1}$$

This model has TRS $T = K$, C_4-rotation symmetry $C_4 = i\sigma_y$, and a mirror symmetry $M_{1\bar{1}0} = \sigma_x$. The corresponding space group is $P4mm$. The model is a trivial insulator for $t' = 0$. As t' is increased, a phase transition happens at $t' = 3/2$, and then the state becomes topological. As shown in Figs. 11(b) and 11(c), the trivial phase and the topological phase have the same irreps. These irreps are the same as the EBR induced from $p_{x,y}$ orbitals at the $1a$ position. (See the Irreducible representations of the Double Point Groups and Band representations of the Double Space Groups on BCS [40] for the definitions of the irreps and EBRs.) Thus, this state cannot be diagnosed by symmetry eigenvalues.

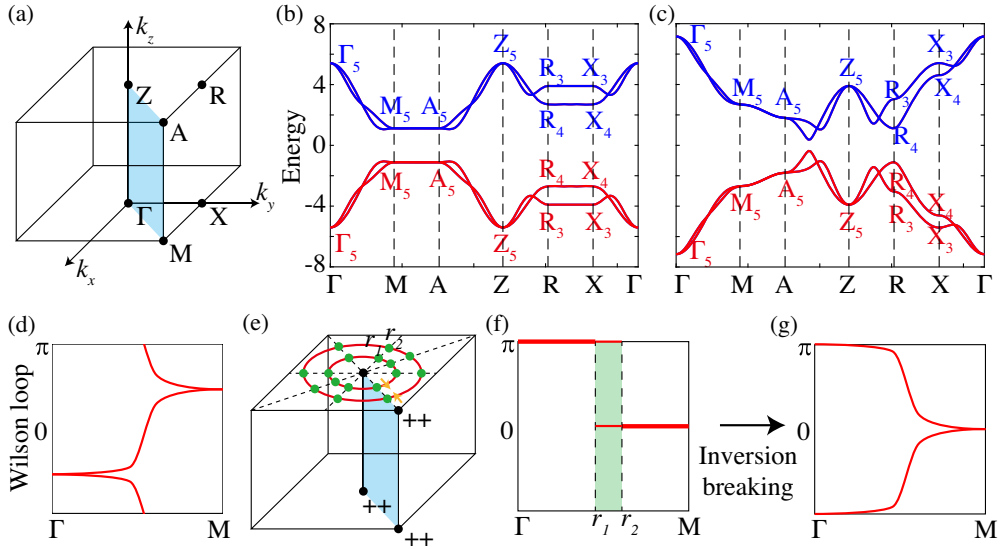

FIG. 11. Fu's topological crystalline insulator [24] and the generalized symmetry eigenvalue criterion. (a) Brillouin zone of the SG $P4$. (b) Band structure and the irreps in the trivial phase of Fu's model ($t' = 0$). (c) Band structure and the irreps in the topological phase of Fu's model ($t' = 2$). The irreps in panels (b,c) are the same as the EBR induced from $p_{x,y}$ orbitals at the $1a$ position. (d) An illustration of the nontrivial Wilson loop spectrum. The Wilson loop operator $W(k_x, k_y)$ is calculated along the k_z direction. The spectrum is plotted along the line $(k_x, k_y) = \Gamma \to \mathrm{M}$. The crossing at Γ and M is protected by C_4 and T. (e) For SG $P4/mmm$, which is a supergroup of $P4$, a $\mathbb{Z}_2$ invariant can be defined based on the inversion eigenvalues [Eq. (E2)]. This $\mathbb{Z}_2$ invariant implies a nodal ring semimetal. The red circles represent the two nodal rings. The four dashed lines represent the four C_2 rotation axes. (f) The discontinuous Wilson loop spectrum of the nodal ring semimetal. (g) If the symmetry is slightly broken such that $P4/mmm$ reduces to $P422$ and no gap closing happens at Γ, M, Z, A, the Wilson loop will have a winding protected by C_4 and T.

2. Topological invariant protected by C_4 and T

We define the topological invariant based on the Wilson loop. The Wilson loop matrix $W(k_x, k_y)$ is given as $W(k_x, k_y) = \lim_{N\to\infty} \prod_{i=0}^{N-1} U^{\dagger}_{k_x,k_y,(2\pi/N)i} U_{k_x,k_y,(2\pi/N)(i+1)}$. Here, $U_{\mathbf{k}}$ is the matrix $(u_{1\mathbf{k}}, u_{2\mathbf{k}}, \cdots)$, with $u_{n\mathbf{k}}$ the periodic part of the nth occupied Bloch wave function at the wave vector $\mathbf{k}$. Now, we show that the spectrum of $W(\mathbf{k}_0)$ for $\mathbf{k}_0 = (0,0), (\pi,\pi)$ must be doubly degenerate. We denote the C_4 representation matrix at $(\mathbf{k}_0, 0)$ as $D_{\mathbf{k}_0}$. Since $C_4^2 = -1$ (because the model consists of $p_{x,y}$ orbitals), $D_{\mathbf{k}_0}$ has only two eigenvalues, i and $-i$, which transform into each other under the action of TRS. As $W(\mathbf{k}_0)$ commutes with $D_{\mathbf{k}_0}$, $W(\mathbf{k}_0)$ is block diagonal in the bases of eigenvectors of $D_{\mathbf{k}_0}$. We denote the blocks in the i and $-i$ sectors as $W_i(\mathbf{k}_0)$ and $W_{-i}(\mathbf{k}_0)$, respectively. Since $W_i(\mathbf{k}_0)$ and $W_{-i}(\mathbf{k}_0)$ are related by TRS, they must have identical eigenvalues. Therefore, each eigenvalue of $W(\mathbf{k}_0)$ is doubly degenerate. Now, we consider the spectra of $W(\mathbf{k}_\perp)$ for a continuous path from $\mathbf{k}_\perp = \Gamma$ to $\mathbf{k}_\perp = \mathrm{M}$. There are two possible types of connectivity: For the trivial phase, a doublet at $\mathbf{k}_\perp = \Gamma$ splits into two branches in the intermediate process, and then the two branches connect to the same doublet at $\mathbf{k}_\perp = \mathrm{M}$; for the topological phase, a doublet at $\mathbf{k} = \Gamma$ splits into two branches in the intermediate process, and the two branches connect to two adjacent doublets at $\mathbf{k} = \mathrm{M}$, as shown Fig. 11(d).

3. Generalized symmetry eigenvalue criterion

In order to obtain the generalized symmetry eigenvalue criterion for the fragile topology protected by C_4 and TRS, we consider two additional symmetries, inversion (P) and C_{2x} rotation. [Equation (E1) does not have these symmetries.] With the additional symmetries, the SG is enhanced to $P4/mmm$. We can think of the subsystem in the line $(0, 0, k_z)$ as a 1D system with TRS, C_4, and P symmetries. Since $C_4^2 = -1$, the 1D system decomposes into a $C_4 = i$ sector and a $C_4 = -i$ sector. The Berry's phase θ_1 in the $C_4 = i$ sector can be calculated from the inversion eigenvalues as $e^{i\pi\theta_1} = \prod_n \xi^{(i)}_{n,\Gamma}\xi^{(i)}_{n,\mathrm{Z}}$, where $\xi^{(i)}_{n\mathbf{k}}$ is the inversion eigenvalue of the nth occupied state in the $C_4 = i$ sector at $\mathbf{k}$. Similarly, the Berry's phase θ_2 in the $C_4 = i$ sector in the line (π, π, k_z) can be calculated as $e^{i\pi\theta_2} = \prod_n \xi^{(i)}_{n,\mathrm{M}}\xi^{(i)}_{n,\mathrm{A}}$. Because of the TRS, the Berry's phases in the $C_4 = -i$ sectors are the same as $\theta_{1,2}$. Then, we define the $\mathbb{Z}_2$ invariant δ as the difference of θ_1 and θ_2,

$$e^{i\pi\delta} = \prod_n \xi^{(i)}_{n,\Gamma}\xi^{(i)}_{n,\mathrm{Z}}\xi^{(i)}_{n,\mathrm{M}}\xi^{(i)}_{n,\mathrm{A}}. \tag{E2}$$

For $\delta = 1$, either Γ and M or Z and A will have opposite products of inversion eigenvalues in each C_4 sector. Since $M_z = C_2 P$ and $C_2 = C_4^2 = -1$, opposite inversion

eigenvalues imply opposite M_z eigenvalues. Therefore, the $\delta = 1$ phase has nodal rings protected by M_z. To be specific, we consider the parities shown in Fig. 11(e), where the two nodal rings are denoted as r_1 and r_2. The M_z eigenvalues $(m_1^{k_z=0} m_2^{k_z=0}, m_1^{k_z=\pi} m_2^{k_z=\pi})$ inside r_1, between r_1 and r_2, and outside r_2 are $(--, ++)$, $(--, +-)$, and $(--, --)$, respectively. According to the correspondence between inversion eigenvalues and Berry's phases [53], the Wilson loop matrices in the three regions have the spectra (π, π), $(0, \pi)$, and (0,0), respectively, as shown in Fig. 11(f).

Now, we consider breaking the inversion symmetry such that the SG reduces to $P422$. Since the mirror symmetry is absent, the nodal rings in Fig. 11(e) will be gapped. However, 16 exceptional gapless points in the four C_2 (C_{2x}, C_{2y}, C_{2xy}, $C_{2x\bar{y}}$) rotation axes will remain. These gapless crossing points are locally protected by the C_2T symmetries and are pinned in the four C_2 axes. There are two ways to gap out these gapless points. The first way is to annihilate two crossings in the same C_2 axes pairwise, which will not close the gap at the high symmetry points. This way is indicated by the yellow arrows in Fig. 11(e). The second way is to annihilate the eight crossings from the same ring at the Z point or the A point. The second way will close the gap at the high symmetry points. Now, we prove that the first way gives the topologically nontrivial phase. As we annihilate the two gapless points, the discontinuous region in the Wilson loop [green region in Fig. 11(f)] will be removed, and the Wilson loop spectrum will become continuous. Because of the $C_{2x\bar{y}}T$ symmetry, the Wilson loop must be "particle-hole" symmetric [55]. Therefore, the Wilson loop must have the connectivity shown in Fig. 11(g), which has a nontrivial winding protected by C_4 and T.

In the end, by a $k \cdot p$ model, we show that the two crossings in the same C_2 axes do annihilate each other. We consider a band inversion of two doublets at the Z point. Each of the two doublets has the C_4 eigenvalues $\pm i$, and the two doublets have opposite inversions. Thus, the symmetries can be represented as $C_4 = i\tau_0\sigma_z$, $P = \tau_z\sigma_0$, $C_{2x} = \tau_0\sigma_x$, and $T = K$. Then, the Hamiltonian for the mirror-protected nodal ring semimetal is

$$H = (M - q_x^2 - q_y^2)\tau_z\sigma_0 + q_z\tau_y\sigma_z, \tag{E3}$$

where $\mathbf{q} = \mathbf{k} - (0, 0, \pi)$. In this Hamiltonian, the two nodal rings are degenerate. One can add perturbation terms to split them. But in order to show that the gapless points can be gapped symmetrically, this Hamiltonian is good enough. The term $m\tau_x\sigma_0$, which breaks P but preserves C_4 and C_{2x}, will fully gap the nodal rings.

APPENDIX F: RELATED MATHEMATICAL THEOREMS

In this section, we summarize the mathematical theorems used in the paper. The theorems are given without proof. Interested readers may look at Ref. [85] for Theorem 2, Ref. [86] for Theorems 3 and 4, and Refs. [79,87,88] for Theorems 5 to 7.

Theorem 2.—(Smith decomposition.) If A is an $n \times m$ integer matrix, then there is an $n \times n$ unimodular matrix L and an $m \times m$ unimodular matrix R such that $A = L\Lambda R$, where $\Lambda_{ij} = \delta_{ij}\lambda_i$ is an $n \times m$ integer matrix. Here, λ_i is positive integer for $1 \le i \le \mathrm{rank}(A)$ and zero for $i > \mathrm{rank}(A)$. Note that Λ is referred to as the Smith normal form of A.

Theorem 3.—(Minkowski-Weyl theorem for polyhedra.) For $P \subseteq \mathbb{R}^d$, the following two statements are equivalent:

(1) (H-representation) P is a polyhedron; *i.e.*, there exist $A \in \mathbb{R}^{m\times d}$, $C \in \mathbb{R}^{m'\times d}$, $b \in \mathbb{R}^m$, and $f \in \mathbb{R}^{m'}$ for some m, m', such that $P = \{x \in \mathbb{R}^d | Ax \ge b, Cx = f\}$.

(2) (V-representation) P is finitely generated; *i.e.*, there exist $V \in \mathbb{R}^{d\times n}$, $\mathrm{Ray} \in \mathbb{R}^{d\times n'}$, and $\mathrm{Line} \in \mathbb{R}^{d\times n''}$, for some n, n', n'', such that $P = \{Vu + \mathrm{Ray}\cdot p + \mathrm{Line}\cdot q | u \in \mathbb{R}^n_+, u_1 + \cdots + u_n = 1,\ p \in \mathbb{R}^{n'}_+,\ q \in \mathbb{R}^{n''}\}$.

The dimension of the polyhedron P, which is given as $d - \mathrm{rank}(C)$, is denoted as $\dim(P)$. The algorithm used to obtain the V-representation from the H-representation or vise versa is available in many mathematical packages. In this work, we use the SageMath package [75]. A special kind of polyhedron is a polyhedral cone, where $b = 0$, $f = 0$, and $V = 0$. For a polyhedral cone, Theorem 3 becomes as follows:

Theorem 4.—(Minkowski-Weyl theorem for polyhedral cones.) For $P \subseteq \mathbb{R}^d$, the following two statements are equivalent:

(1) (H-representation) P is a polyhedral cone; *i.e.*, there exist $A \in \mathbb{R}^{m\times d}$ and $C \in \mathbb{R}^{m'\times d}$ for some m, m', such that $P = \{x \in \mathbb{R}^d | Ax \ge 0, Cx = 0\}$.

(2) (V-representation) P is a finitely generated cone; *i.e.*, there exist $\mathrm{Ray} \in \mathbb{R}^{d\times n}$, and $\mathrm{Line} \in \mathbb{R}^{d\times n'}$, for some n, n', such that $P = \{\mathrm{Ray}\cdot p + \mathrm{Line}\cdot q | p \in \mathbb{R}^n_+, q \in \mathbb{R}^{n'}\}$.

A polyhedral cone is called *pointed* if it does not contain lines, i.e., $\mathrm{Line} = 0$. $\mathrm{Line} = 0$ if $\binom{C}{A}$ is a full-rank matrix. In the case $C = 0$, $\mathrm{Line} = 0$ if the A is a full-rank matrix.

Definition 5.—An affine monoid, denoted as M, is a finitely generated submonoid of a lattice $\mathbb{Z}^d$; *i.e.*, there exist $r_1, r_2, \cdots r_n \in \mathbb{Z}^d$ such that $M = \{r_1p_1 + r_2p_2 + \cdots r_np_n | p_1 \cdots p_n \in \mathbb{N}\}$. Note that M is called positive if $a, -a \in M \Rightarrow a = 0$.

Theorem 6.—(Van der Corput theorem.) Let M be a positive affine monoid. The elements in M that cannot be written as a sum of other elements with positive coefficients are referred to as irreducible elements. Then, (i) every element of M is a sum of irreducible elements with positive coefficients, (ii) M has only finitely many irreducible elements, and (iii) the irreducible elements form the unique

minimal system of generators $\mathrm{Hil}(M) = \{b_1, b_2, \cdots\}$ of M, the Hilbert bases.

Algorithms to find the Hilbert bases include the Normaliz algorithm [79] and the Hemmecke algorithm [80], which are available in the *Normaliz* package and the *4ti2* package, respectively.

Theorem 7.—(Gordan's Lemma.) Let $P \subseteq \mathbb{R}^d$ be a polyhedral cone. Then, $P \cap \mathbb{Z}^d$ is an affine monoid. And when P is pointed, $P \cap \mathbb{Z}^d$ is a positive affine monoid.

Definition 8.—(Monoid homomorphisms.) A homomorphism between two affine monoids M and N is a function $f: M \to N$ such that (i) $f(x+y) = f(x) + f(y)$ for all x, y in M, and (ii) $f(0) = 0$. A bijective monoid homomorphism is called a monoid isomorphism.

[1] C. L. Kane and E. J. Mele, *Quantum Spin Hall Effect in Graphene*, Phys. Rev. Lett. **95**, 226801 (2005).

[2] C. L. Kane and E. J. Mele, Z_2 *Topological Order and the Quantum Spin Hall Effect*, Phys. Rev. Lett. **95**, 146802 (2005).

[3] B. A. Bernevig, T. L. Hughes, and S.-C. Zhang, *Quantum Spin Hall Effect and Topological Phase Transition in HgTe Quantum Wells*, Science **314**, 1757 (2006).

[4] M. König, S. Wiedmann, C. Brüne, A. Roth, H. Buhmann, L. W. Molenkamp, X.-L. Qi, and S.-C. Zhang, *Quantum Spin Hall Insulator State in HgTe Quantum Wells*, Science **318**, 766 (2007).

[5] L. Fu, C. L. Kane, and E. J. Mele, *Topological Insulators in Three Dimensions*, Phys. Rev. Lett. **98**, 106803 (2007).

[6] H. Zhang, C.-X. Liu, X.-L. Qi, X. Dai, Z. Fang, and S.-C. Zhang, *Topological Insulators in* Bi_2Se_3, Bi_2Te_3 *and* Sb_2Te_3 *with a Single Dirac Cone on the Surface*, Nat. Phys. **5**, 438 (2009).

[7] Y. L. Chen, J. G. Analytis, J.-H. Chu, Z. K. Liu, S.-K. Mo, X.-L. Qi, H. J. Zhang, D. H. Lu, Xi Dai, Z. Fang *et al.*, *Experimental Realization of a Three-Dimensional Topological Insulator,* Bi_2Te_3, Science **325**, 178 (2009).

[8] Y. Xia, D. Qian, D. Hsieh, L. Wray, A. Pal, H. Lin, A. Bansil, D. H. Y. S. Grauer, Y. S. Hor, R. J. Cava *et al.*, *Observation of a Large-Gap Topological-Insulator Class with a Single Dirac Cone on the Surface*, Nat. Phys. **5**, 398 (2009).

[9] A. Kitaev, *Periodic Table for Topological Insulators and Superconductors*, AIP Conf. Proc. **1134**, 22 (2009).

[10] X.-L. Qi and S.-C. Zhang, *Topological Insulators and Superconductors*, Rev. Mod. Phys. **83**, 1057 (2011).

[11] M. Z. Hasan and C. L. Kane, *Colloquium: Topological Insulators*, Rev. Mod. Phys. **82**, 3045 (2010).

[12] J. E. Moore, *The Birth of Topological Insulators*, Nature (London) **464**, 194 (2010).

[13] S. Murakami, *Phase Transition between the Quantum Spin Hall and Insulator Phases in 3D: Emergence of a Topological Gapless Phase*, New J. Phys. **9**, 356 (2007).

[14] X. Wan, A. M. Turner, A. Vishwanath, and S. Y. Savrasov, *Topological Semimetal and Fermi-Arc Surface States in the Electronic Structure of Pyrochlore Iridates*, Phys. Rev. B **83**, 205101 (2011).

[15] G. Xu, H. Weng, Z. Wang, X. Dai, and Z. Fang, *Chern Semimetal and the Quantized Anomalous Hall Effect in* $HgCr_2Se_4$, Phys. Rev. Lett. **107**, 186806 (2011).

[16] A. A. Burkov, *Topological Semimetals*, Nat. Mater. **15**, 1145 (2016).

[17] H. Weng, C. Fang, Z. Fang, B. A. Bernevig, and X. Dai, *Weyl Semimetal Phase in Noncentrosymmetric Transition-Metal Monophosphides*, Phys. Rev. X **5**, 011029 (2015).

[18] S.-Y. Xu, I. Belopolski, N. Alidoust, M. Neupane, G. Bian, C. Zhang, R. Sankar, G. Chang, Z. Yuan, C.-C. Lee, S.-M. Huang, H. Zheng, J. Ma, D. S. Sanchez, B. Wang, A. Bansil, F. Chou, P. P. Shibayev, H. Lin, S. Jia, and M. Z. Hasan, *Discovery of a Weyl Fermion Semimetal and Topological Fermi Arcs*, Science **349**, 613 (2015).

[19] L. Yang, Z. Liu, Y. Sun, H. Peng, H. Yang, T. Zhang, B. Zhou, Y. Zhang, Y. Guo, M. Rahn, D. Prabhakaran, Z. Hussain, S.-K. Mo, C. Felser, B. Yan, and Y. Chen, *Discovery of a Weyl Semimetal in Non-Centrosymmetric Compound TaAs*, arXiv:1507.00521.

[20] Z. Wang, Y. Sun, X.-Q. Chen, C. Franchini, G. Xu, H. Weng, X. Dai, and Z. Fang, *Dirac Semimetal and Topological Phase Transitions in* A_3Bi *(*$A =$ Na*, K, Rb)*, Phys. Rev. B **85**, 195320 (2012).

[21] S. M. Young, S. Zaheer, J. C. Y. Teo, C. L. Kane, E. J. Mele, and A. M. Rappe, *Dirac Semimetal in Three Dimensions*, Phys. Rev. Lett. **108**, 140405 (2012).

[22] B.-J. Yang and N. Nagaosa, *Classification of Stable Three-Dimensional Dirac Semimetals with Nontrivial Topology*, Nat. Commun. **5**, 4898 (2014).

[23] J. C. Y. Teo, L. Fu, and C. L. Kane, *Surface States and Topological Invariants in Three-Dimensional Topological Insulators: Application to* $Bi_{1-x}Sb_x$, Phys. Rev. B **78**, 045426 (2008).

[24] L. Fu, *Topological Crystalline Insulators*, Phys. Rev. Lett. **106**, 106802 (2011).

[25] T. H. Hsieh, H. Lin, J. Liu, W. Duan, A. Bansil, and L. Fu, *Topological Crystalline Insulators in the SnTe Material Class*, Nat. Commun. **3**, 982 (2012).

[26] R.-J. Slager, A. Mesaros, V. Juričić, and J. Zaanen, *The Space Group Classification of Topological Band-Insulators*, Nat. Phys. **9**, 98 (2013).

[27] K. Shiozaki and M. Sato, *Topology of Crystalline Insulators and Superconductors*, Phys. Rev. B **90**, 165114 (2014).

[28] C.-X. Liu, R.-X. Zhang, and B. K. VanLeeuwen, *Topological Nonsymmorphic Crystalline Insulators*, Phys. Rev. B **90**, 085304 (2014).

[29] C. Fang and L. Fu, *New Classes of Three-Dimensional Topological Crystalline Insulators: Nonsymmorphic and Magnetic*, Phys. Rev. B **91**, 161105(R) (2015).

[30] W. A. Benalcazar, B. A. Bernevig, and T. L. Hughes, *Quantized Electric Multipole Insulators*, Science **357**, 61 (2017).

[31] W. A. Benalcazar, B. A. Bernevig, and T. L. Hughes, *Electric Multipole Moments, Topological Multipole Moment Pumping, and Chiral Hinge States in Crystalline Insulators*, Phys. Rev. B **96**, 245115 (2017).

[32] F. Schindler, A. M. Cook, M. G. Vergniory, Z. Wang, S. S. P. Parkin, B. A. Bernevig, and T. Neupert, *Higher-Order Topological Insulators*, Sci. Adv. **4**, eaat0346 (2018).

[33] J. Langbehn, Y. Peng, L. Trifunovic, F. von Oppen, and P. W. Brouwer, *Reflection-Symmetric Second-Order*

Topological Insulators and Superconductors, Phys. Rev. Lett. **119**, 246401 (2017).

[34] Z. Song, Z. Fang, and C. Fang, *$(d-2)$-Dimensional Edge States of Rotation Symmetry Protected Topological States*, Phys. Rev. Lett. **119**, 246402 (2017).

[35] C. Fang and L. Fu, *Rotation Anomaly and Topological Crystalline Insulators*, Sci. Adv. **5**, eaat2374 (2019).

[36] M. Ezawa, *Higher-Order Topological Insulators and Semimetals on the Breathing Kagome and Pyrochlore Lattices*, Phys. Rev. Lett. **120**, 026801 (2018).

[37] B. Bradlyn, L. Elcoro, J. Cano, M. G. Vergniory, Z. Wang, C. Felser, M. I. Aroyo, and B. A. Bernevig, *Topological Quantum Chemistry*, Nature (London) **547**, 298 (2017).

[38] H. C. Po, A. Vishwanath, and H. Watanabe, *Complete Theory of Symmetry-Based Indicators of Band Topology*, Nat. Commun. **8**, 50 (2017).

[39] J. Kruthoff, J. de Boer, J. van Wezel, C. L. Kane, and R.-J. Slager, *Topological Classification of Crystalline Insulators through Band Structure Combinatorics*, Phys. Rev. X **7**, 041069 (2017).

[40] L. Elcoro, B. Bradlyn, Z. Wang, M. G. Vergniory, J. Cano, C. Felser, B. A. Bernevig, D. Orobengoa, G. de la Flor, and M. I. Aroyo, *Double Crystallographic Groups and Their Representations on the Bilbao Crystallographic Server*, J. Appl. Crystallogr. **50**, 1457 (2017).

[41] M. G. Vergniory, L. Elcoro, Z. Wang, J. Cano, C. Felser, M. I. Aroyo, B. A. Bernevig, and B. Bradlyn, *Graph Theory Data for Topological Quantum Chemistry*, Phys. Rev. E **96**, 023310 (2017).

[42] J. Cano, B. Bradlyn, Z. Wang, L. Elcoro, M. G. Vergniory, C. Felser, M. I. Aroyo, and B. A. Bernevig, *Topology of Disconnected Elementary Band Representations*, Phys. Rev. Lett. **120**, 266401 (2018).

[43] E. Khalaf, H. C. Po, A. Vishwanath, and H. Watanabe, *Symmetry Indicators and Anomalous Surface States of Topological Crystalline Insulators*, Phys. Rev. X **8**, 031070 (2018).

[44] Z. Song, T. Zhang, Z. Fang, and C. Fang, *Quantitative Mappings between Symmetry and Topology in Solids*, Nat. Commun. **9**, 3530 (2018).

[45] Z. Song, T. Zhang, and C. Fang, *Diagnosis for Nonmagnetic Topological Semimetals in the Absence of Spin-Orbital Coupling*, Phys. Rev. X **8**, 031069 (2018).

[46] M. G. Vergniory, L. Elcoro, C. Felser, N. Regnault, B. A. Bernevig, and Z. Wang, *A Complete Catalogue of High-Quality Topological Materials*, Nature (London) **566**, 480 (2019).

[47] T. Zhang, Y. Jiang, Z. Song, H. Huang, Y. He, Z. Fang, H. Weng, and C. Fang, *Catalogue of Topological Electronic Materials*, Nature (London) **566**, 475 (2019).

[48] F. Tang, H. C. Po, A. Vishwanath, and X. Wan, *Comprehensive Search for Topological Materials Using Symmetry Indicators*, Nature (London) **566**, 486 (2019).

[49] F. Tang, H. C. Po, A. Vishwanath, and X. Wan, *Efficient Topological Materials Discovery Using Symmetry Indicators*, Nat. Phys.**15**, 470 (2019).

[50] J. Cano, B. Bradlyn, Z. Wang, L. Elcoro, M. G. Vergniory, C. Felser, M. I. Aroyo, and B. A. Bernevig, *Building Blocks of Topological Quantum Chemistry: Elementary Band Representations*, Phys. Rev. B **97**, 035139 (2018).

[51] M. I. Aroyo, J. M. Perez-Mato, D. Orobengoa, E. Tasci, G. De La Flor, and A. Kirov, *Crystallography Online: Bilbao Crystallographic Server*, Bulg Chem Commun **43**, 183 (2011); M. I. Aroyo, J. Manuel Perez-Mato, C. Capillas, E. Kroumova, S. Ivantchev, G. Madariaga, A. Kirov, and H. Wondratschek, *Bilbao Crystallographic Server: I. Databases and Crystallographic Computing Programs*, Crystalline Mater. **221**, 15 (2006); M. I. Aroyo, A. Kirov, C. Capillas, J. M. Perez-Mato, and H. Wondratschek, *Bilbao Crystallographic Server. II. Representations of Crystallographic Point Groups and Space Groups*, Acta Crystallogr. Sect. A **62**, 115 (2006).

[52] R. Yu, X. L. Qi, A. Bernevig, Z. Fang, and X. Dai, *Equivalent Expression of $\mathbb{Z}_2$ Topological Invariant for Band Insulators Using the Non-Abelian Berry Connection*, Phys. Rev. B **84**, 075119 (2011).

[53] A. Alexandradinata, X. Dai, and B. A. Bernevig, *Wilson-Loop Characterization of Inversion-Symmetric Topological Insulators*, Phys. Rev. B **89**, 155114 (2014).

[54] A. Bouhon, A. M. Black-Schaffer, and R.-J. Slager, *Wilson Loop Approach to Topological Crystalline Insulators with Time Reversal Symmetry*, Phys. Rev. B **100**, 195135 (2019).

[55] Z. Song, Z. Wang, W. Shi, G. Li, C. Fang, and B. A. Bernevig, *All Magic Angles in Twisted Bilayer Graphene are Topological*, Phys. Rev. Lett. **123**, 036401 (2019).

[56] B. Bradlyn, Z. Wang, J. Cano, and B. A. Bernevig, *Disconnected Elementary Band Representations, Fragile Topology, and Wilson Loops as Topological Indices: An Example on the Triangular Lattice*, Phys. Rev. B **99**, 045140 (2019).

[57] H. C. Po, H. Watanabe, and A. Vishwanath, *Fragile Topology and Wannier Obstructions*, Phys. Rev. Lett. **121**, 126402 (2018).

[58] J. Ahn, S. Park, and B.-J. Yang, *Failure of Nielsen-Ninomiya Theorem and Fragile Topology in Two-Dimensional Systems with Space-Time Inversion Symmetry: Application to Twisted Bilayer Graphene at Magic Angle*, Phys. Rev. X **9**, 021013 (2019).

[59] H. C. Po, L. Zou, T. Senthil, and A. Vishwanath, *Faithful Tight-Binding Models and Fragile Topology of Magic-Angle Bilayer Graphene*, Phys. Rev. B **99**, 195455 (2019).

[60] M. B. de Paz, M. G. Vergniory, D. Bercioux, A. García-Etxarri, and B. Bradlyn, *Engineering Fragile Topology in Photonic Crystals: Topological Quantum Chemistry of Light*, Phys. Rev. Research **1**, 032005 (2019).

[61] J. L. Mañes, *Fragile Phonon Topology on the Time-Reversal Symmetric Honeycomb*, arXiv:1904.06997.

[62] D. V. Else, H. C. Po, and H. Watanabe, *Fragile Topological Phases in Interacting Systems*, Phys. Rev. B **99**, 125122 (2019).

[63] R. Bistritzer and A. H. MacDonald, *Moiré Bands in Twisted Double-Layer Graphene*, Proc. Natl. Acad. Sci. U.S.A. **108**, 12233 (2011).

[64] K. Kim, A. DaSilva, S. Huang, B. Fallahazad, S. Larentis, T. Taniguchi, K. Watanabe, B. J. LeRoy, A. H. MacDonald, and E. Tutuc, *Tunable Moiré Bands and Strong Correlations in Small-Twist-Angle Bilayer Graphene*, Proc. Natl. Acad. Sci. U.S.A. **114**, 3364 (2017).

[65] Y. Cao, V. Fatemi, A. Demir, S. Fang, S. L. Tomarken, J. Y. Luo, J. D. Sanchez-Yamagishi, K. Watanabe, T. Taniguchi,

E. Kaxiras *et al.*, *Correlated Insulator Behaviour at Half-Filling in Magic-Angle Graphene Superlattices*, Nature (London) **556**, 80 (2018).

[66] Y. Cao, V. Fatemi, S. Fang, K. Watanabe, T. Taniguchi, E. Kaxiras, and P. Jarillo-Herrero, *Unconventional Superconductivity in Magic-Angle Graphene Superlattices*, Nature (London) **556**, 43 (2018).

[67] S. Huang, K. Kim, D. K. Efimkin, T. Lovorn, T. Taniguchi, K. Watanabe, A. H. MacDonald, E. Tutuc, and B. J. LeRoy, *Topologically Protected Helical States in Minimally Twisted Bilayer Graphene*, Phys. Rev. Lett. **121**, 037702 (2018).

[68] M. Yankowitz, S. Chen, H. Polshyn, Y. Zhang, K. Watanabe, T. Taniguchi, D. Graf, A. F. Young, and C. R. Dean, *Tuning Superconductivity in Twisted Bilayer Graphene*, Science **363**, 1059 (2019).

[69] G. Tarnopolsky, A. J. Kruchkov, and A. Vishwanath, *Origin of Magic Angles in Twisted Bilayer Graphene*, Phys. Rev. Lett. **122**, 106405 (2019).

[70] J. Liu, J. Liu, and X. Dai, *A Complete Picture for the Band Topology in Twisted Bilayer Graphene*, arXiv:1810.03103.

[71] J. Zak, *Band Representations of Space Groups*, Phys. Rev. B **26**, 3010 (1982).

[72] L. Michel and J. Zak, *Elementary Energy Bands in Crystals Are Connected*, Phys. Rep. **341**, 377 (2001).

[73] L. Elcoro, Z. Song, and B. A. Bernevig, *Application of the Induction Procedure and the Smith Decomposition in the Calculation and Topological Classification of Electronic Band Structures in the 230 Space Groups*, arXiv:2002.03836.

[74] See Supplemental Material at http://link.aps.org/supplemental/10.1103/PhysRevX.10.031001 for tables about materials, parametrization of band irreps, fragile criteria, and fragile roots.

[75] The Sage Developers, *sageMath, The Sage Mathematics Software System (Version 8.4)* (2018).

[76] D. J. Thouless, M. Kohmoto, M. P. Nightingale, and M. den Nijs, *Quantized Hall Conductance in a Two-Dimensional Periodic Potential*, Phys. Rev. Lett. **49**, 405 (1982).

[77] F. D. M. Haldane, *Model for a Quantum Hall Effect without Landau Levels: Condensed-Matter Realization of the "Parity Anomaly"*, Phys. Rev. Lett. **61**, 2015 (1988).

[78] Y. Hatsugai, *Chern Number and Edge States in the Integer Quantum Hall Effect*, Phys. Rev. Lett. **71**, 3697 (1993).

[79] W. Bruns and B. Ichim, *Normaliz: Algorithms for Affine Monoids and Rational Cones*, J. Algebra **324**, 1098 (2010).

[80] R. Hemmecke, *On the Computation of Hilbert Bases of Cones*, in *Mathematical Software* (World Scientific, Singapore, 2002), pp. 307–317.

[81] L. Fu and C. L. Kane, *Topological Insulators with Inversion Symmetry*, Phys. Rev. B **76**, 045302 (2007).

[82] T. L. Hughes, E. Prodan, and B. A. Bernevig, *Inversion-Symmetric Topological Insulators*, Phys. Rev. B **83**, 245132 (2011).

[83] B. J. Wieder and B. A. Bernevig, *The Axion Insulator as a Pump of Fragile Topology*, arXiv:1810.02373.

[84] A. Alexandradinata, C. Fang, M. J. Gilbert, and B. A. Bernevig, *Spin-Orbit-Free Topological Insulators without Time-Reversal Symmetry*, Phys. Rev. Lett. **113**, 116403 (2014).

[85] Wikipedia contributors, *Wikipedia, Smith Normal Form* (2019).

[86] K. Fukuda, *Lecture: Polyhedral Computation* (Institute for Operations Research and Institute of Theoretical Computer Science, Zurich, 2013).

[87] L. E. Renner, *Linear Algebraic Monoids* (Springer-Verlag Berlin Heidelberg, 2006), Vol. 134.

[88] W. Bruns and J. Gubeladze, *Polytopes, Rings, and K-theory* (Springer, New York, 2009), Vol. 27.